The mechanics of static non-planar faults in linear elasticity

Pierre ROMANET[1,2], Tatsuhiko SAITO[3], and Eiichi FUKUYAMA[3]

[1]Department of Earth Sciences, La Sapienza Università di Roma, Rome, Italy
[2]Université Côte d'Azur, IRD, CNRS, Observatoire de la Côte d'Azur, Géoazur, Sophia-Antipolis, France, email: romanet@geoazur.unice.fr
[3]Earthquake and Tsunami research division, NIED, Tsukuba, Japan

August 2, 2023

Abstract

Fault geometry is a key factor in controling the mechanics of faulting. However, there is currently limited theoretical knowledge regarding the effect of non-planar fault geometry on earthquake mechanics. Here, we address this gap by introducing an expansion of the relation between fault traction and slip, up to second order, relative to the deviation from a planar fault geometry. This expansion enables the separation of the effects of non-planarities from those of planar faults. This expansion is realised in the boundary integral equation, assuming a small fault slope. It provides an interpretation for the effect of complex fault geometry on fault traction, for any fault geometry and any slip distribution. Hence the results are also independent of the friction that applies on the fault. The findings confirm that fault geometry has a strong influence on in-plane faulting (mode II) by altering the normal traction on the fault and making it more resistant to slipping for any fault geometry. On the contrary, for out-of-plane faulting (mode III), fault geometry has a much smaller influence.

Additionally, we analyse some singularities that arise for specific fault geometries often used in earthquake simulations and provide guidelines for their elimination. To conclude this study, we discuss the limits of the small strain approximation when non-planar faults are considered.

1 Introduction

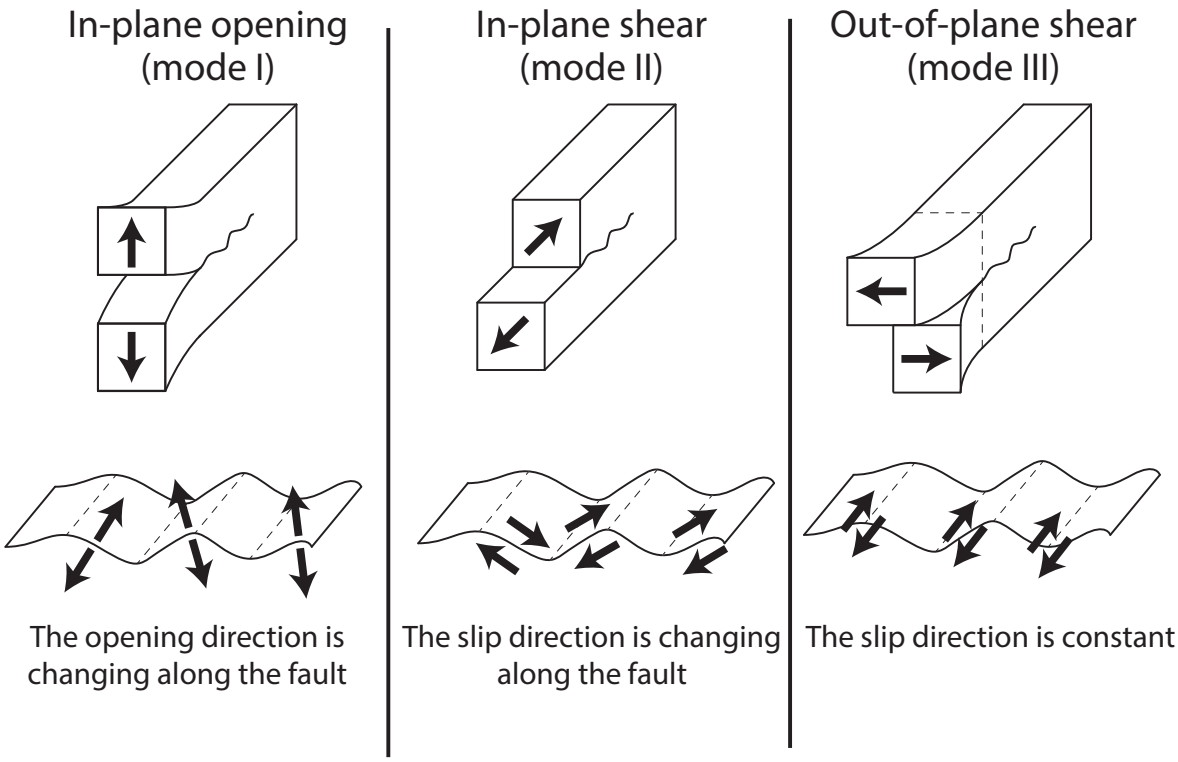

Figure 1: Description of the different modes of slip for a non-planar fault. Please note that we are using a slight abuse of language by calling them mode I, mode II, and mode III.

Understanding the mechanical effect of fault geometry is an important question for seismology, as it can influence various aspects of earthquake mechanics, such as the areas of the fault that will nucleate, the size of the rupture, or the slip distribution (*Aki*, 1979; *King and Nabelek*, 1985; *Schwartz and Sibson*, 1989; *Klinger et al.*, 2006; *Wesnousky*, 2006, 2008; *Milliner et al.*, 2015). Previous theoretical efforts to understand the effect of fault non-planarities have been primarily focusing on particular fault geometries such as sinusoidale geometry (*Saucier et al.*, 1992; *Chester and Chester*, 2000), or rough faults (*Dieterich and Smith*, 2009; *Dunham et al.*, 2011; *Fang and Dunham*, 2013), limiting the generalizability

of the results.

In this paper, we extract the effect of non-planarities from the effect of planar fault by performing an expansion of the boundary integral equation. It makes the results presented in this paper very general as they do not depend on one specific geometry, or one specific slip distribution. It also makes the results presented here independent of the friction law that applies on the fault.

Our emphasis will be on the two modes of shearing fault: in-plane faulting and out-of-plane faulting. However, the results presented in this paper can also be applied to opening faults, and the associated findings can be found in Appendix G. We will use a slight abuse of language by sometimes calling mode I, mode II, and mode III what should respectively be called in-plane opening, in-plane shearing, and out-of-plane shearing. Mode I corresponds to pure opening, Mode II corresponds to a pure shear fault, where the direction of rupture is parallel to the direction of slip. Mode III corresponds to a pure shear fault where the direction of rupture is perpendicular to the direction of slip (see Fig. 1). The primary objective of this paper is to provide a comprehensive explanation of the main effects of non-planar fault geometry on the traction that applies on the fault.

2 Tractions on a non-planar fault

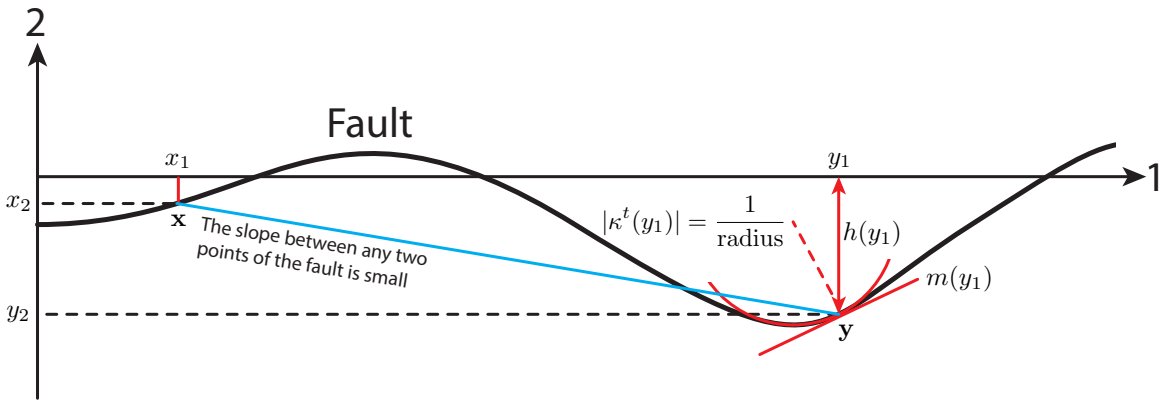

Figure 2: Definition of the parameters used in this study. The flat fault approximation is when the slope between any two points of the fault is considered small. This figure is modified from *Romanet et al.* (2020).

This paper derives exact semi-analytical solutions for the strains and stresses within a homogeneous, infinite, linear, static, two-dimensional (2D) medium caused by a finite, non-planar fault (see Appendix G, H and I). It can be viewed as the static, 2D extension of the previous work by *Romanet et al.* (2020), where the semi-analytical solution was derived for a fully-dynamic, three-dimensional (3D) medium using the Einstein notation.

The geometry of the fault is described by a function $h(y_1)$ representing the height of the fault at given position $\mathbf{y} = (y_1, y_2) = (y_1, h(y_1))$ (Fig. 2). The derivative of the height with respect to the coordinate y_1 (the fault slope) is denoted as $m(y_1) = \frac{d}{dy_1}h(y_1)$. When the fault slope is small ($m(y_1) << 1$), the second order derivative of height with respect

to the coordinate y_1 can be linked to the curvature along the fault κ^t by:

$$\begin{aligned}\kappa^t(y_1) &= \frac{\frac{d}{dy_1}m(y_1)}{(1+m^2(y_1))^{\frac{3}{2}}} \\ &\simeq \frac{d}{dy_1}m(y_1) = \frac{d^2}{dy_1^2}h(y_1), \text{ if } m(y_1) << 1\end{aligned} \tag{1}$$

The absolute value of the fault curvature $|\kappa^t|$ can be interpreted geometrically as the inverse radius of the tangential circle to the fault (see Fig. 2). When the fault is locally flat, the curvature is zero ($\kappa^t(y_1) = 0$).

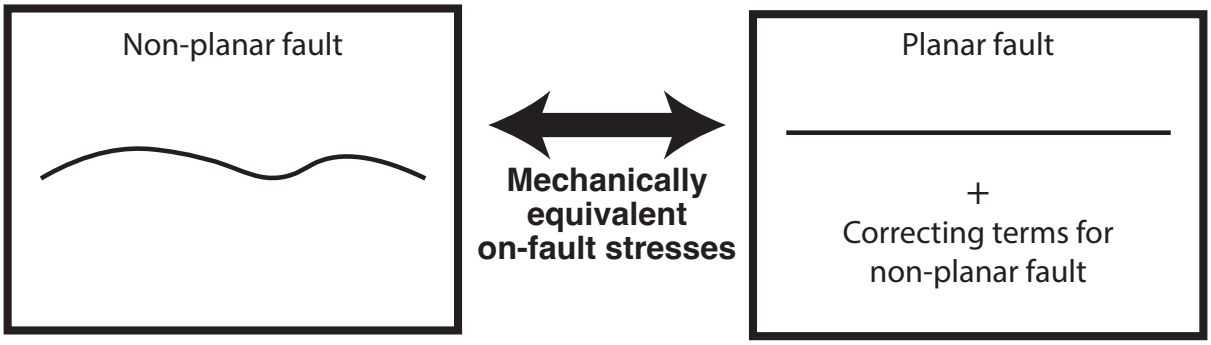

Figure 3: A non-planar fault can be made equivalent to a planar fault with additional on-fault stresses correction. This is not working for off-fault stresses.

This paper demonstrates that the semi-analytical solution for the on-fault stresses can be significantly simplified when assuming a small fault slope. **For the on-fault stresses**, it is possible to identify the exact mechanical corrections that renders a planar fault mechanically equivalent to a non-planar fault by including additional terms that account for the non-planar geometry (see Fig. 3). In order not to distract the reader from the main points of this paper, most of the derivation is provided in appendix B. In the following, we just provide a summary of the principal steps involved in the derivation:

1. We start from the representation theorem (*Aki and Richards* (2002), chapter 2.5)

which allows to calculate the displacement u_k anywhere in the medium by evaluating an integral over the fault involving the Green's function G_{kp} (*Tada and Yamashita*, 1997) and the displacement discontinuity Δu_i across the fault. The subscripts refer to specific component of the vector, for example u_k is the k^{th} component of the slip vector $\mathbf{u}$. c_{ijpq} is the Hooke tensor, and $\mathbf{n}$ is the normal vector to the fault.

$$u_k(\mathbf{x}) = -\int_{\text{fault}} c_{ijpq}\Delta u_i(\mathbf{y})n_j(\mathbf{y})\frac{\partial}{\partial x_q}G_{kp}(\mathbf{x},\mathbf{y})dl(\mathbf{y}) \tag{2}$$

2. By using the strain definition $\epsilon_{cd} = \frac{1}{2}\left(\frac{\partial}{\partial x_c}u_d + \frac{\partial}{\partial x_d}u_c\right)$ and the Hooke's law ($\sigma_{ab} = c_{abcd}\epsilon_{cd}$), we can obtain the stresses σ_{ab} at any point within the medium. It leads to an integral linking the stresses to the Green's function and the displacement discontinuity along the fault. Unfortunately the resulting integral is hypersingular for the on-fault stresses. This hypersingularity arises because of the second-order derivative of the Green's functions. As a result, conventional numerical integration technics cannot be used (*Koller et al.*, 1992; *Tada and Yamashita*, 1997).

$$\sigma_{ab}(\mathbf{x}) = -c_{abcd}\int_{\text{fault}} c_{ijpq}\Delta u_i(\mathbf{y})n_j(\mathbf{y})\frac{\partial}{\partial x_q}\frac{\partial}{\partial x_d}G_{cp}(\mathbf{x},\mathbf{y})dl(\mathbf{y}) \tag{3}$$

3. We regularize this integral using the tangential differential operator (*Bonnet*, 1999; *Sato et al.*, 2020) and project the slip vector onto the fault (*Romanet et al.*, 2020). This makes appear the curvature term and the gradient term into the equation:

$$\sigma_{ij}(\mathbf{x}) = \underbrace{\int_{\text{fault}} \underbrace{c_{abcd}c_{ijpq}\frac{\partial}{\partial x_q}G_{cp}[n_d t_j - n_j t_d]t_i}_{\text{Kernel}} \underbrace{\frac{\partial}{\partial y^t}\Delta u(\mathbf{y})}_{\text{Gradient of slip}} \, \mathrm{d}l(\mathbf{y})}_{\text{Gradient term}} + \underbrace{\int_{\text{fault}} \underbrace{c_{abcd}c_{ijpq}\frac{\partial}{\partial x_q}G_{cp}[n_d t_j - n_j t_d]n_i}_{\text{Kernel}} \underbrace{\kappa^t(\mathbf{y})\Delta u(\mathbf{y})}_{\text{Curvature} \times \text{Slip}} \, \mathrm{d}l(\mathbf{y})}_{\text{Curvature term}} \tag{4}$$

This equation is now Cauchy integrable, and **no longer** hypersingular. In the gradient term, $\frac{\partial}{\partial y^t}\Delta u(\mathbf{y})$ represents the derivative along the fault direction (see Appendix B.1). In the curvature term, the local curvature of the fault κ^t can be seen. The t upper-script emphasizes that the curvature is the one in the direction of the tangential vector to the fault $\mathbf{t}$.

4. **For on-fault shear ($\tau_{\mathbf{el}} = t_i\sigma_{ij}n_j$) and normal ($\sigma_{\mathbf{el}} = n_i\sigma_{ij}n_j$) tractions only**, we can develop the integrand that consists of Green's function and Hooke tensor while making the small slope approximation of the fault geometry (see Fig. 2, *Romanet et al.* (2020); *Romanet and Ozawa* (2021)). This approach allows to derive a simplified expansion for the **elastic tractions on the fault** due to a slip distribution:

$$\begin{aligned} \underbrace{\tau_{\text{el}}(\mathbf{x})}_{\substack{\text{Full solution}\\ \text{Elastic shear traction}}} &= \underbrace{\tau^0_{\text{el}}(x_1)}_{0^{\text{th}}\text{ order}} + \underbrace{\tau^1_{\text{el}}(x_1)}_{1^{\text{st}}\text{ order}} + \underbrace{\ldots}_{\text{higher orders}} \\ \underbrace{\sigma_{\text{el}}(\mathbf{x})}_{\substack{\text{Full solution}\\ \text{Elastic normal traction}}} &= \underbrace{\sigma^0_{\text{el}}(x_1)}_{0^{\text{th}}\text{ order}} + \underbrace{\sigma^1_{\text{el}}(x_1)}_{1^{\text{st}}\text{ order}} + \underbrace{\ldots}_{\text{higher orders}} \end{aligned} \tag{5}$$

The 0^{th} order terms in the previous equation represent terms that are independent of the slope between any two points of the fault. The 1^{st} order terms are terms whose integrands are proportional to the fault slope $\propto \frac{x_2 - y_2}{x_1 - y_1}$, and the 2^{nd} order

terms are terms whose integrands are proportional to the square of the fault slope $\propto \left(\frac{x_2-y_2}{x_1-y_1}\right)^2$ and so on. This decomposition process may appear complex, but it offers two significant advantages when it comes to decomposing shear and normal traction:

(a) **Interpretability:** Breaking down the tractions into terms based on fault slope provides a clearer understanding of the physical processes at play. Each order of terms corresponds to a specific level of importance regarding the effect of fault geometry, allowing for easier interpretation and analysis.

(b) **Approximation:** The small slope approximation in the decomposition process enables us to simplify the mathematical expressions and calculations involved. This approximation is often valid in many practical scenarios, because faults are more or less linear structures. As a result, more computationally efficient numerical methods can be employed while still capturing essential aspects of fault behavior (*Romanet and Ozawa*, 2021).

The discretisation of the integrals needed for the calculation of the stresses (eq.(4)) and the on-fault shear and normal traction (eq. (5)) is done using a piecewise discretisation of the fault geometry, together with a piecewise discretisation of the slip (see Appendix 17).

2.1 In-plane shear (mode II)

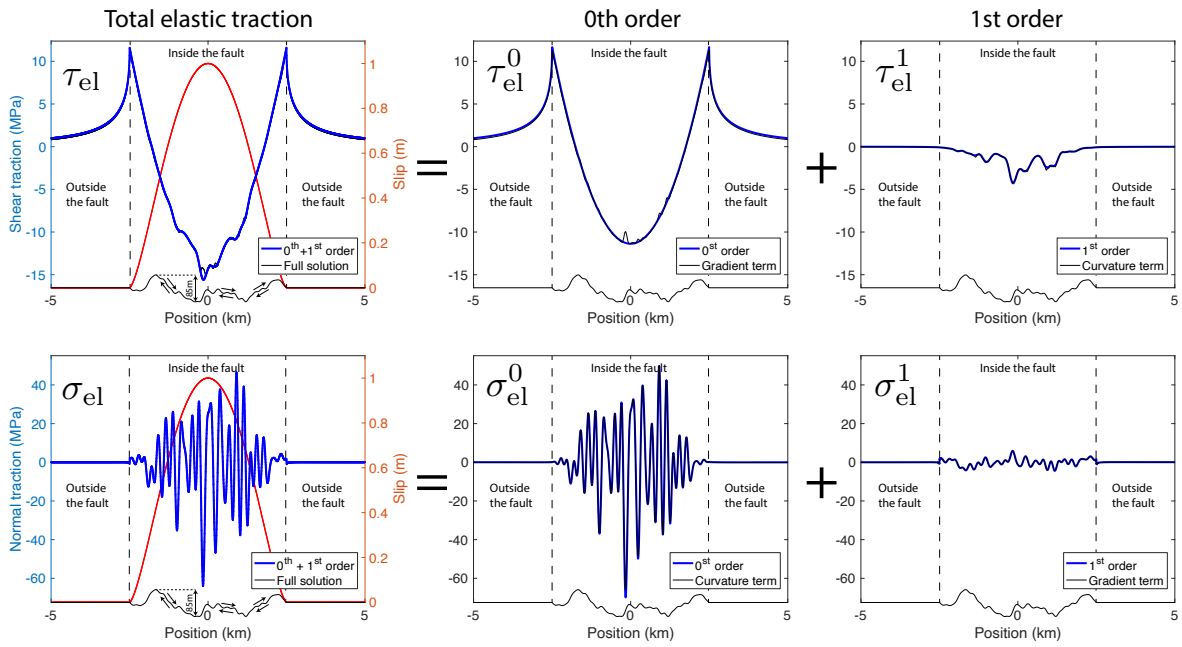

Figure 4: Assuming the fault geometry (as shown by the x-axis) and the slip distribution $\Delta u(y_1) = (1-4\frac{y_1^2}{L^2})^{3/2}$ (red curve), L being the length of the fault, the shear traction (upper panels) and the normal traction (lower panels) term can be decomposed into 0^{th} order term and 1^{st} order term. The 0^{th} order and the 1^{st} order (blue lines), are respectively calculated using the expressions (8) and (9) (more precisely the spectral version of these equations as given by (74) and (76) in appendix H). The full solution and associated gradient and curvature terms (black lines) are calculated using eq. (72).

By employing the small slope approximation, the shear and normal tractions can be expanded as:

$$\underbrace{\tau_{\mathrm{el}}}_{\substack{\text{Elastic shear traction}\\ \text{of a non-planar fault}}} = \underbrace{\tau^0_{\mathrm{el}}}_{\text{Planar fault response}} + \underbrace{\tau^1_{\mathrm{el}}}_{\text{Shear traction drag}} + \underbrace{\ldots}_{\text{Higher order terms}} \tag{6}$$

$$\underbrace{\sigma_{\mathrm{el}}}_{\substack{\text{Elastic normal traction}\\ \text{Only if the fault is non-planar}}} = \underbrace{\sigma^0_{\mathrm{el}}}_{\substack{\text{Normal traction perturbation}\\ \propto \kappa^t \Delta u^t}} + \underbrace{\sigma^1_{\mathrm{el}}}_{\substack{1^{\mathrm{st}}\text{order}\\ \text{Normal traction perturbations}}} + \underbrace{\ldots}_{\text{Higher order terms}} \tag{7}$$

with the expressions:

$$\begin{aligned}
\tau^0_{\mathrm{el}}(x_1) &= -\frac{\mu}{\pi}\left(1-\frac{c_s^2}{c_p^2}\right)\int_{-\infty}^{+\infty}\left[\frac{1}{x_1-y_1}\frac{d}{dy_1}\Delta u^t(y_1)\right]\mathrm{d}y_1 \\
\sigma^0_{\mathrm{el}}(x_1) &= -\frac{\mu}{\pi}\left(1-\frac{c_s^2}{c_p^2}\right)\int_{-\infty}^{+\infty}\left[\frac{1}{x_1-y_1}\kappa^t(y_1)\Delta u^t(y_1)\right]\mathrm{d}y_1
\end{aligned} \tag{8}$$

$$\begin{aligned}
\tau^1_{\mathrm{el}}(x_1) &= \frac{\mu}{\pi}\left(1-\frac{c_s^2}{c_p^2}\right)\int_{-\infty}^{+\infty}\left[\frac{m(y_1)}{x_1-y_1}-\frac{x_2-y_2}{(x_1-y_1)^2}\right]\kappa^t(y_1)\Delta u^t(y_1)\mathrm{d}y_1 \\
\sigma^1_{\mathrm{el}}(x_1) &= \frac{\mu}{\pi}\left(1-\frac{c_s^2}{c_p^2}\right)\int_{-\infty}^{+\infty}\left[\frac{2m(x_1)}{x_1-y_1}-\frac{m(y_1)}{x_1-y_1}-\frac{x_2-y_2}{(x_1-y_1)^2}\right]\frac{d}{dy_1}\Delta u^t(y_1)\mathrm{d}y_1
\end{aligned} \tag{9}$$

Contrary to the general expression given in eq. (5), the integrals in this decomposition are over the line ($\mathrm{d}y_1$) and not over the fault ($\mathrm{d}l(\mathbf{y})$). An example of this decomposition of shear and normal traction into 0^{th} order term and 1^{st} order term is illustrated in figure 4. The exemple considers a rough fault with an assumed slip distribution $\Delta u(y_1) = (1-4\frac{y_1^2}{L^2})^{3/2}$, where L is the length of the fault. It can be observed that for a rough fault, the 0^{th} and 1^{st} order terms are already capturing a significant portion of the physics of the shear and normal traction. In the subsequent section, a physical interpretation of the 0^{th} and 1^{st} order terms for both shear and normal traction is provided. Additionally, analytical results and possible other approximations will be presented.

The 0^{th} order contribution to shear traction τ^0_{el}: the planar fault response

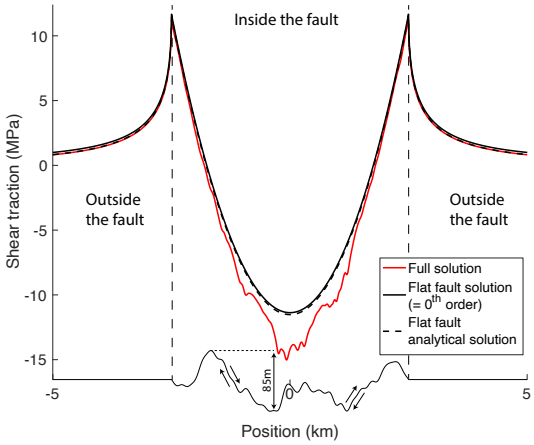

Figure 5: Assuming a flat fault geometry and the slip distribution $\Delta u(y_1) = (1 - 4\frac{y_1^2}{L^2})^{3/2}$ (red curve), L being the length of the fault , the shear traction can be calculated analytically (black dash line, see appendix E). It is compared with the full solution as given by eq (72), and the 0^{th} order solution as calculated by eq. (74) in the spectral domain. The 0^{th} order solution for the shear traction is exactly the one for a planar fault. The slight difference between the analytical solution and the 0^{th} order solution are coming from the fact that the calculation was performed in spectral domain, hence there is a periodic replication of the fault that slighly increase the shear traction of the 0^{th} order solution.

The 0^{th} order response of the shear traction, denoted as τ^0_{el}, is exactly the same as if the fault was flat (*Segall* (2010), section 4.7). In other words, It means that the main contribution for the shear traction of a non-planar fault is the flat fault response. In figure 5, the shear traction response for a rough fault that is subject to a slip distribution $\Delta u(y_1) = (1-4\frac{y_1^2}{L^2})^{3/2}$ in meter, L being the length of the fault, can be seen. This represents the shear traction for a right lateral fault. Inside the fault, the shear traction exhibits a globally negative value, resulting in decreasing the shear traction on the fault. This overall

shear traction reduction is usually called the shear stress drop in seismology. On the other hand, outside the fault, the presence of the fault increases the shear traction.

The 0^{th} order contribution to normal traction σ^0_{el}: the main source of normal traction variations

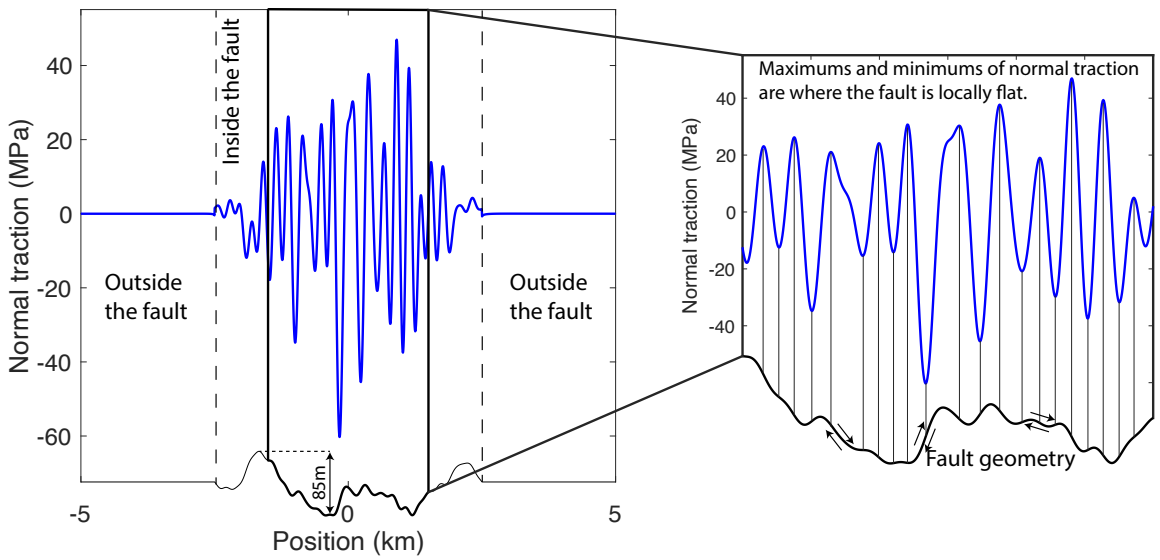

Figure 6: Zoom on the normal traction in Fig. 4. It can be seen that minimums and maximums of the normal traction correspond to area where the fault is locally flat ($\kappa^t = 0$).

One of the main effect of non-planar geometry on an in-plane shear fault is the introduction of normal traction variations. This effect is well-documented in the literature (*Nielsen and Knopoff*, 1998; *Dunham et al.*, 2011; *Romanet et al.*, 2020; *Cattania and Segall*, 2021). Figure 6 provides a closer look at the normal traction depicted in figure 4, for a rough fault whose slip distribution is assumed. It can be seen that the maximums and minimums of normal traction correspond to the areas where the fault is locally flat ($\kappa^t = 0$). This relationship can be analytically demonstrated with the 0^{th} order elastic normal traction

(which is the main contribution to the normal traction) given by:

$$\sigma^0_{\text{el}}(x_1) = -\frac{\mu}{\pi}\left(1 - \frac{c_s^2}{c_p^2}\right)\int_{-\infty}^{+\infty} \frac{1}{x_1 - y_1}\kappa^t(y_1)\Delta u^t(y_1)\mathrm{d}y_1 \tag{10}$$

To identify the areas of minimums and maximums of normal traction, we can differentiate the previous expression and find where the derivative equals zero.

$$\frac{d}{dx_1}\sigma^0_{\text{el}}(x_1) = \underbrace{\frac{\mu}{\pi}\left(1 - \frac{c_s^2}{c_p^2}\right)}_{>0}\int_{-\infty}^{+\infty} \underbrace{\frac{1}{(x_1 - y_1)^2}}_{>0}\,\kappa^t(y_1)\,\underbrace{\Delta u^t(y_1)}_{>0}\,\mathrm{d}y_1 \tag{11}$$

Since the slip is always positive, the only way that the previous integral to be 0 is if the curvature reverses sign. Moreover, due to the weight $1/(x_1 - y_1)^2$, the maximums and minimums of normal traction occur very close to the areas where the curvature changes sign. Although it may not precisely coincide with the location of the curvature reversing sign, it generally occurs very close. Similar reasoning can be applied for the extremas of the shear traction for pure opening faults (see appendix G).

Lastly, it is worth noting an interesting approximation for a rough fault that is not applicable to general fault geometries. If the slip distribution in Fourier domain has mainly low wavelength, so that it exists k_c such that $\Delta u^t(k > k_c) = 0$, and that the curvature along the fault in Fourier domain has mainly high wavelength such that $\kappa^t(k < k_c) = 0$, then the Hilbert transform of the curvature that multiplies the slip can be simplified using Bedrosian's theorem (*Bedrosian* (1963)):

$$\sigma^0_{\text{el}}(x_1) \simeq -\frac{\mu}{\pi}\left(1 - \frac{c_s^2}{c_p^2}\right)\Delta u^t(x_1)\int_{-\infty}^{+\infty} \frac{\kappa^t(y_1)}{x_1 - y_1}\mathrm{d}y_1. \tag{12}$$

Although this approximation is not entirely accurate as the slip and curvature do have overlapping bandwidth, it can be considered a reasonable assumption for rough faults, as

shown in Fig. 7.

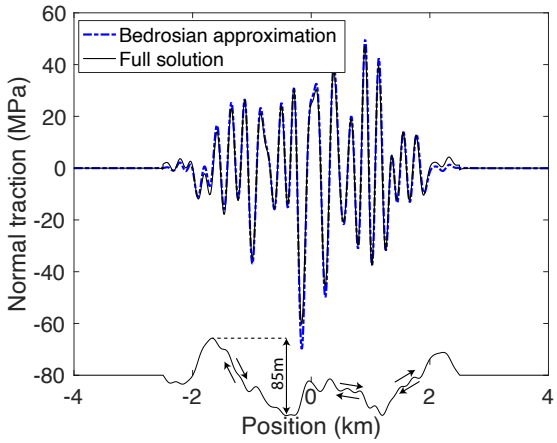

Figure 7: Assuming the fault geometry and the slip distribution $\Delta u(y_1) = (1 - 4\frac{y_1^2}{L^2})^{3/2}$, the full solution for normal traction (black curved) can be calculated using equation (72). The solution using the Bedrosian's approximation eq. (12) (blue dash curve) is very close to the full solution and allows to give some interpretations.

Scaling of slip vs geometry

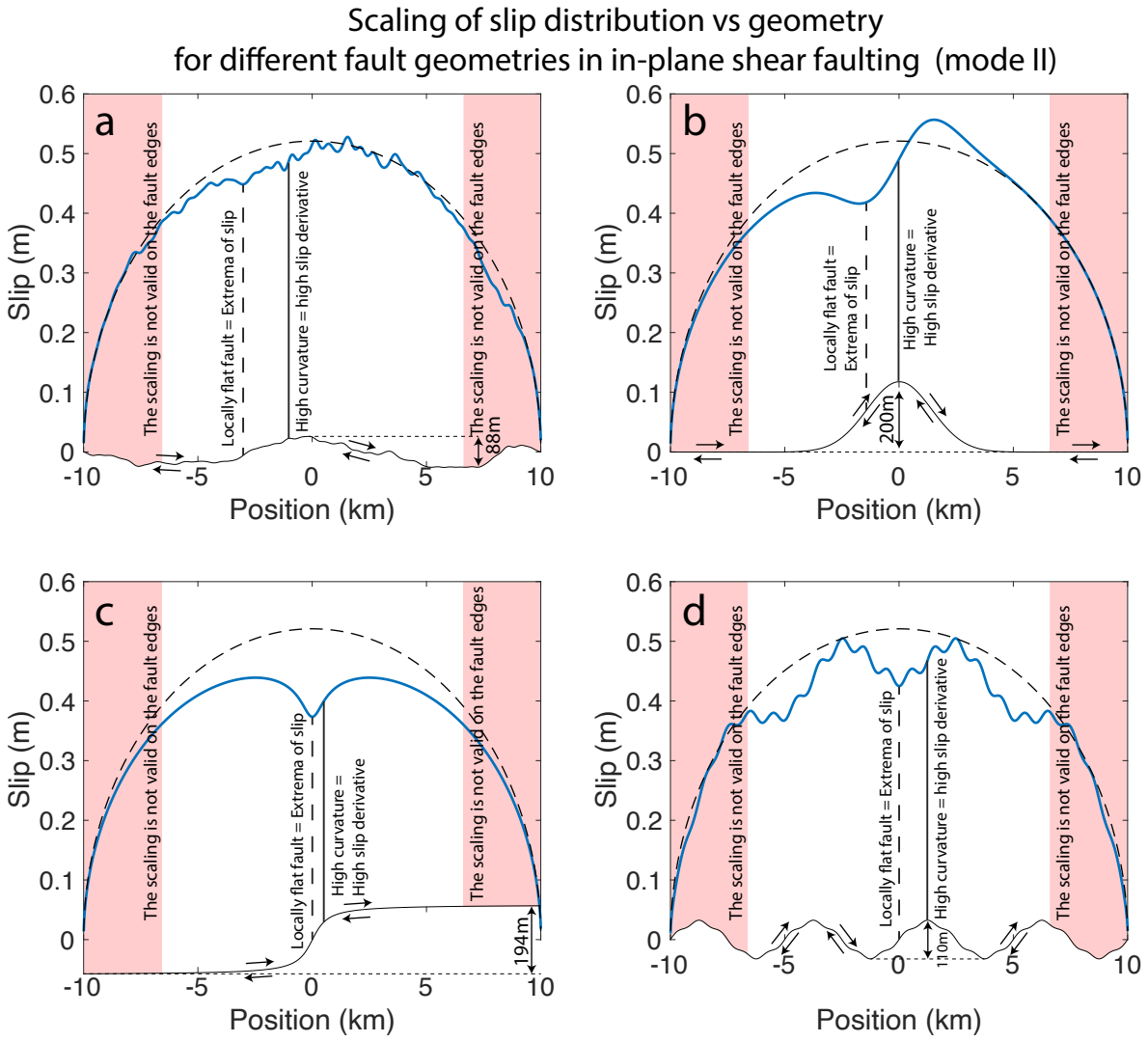

Figure 8: Scaling of geometry and slip distribution for a static, in-plane shear (mode II) fault subject to a constant loading and that follows Coulomb friction. The black dash line is the planar fault solution. The solution for a non-planar fault geometry is shown as a blue line: a) a rough fault, b) a seamount fault geometry, c) an arctan fault geometry and d) a sum of two sinusoidal functions geometry.

First and foremost, please note that in this section, we are introducing a new approach by solving the mechanical problem using the momentum balance equation, without assuming a specific slip distribution along the fault. If the fault follows the Coulomb friction law (f being the friction coefficient) and that the loading can be considered constant at 0^{th} order along the fault, we can write the momentum balance equation at 0^{th} order as:

$$\underbrace{-f(\sigma^0_{\text{el}} + \sigma^0_{\text{load}})}_{\text{Friction}} = \underbrace{\tau^0_{\text{el}}}_{\substack{\text{Shear traction} \\ \text{due to elasticity}}} + \underbrace{\tau^0_{\text{load}}}_{\text{Loading}} . \tag{13}$$

By utilizing the momentum balance equation mentioned above, it becomes possible to solve for the distribution of slip along the fault.

This approach was applied for the different non-planar fault geometry in figure 8. The figure illustrates a clear scaling relationship between the geometry of the fault and the slip distribution: locally flat areas exhibit extrema of slip while highly curved areas show a strong slip gradient. It can be seen that this scaling is not working near the edges of the fault. Remarkably, the scaling appears to be linear and preserves the wavelength of the fault geometry. Indeed, in figure 8-d, the fault geometry is a sum of two sinusoids with different amplitude and wavelength. The amplitude and wavelength of the fault geometry can be retrieved in the resulting slip distribution.

This scaling has been analytically derived in *Romanet et al.* (2020), and is presented again in this paper for consistency. This scaling arises from the relationship between the shear traction and the normal traction through the friction law. For an in-plane shear fault, as shown in the previous section, the shear traction τ^0_{el} is mainly controlled by the gradient term along the fault while the normal traction σ^0_{el} is mainly controlled by the curvature term:

$$\begin{aligned}\tau^0_{\mathrm{el}}(x_1) &= -\frac{\mu}{\pi}\left(1-\frac{c_s^2}{c_p^2}\right)\int_{-\infty}^{+\infty}\left[\frac{1}{x_1-y_1}\frac{d}{dy_1}\Delta u^t(y_1)\right]\mathrm{d}y_1 \\ \sigma^0_{\mathrm{el}}(x_1) &= -\frac{\mu}{\pi}\left(1-\frac{c_s^2}{c_p^2}\right)\int_{-\infty}^{+\infty}\left[\frac{1}{x_1-y_1}\kappa^t(y_1)\Delta u^t(y_1)\right]\mathrm{d}y_1\end{aligned} \tag{14}$$

The Coulomb friction on the fault links the curvature term (the fault geometry) that controls normal traction and the gradient term (the slip distribution gradient) that controls shear traction. It is possible to invert the two Hilbert's transform, by using Chebitchev polynomials (*Segall* (2010), section 4.1), to obtain a non-linear ordinary differential equation:

$$\underbrace{\frac{d}{dx_1}\Delta u^t(x_1)}_{\text{Gradient of slip}} + \underbrace{f\kappa^t(x_1)\Delta u^t(x_1)}_{\text{Effect of geometry}} = -\underbrace{\frac{f\sigma^{\mathrm{load}}+\tau^{\mathrm{load}}}{\mu(1-c_s^2/c_p^2)}\frac{x_1-L/2}{L\sqrt{(1-\frac{4(x_1-L/2)^2}{L^2}})}}_{\text{Effect of loading}}, \tag{15}$$

In the center of fault the effect of loading cancels so that we obtained the scaling:

$$\frac{\mathrm{d}\Delta u^t}{\Delta u^t} = -f\mathrm{d}m. \tag{16}$$

where the property $\kappa^t \mathrm{d}x = \mathrm{d}m$ has been used.

This scaling exist only for in-plane shear fault (mode II) as shown in Fig. 8, but not for out-of-plane shear fault (mode III) as depicted in Fig. 13. Although his scaling has not been yet confirmed in observations (*Bruhat et al.*, 2020), it was verified for fully-dynamic simulations using rate and state friction (*Romanet and Ozawa*, 2021).

This scaling is an important theoretical finding as it provides a link between three crucial parameters of the fault, i.e. the fault geometry, the slip distribution and the friction coefficient.

The shear traction drag $\tau^1_{\mathbf{el}}$

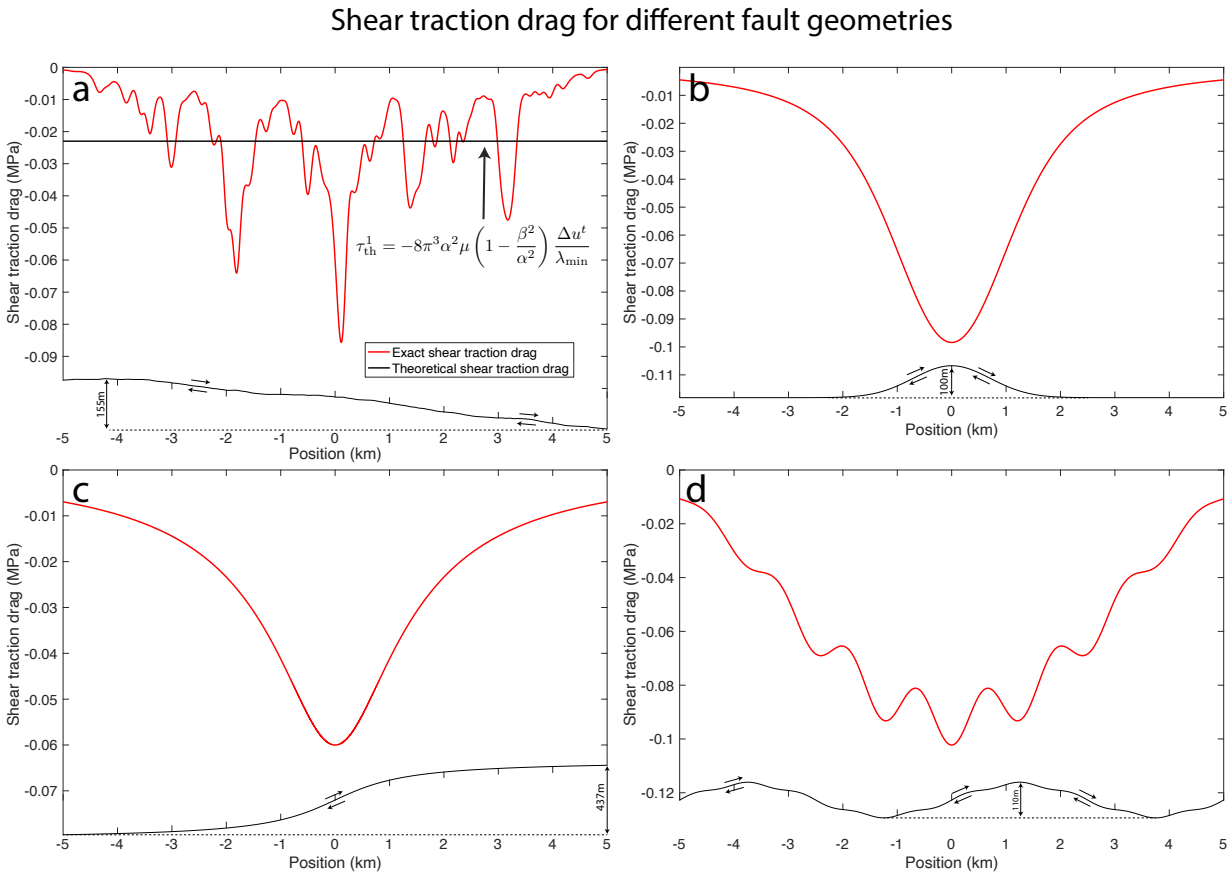

Figure 9: Calculation of the exact shear traction drag as expressed by equation (18) for different geometries. The fault geometry is shown as the x-axis. a) a finite rough fault. In the case of the rough fault geometry, the theoretical shear traction drag derived by *Fang and Dunham* (2013) is also shown as a black line. b) a finite fault with a seamount geometry, c) a finite fault with arctan geometry, and d) a finite fault whose geometry is the sum of two sinusoidal functions. The calculation is done for the prescribed slip distribution $\Delta u(y_1) = (1 - 4\frac{y_1^2}{L^2})^{3/2}$ in meter, where L is the length of the fault.

A key theoretical result on rough fault was obtained by *Dieterich and Smith* (2009) and *Fang and Dunham* (2013). It states that a rough fault is harder to slip than a flat fault. In other words, it says that a rough fault has an additional shear resistance when compared to a flat fault. This term will be referred as the shear traction drag in the following. Originally, it was derived as the 1st order effect* of a rough fault on the shear traction . They have shown that this term is mainly resisting movement. Figure 9 illustrates the 1st order term for shear traction for different fault geometries when assuming the slip distribution $\Delta u(y_1) = (1 - 4\frac{y_1^2}{L^2})^{3/2}$.

$$\tau^1_{\text{el}}(x_1) = \frac{\mu}{\pi}\left(1 - \frac{c_s^2}{c_p^2}\right)\int_{-\infty}^{+\infty}\left[\frac{m(y_1)}{x_1 - y_1} - \frac{x_2 - y_2}{(x_1 - y_1)^2}\right]\kappa^t(y_1)\Delta u^t(y_1)\mathrm{d}y_1 \tag{17}$$

This figure shows that the additional shear resistance coming from the shear traction drag is not only valid for rough fault (Fig. 9, a), but for any non planar fault geometry (Fig. 9, b,c,d). It can be seen that as long as the fault is non-planar, this term is resisting to movement. It leads to the very intuitive result that it is harder to slide a fault if it is non-planar. Contrary to the expression given in *Fang and Dunham* (2013), the expression presented here for the shear traction drag is exact for any fault geometry, and any slip distribution. It can be viewed as the generalisation of their work. It is also independent of the friction on the fault, making it a highly general result. Here are some properties of the shear traction drag:

1. The shear traction drag is valid for any geometry and any slip distribution. There is more resistance to slip for a non-planar fault compared to a planar fault (for in-plane shear -mode II-).

2. It is only associated with in-plane faulting (mode II), there is no shear traction drag

*A 2nd order effect, but there is a mistake in their derivation.

for out-of-plane shearing (mode III).

3. Since the stresses in the Fourier domain in three dimensional can be understood as a combinaison of of mode II and mode III (*Geubelle and Rice*, 1995), the analytical result mentionned above can be used to calculate the shear traction drag in 3D.

4. Since the curvature term for shear traction as given by equation (4), and the 1st order term (equation (9)) are the same at order 1, the two terms can both be used to calculate the shear traction drag.

5. An interpretation is that for equivalent slip distribution, the shear stress drop will be higher for a non-planar fault than for a planar fault. This interpretation may seem to contradict the fact that the fault is more difficult to slip, but this is not the case. To get an equivalent slip, the loading traction on a non-planar fault will be required to be higher than on a planar fault, hence it is more difficult to slip on a non planar fault.

6. This definition of the shear traction drag includes the result obtained by *Fang and Dunham* (2013) for the shear traction drag on a rough fault: $\tau^1_{\text{th}} = -8\pi^3\alpha^2\mu\left(1-\frac{c_s^2}{c_p^2}\right)\frac{\Delta u^t}{\lambda_{\min}}$. The previous result was derived for a constant slip on an infinite friction less fault, where α represents the amplitude to wavelength ratio, and $\lambda_{\min}$ is the minimum roughness wavelength.

In the following, we will show that our result encompasses the result by *Fang and Dunham* (2013). Assuming that the slip is constant, and that the fault slope is small ($m << 1$), it is possible to replace the curvature by the second order derivative of the height of the fault: $\kappa^t(x) = \frac{m'(x)}{(1+m(x)^2)^{3/2}} \simeq m'(x)$. The previous exact equation for the shear traction drag simplifies to

$$\tau^1_{\text{el}}(x_1) = \frac{\mu}{\pi}\left(1 - \frac{c_s^2}{c_p^2}\right)\Delta u^t \int_{-\infty}^{+\infty}\left[\frac{m(y_1)}{x_1 - y_1} - \frac{x_2 - y_2}{(x_1 - y_1)^2}\right] m'(y_1)\mathrm{d}y_1 \tag{18}$$

Another simplification can be made because the term $\frac{x_2-y_2}{(x_1-y_1)^2}$ is usually small compare to $\frac{m(y)}{x_1-y_1}$. Then the equation becomes:

$$\tau^1_{\text{el}}(x_1) = \frac{\mu}{\pi}\left(1 - \frac{c_s^2}{c_p^2}\right)\Delta u^t \int_{-\infty}^{+\infty}\left[\frac{m(y_1)}{x_1 - y_1}\right] m'(y_1)\mathrm{d}y_1 \tag{19}$$

Finally, using the Bedrosian theorem (*Bedrosian*, 1963), it can be obtained:

$$\tau^1_{\text{el}}(x_1) = \frac{\mu}{\pi}\left(1 - \frac{c_s^2}{c_p^2}\right)\Delta u^t(x_1) m(x_1) \int_{-\infty}^{+\infty}\left[\frac{m'(y)}{x_1 - y_1}\right] \mathrm{d}y_1 \tag{20}$$

which is the same equation A61 as in *Fang and Dunham* (2013). Hence the mean roughness drag can be written as:

$$\tau^1_{\text{th}} = -8\pi^3\alpha^2\mu\left(1 - \frac{c_s^2}{c_p^2}\right)\frac{\Delta u^t}{\lambda_{\min}} \tag{21}$$

To further validate our derivations and assess the accuracy of the approximations made, we conducted numerical tests comparing the two expressions. In figure 10-a, we computed the shear traction drag (red line) using eq. (18) for an infinitely long fault with constant slip. To achieve the infinite fault, we calculated the shear traction drag in the spectral domain (eq. (76)), hence it is infinite with periodic replication. The theoretical expression proposed by *Fang and Dunham* (2013) is shown in black. The mean value of our definition for the shear traction drag closely aligns with the expression derived in *Fang and Dunham* (2013). Additionally, in figure 10-b, we calculated the relative difference between the mean of the exact expression (eq. (18)) and the theoretical expression (eq (21)) for the shear traction drag for 100,000 different rough fault profiles. The mean of the relative difference

is less that 1%, with a standard deviation of approximately 5%. The discrepancy can be explained by the neglect of the term $\frac{x_2-y_2}{(x_1-y_1)^2}$, and the utilization of the Bedrosian theorem whose assumptions are not entirely verified. These numerical comparisons further support the validity and accuracy of our derived expressions.

Finally, it can be demonstrated through an integration by parts that the expression for the shear traction drag , under the assumptions that $\frac{x_2-y_2}{(x_1-y_1)^2}$ can be neglected and that the Bedrosian theorem can be applied, is always negative :

$$\begin{aligned}
\tau^1_{\text{el}}(x_1) &= \frac{\mu}{\pi}\left(1-\frac{c_s^2}{c_p^2}\right)\int_{-\infty}^{+\infty}\frac{1}{x_1-y_1}\Delta u^t(y_1)m(y_1)\frac{d}{dy_1}m(y_1)\mathrm{d}y_1 \\
&= \frac{\mu}{\pi}\left(1-\frac{c_s^2}{c_p^2}\right)\Delta u^t(x_1)\int_{-\infty}^{+\infty}\frac{1}{x_1-y_1}\frac{1}{2}\frac{d}{dy_1}m^2(y_1)\mathrm{d}y_1 \\
&= -\underbrace{\frac{\mu}{2\pi}\left(1-\frac{c_s^2}{c_p^2}\right)}_{>0}\Delta u^t(x_1)\int_{-\infty}^{+\infty}\underbrace{\frac{1}{(x_1-y_1)^2}m^2(y_1)}_{>0}\,\mathrm{d}y_1
\end{aligned} \tag{22}$$

The last expression, which is valid for any fault geometry, is always opposite sign of the slip Δu^t, hence resisting movement.

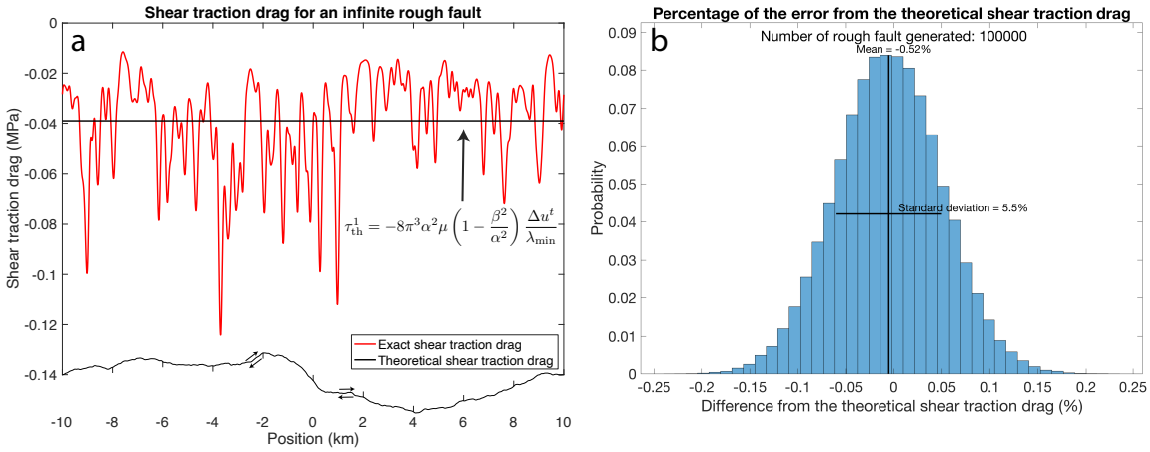

Figure 10: a) Exact -red line- (from eq (18)) and theoretical -black line- (from eq (21)) shear traction drag for an infinite rough fault. The exact shear traction drag was calculating in the Fourier domain (eq. (76), in appendix H) to make it infinite with periodic replication. b) In order to check the equivalence of the two expressions in the case of an infinite rough fault, we generated 100000 rough fault profiles and computed the distance of the mean value for the exact shear traction drag compared with the theoretical shear traction drag. The mean difference is less than 1% with a standard deviation of 5.5%.

1^{st} order response of normal traction

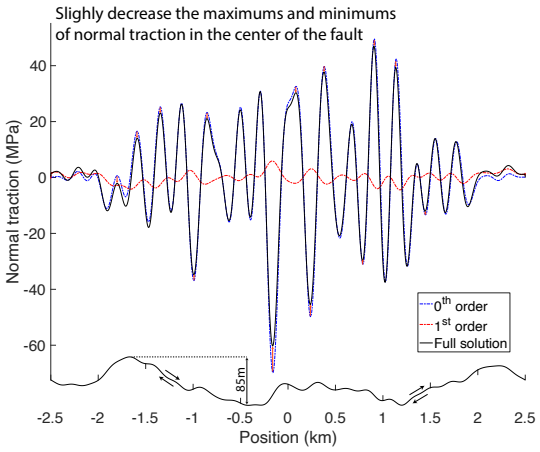

Figure 11: The 1^{st} order effect on normal traction. If can seen that the main effect is to slightly reduce the minimums and maximums of the normal traction. The full solution was calculated with the equation (72) in appendix H.

Although there is a 1st order response on normal traction, its effect is not as important as the shear traction drag. The main effect is to slightly oppose the effect of the 0^{th} order, so that the full normal traction at maximum and minimums are slightly reduced compare to the 0^{th} order effect. This effect can be seen on figure 11, where the maximums and minimums of normal traction at 0^{th} order σ^0_{el} are slighly reduced by the 1^{st} order of normal traction σ^1_{el}.

2.2 Out-of-plane shear (mode III)

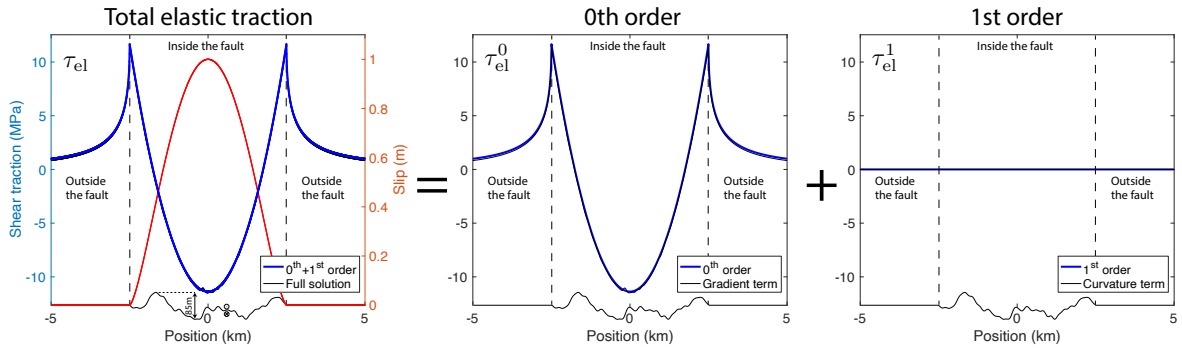

Figure 12: Total elastic traction for an out-of-plane fault (mode III). Assuming the fault geometry (as shown by the x-axis) and the slip distribution $\Delta u(y_1) = (1 - 4\frac{y_1^2}{L^2})^{3/2}$ in meter (red curve), the full solution, the gradient term and the curvature term (black lines) can be calculated using equation (77) (more precisely using the spectral expressions eq. (79) and eq. (81)). The 0^{th} order and the 1^{st} order (blue lines), are respectively calculated using the expressions (25) and (26).

Similarly as for the in-plane (mode II) case, the out-of-plane (mode III) shear and normal traction can be decomposed into 0^{th} and 1^{st} order responses.

$$\underbrace{\tau_{\text{el}}}_{\substack{\text{Elastic shear traction} \\ \text{of non-planar fault}}} = \underbrace{\tau_{\text{el}}^0}_{\text{Planar fault response}} + \underbrace{\tau_{\text{el}}^1}_{=0} + \underbrace{\dots}_{\text{Higher order terms}} \tag{23}$$

$$\underbrace{\sigma_{\text{el}}}_{\substack{\text{Elastic normal traction} \\ =0}} = \underbrace{\sigma_{\text{el}}^0}_{=0} + \underbrace{\sigma_{\text{el}}^1}_{=0} + \underbrace{\dots}_{\substack{\text{Higher order terms} \\ =0}} \tag{24}$$

However, in this case, only the shear traction at 0^{th} order is non-zeros.

$$\tau_t^0(x_1) = \frac{\mu}{2\pi} \int_{-\infty}^{+\infty} \frac{1}{x_1 - y_1} \frac{d}{dy_1} \Delta u^s(y_1) \mathrm{d}y_1$$
$$\sigma_n^0(x_1) = 0 \tag{25}$$

$$\tau_t^1(x_1) = 0$$
$$\sigma_n^1(x_1) = 0 \tag{26}$$

For an out-of-plane shear fault, the contribution of non-planar fault geometry to the stresses is only a 2^{nd} order effect. This means that fault geometry has a small effect for an out-of-plane shear fault (mode III). Figure 13 illustrates the slip distribution for non-planar fault geometries with Coulomb friction and constant loading, using the same parameters as in the in-plane shear case (mode II) shown in Figure 8. In the case of out-of-plane shear (mode III), there is no scaling of the slip distribution with respect to fault geometry. The slip distribution for the planar fault (dashed black line) perfectly overlaps with the slip distributions for the non-planar faults (continuous blue lines).

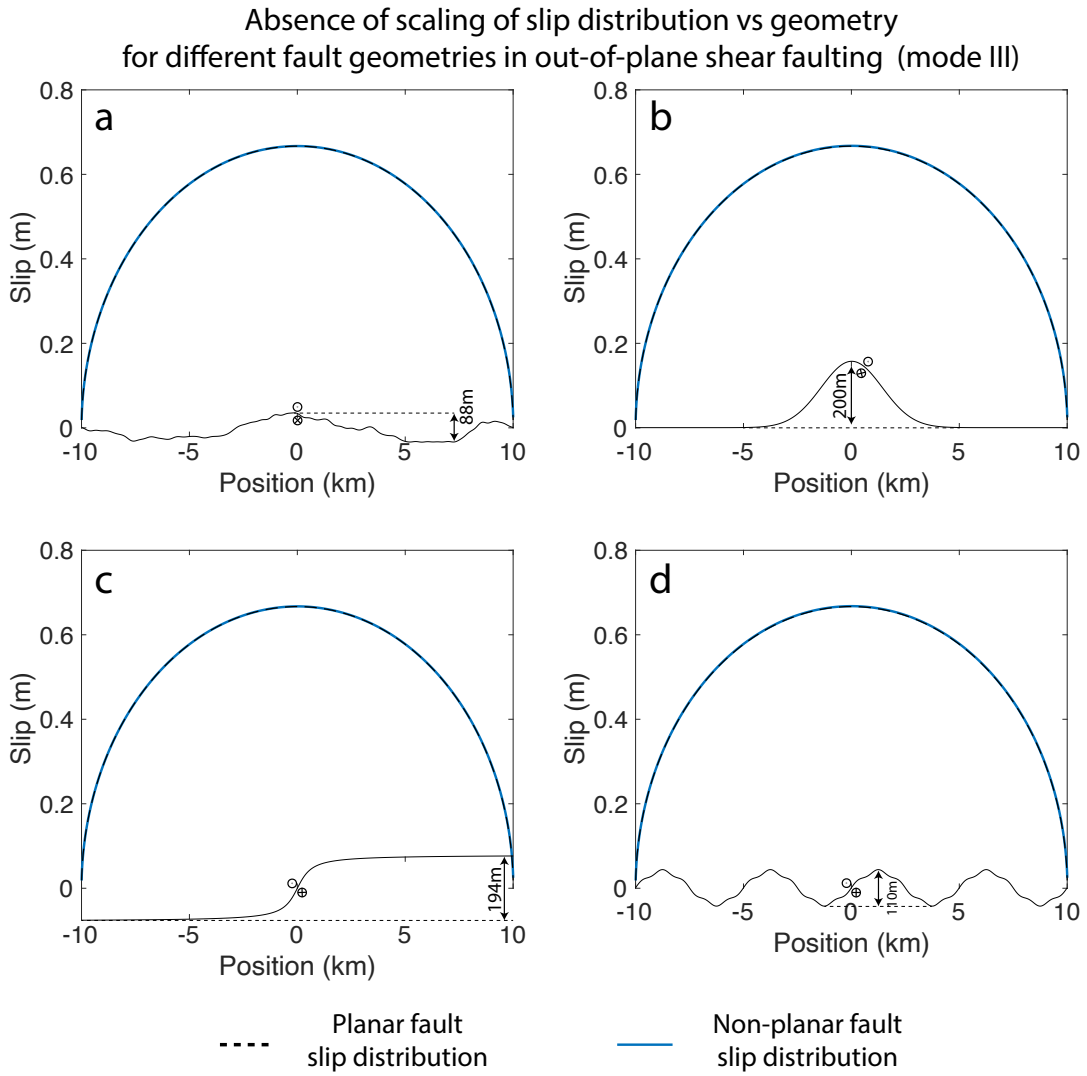

Figure 13: Scaling of geometry and slip distribution for a static, out-of-plane shear (mode III) fault subject to a constant loading and that follows Coulomb friction. The black dash line is the planar fault solution. The slip distribution does not show any scaling with fault geometry. Fault geometry: a) a rough fault, b) a seamount fault geometry, c) an arctan fault geometry and d) a sum of two sinusoidal functions geometry.

3 Discussion

3.1 Physical singularities that appear on non-planar fault

3.1.1 Non-zeros slip at kinks of the fault.

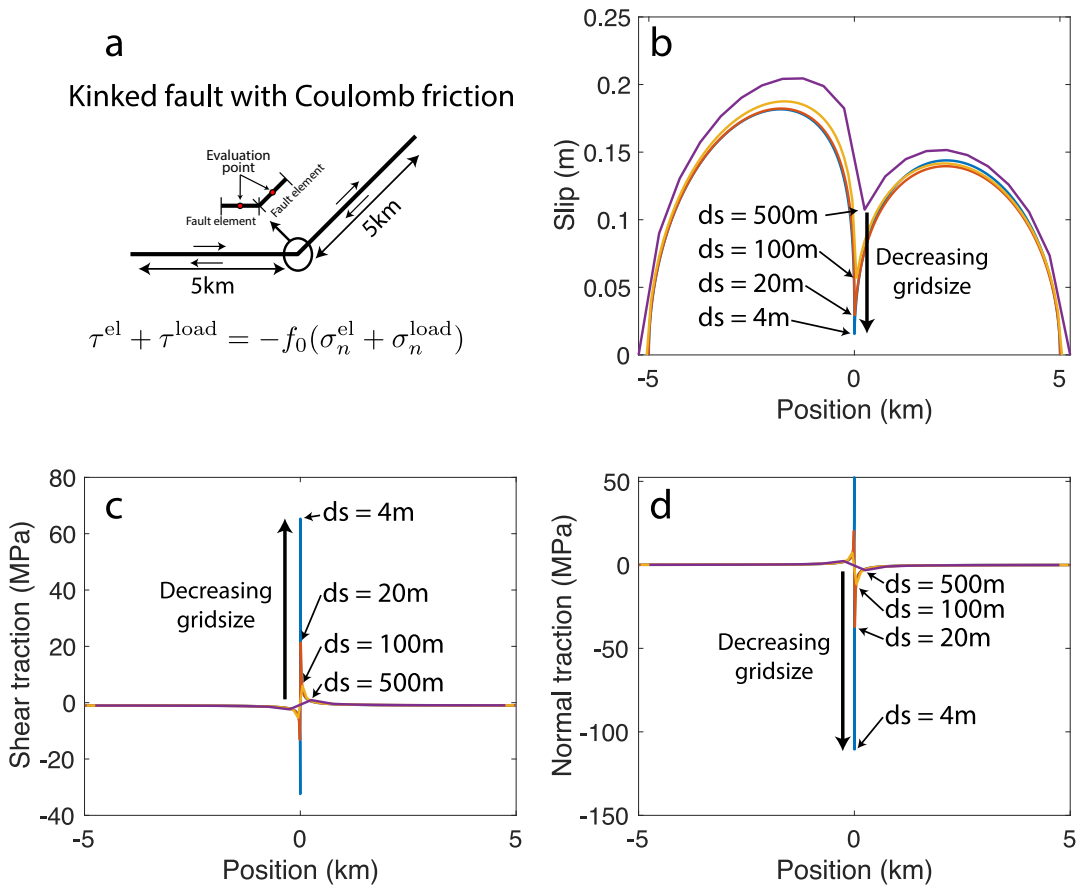

Figure 14: Figure showing the grid dependency of a kinked faults. a) The geometry of the fault and the momentum equation. b) The slip distribution versus position along the fault. The slip distribution is changing with gridsize. Please note the only physically acceptable slip at the kink is zero. c) The shear traction distribution versus the position along the fault. The shear traction is closely following the normal traction because they are linked by the friction law. It is also diverging with the refinement of the mesh. d) The normal traction distribution vs position along the fault. The normal traction is diverging with the refinement of the mesh.

Many literature sources make the mistake of modeling kinks while assuming small strain elasticity and no opening (*Tada and Yamashita*, 1996; *Aochi et al.*, 2000a; *Duan and Oglesby*, 2005; *Ely et al.*, 2009; *Lozos et al.*, 2011; *Fukuyama and Hok*, 2015; *Sathiakumar and Barbot*, 2021). A kink on a fault with non-zeros slip create a $1/r$ singularity, where r is the distance from the kink. This is a non-physical singularity that results to infinite strain energy near the kink. We can demonstrate this result in the small slope approximation, for the 0^{th} order on normal traction:

$$\sigma_{\text{el}}^{0}(x_1) = -\frac{\mu}{\pi}\left(1 - \frac{c_s^2}{c_p^2}\right)\int_{-\infty}^{+\infty}\left[\frac{1}{x_1 - y_1}\frac{d}{dy_1}m(y_1)\Delta u^t(y_1)\right]\mathrm{d}y_1 \tag{27}$$

If we assume that the curvature is $\kappa^t(y_1) = \frac{d}{dy_1}m(y_1)$. For a kink at the position $y_1 = 0$, the slope is discontinuous so that we can assume that $m(y_1) = AH(y_1)$, where H is the Heaviside function and A the fault slope after the kink. In this case, the previous equation becomes:

$$\begin{aligned}\sigma_{\text{el}}^{0}(x_1) &= -\frac{\mu}{\pi}\left(1 - \frac{c_s^2}{c_p^2}\right)\int_{-\infty}^{+\infty}\left[\frac{A\Delta u(y_1)}{x_1 - y_1}\delta(y_1)\right]\mathrm{d}y_1 \\ &= -\frac{\mu}{\pi}\left(1 - \frac{c_s^2}{c_p^2}\right)\frac{A\Delta u^t(0)}{x_1}\end{aligned} \tag{28}$$

This reveals a $1/x_1$ singularity of normal traction on the fault. One straightforward way to eliminate this singularity is by imposing the slip to be null at the kink $\Delta u^t(0) = 0$, which is evident from the previous equation. Another approach would be to allow for fault opening or adding a third fault and imposing the closure of slip at the kink (*Andrews*, 1989). In the boundary element method, the maximum normal traction concentration due to the discretization is typically proportional to the gridsize Δs. Thus, the maximum normal

traction on the fault is:

$$\sigma^0_{\text{el}}(x_1 = 0) \propto -\frac{\mu}{\pi}\left(1 - \frac{c_s^2}{c_p^2}\right)\frac{A\Delta u^t(0)}{\Delta s} \tag{29}$$

The problem is that the usual gridsize for the modeling of fault is of the order $\Delta s \sim 1000m$, as a result, the stress concentration at the kink, which is normally infinite, is of the order of $\sigma^0_{\text{el}}(x_1) \simeq 1$ MPa for typical shear modulus μ (30 GPa), P-wave velocity (5000 m/s) and S wave velocity (3000 m/s) and a slip at the kink of $\Delta u^t(0) = 1$m. This is why the issue of diverging traction at kinks has remained unknown in numerical work so far. An example of this effect is shown in figure 14, where the slip, normal traction and shear traction was calculated for a fault following Coulomb friction with constant loading. The maximum values of normal traction and shear traction are largely underestimate ($\sim$ 1MPa) for the gridsize $\Delta s = 500$ m. It is worth noting that adding plasticity or viscosity is not an entirely satisfying solution. In most of seismological research, the small strain approximation is used together with plasticity/viscosity and the plastic/viscous effects are driven by the linear elastic interaction. If the elastic interactions are underestimated, the plastic/viscous effect will also be significantly underestimated. It means all the quantitative work done using kinks in linear elasticity (with the small strain assumption) is grid-dependent and does not converge numerically.

Finally, it is still possible to observe that modeling a kink is still possible in out-of-plane faulting (mode III), because there is no curvature term.

3.1.2 Discontinuous curvature along the fault

A discontinuity in the curvature of the fault also creates a singularity in stresses. However, this singularity can be compensated by a singularity in the slip derivative (hence the slip will still be continuous). Using the scaling of slip vs curvature -that is valid only when the

fault follows Coulomb friction- (eq. (16)):

$$\frac{d}{dx_1}\Delta u^t(x_1) = -f\kappa^t(x_1)\Delta u^t(x_1). \tag{30}$$

So that if the curvature has a discontinuity of Amplitude B at $x_1 = 0$, $\kappa^t(x_1) = BH(x_1)$, the discontinuity in slip gradient will be: $\frac{d}{dx_1}\Delta u^t(x_1) = -fBH(x_1)\Delta u^t(x_1)$. This effect is well observed on figure 15-b, where there is a discontinuity in slip gradient due to the discontinuity of the curvature along the fault.

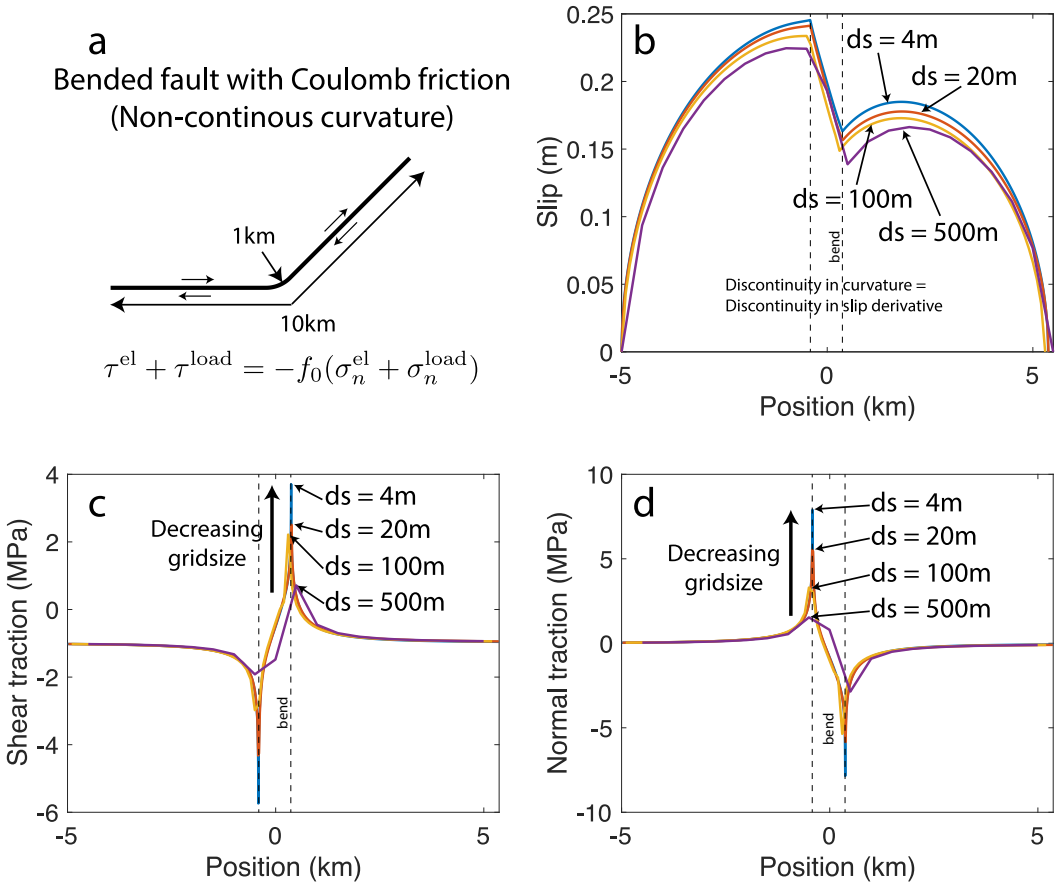

Figure 15: Figure showing the grid dependency of a bended fault with discontinuous curvature. a) The geometry of the fault and the momentum equation. b) The slip distribution versus position along the fault. The slip distribution is changing with gridsize. c) The shear traction distribution versus the position along the fault. The shear traction is closely following the normal traction because they are linked by the friction law. It is also diverging with the refinement of the mesh. d) The normal traction distribution vs position along the fault. The normal traction is diverging with the refinement of the mesh.

The discontinuity in curvature creates a singularity of the stresses that is $\propto \log(x_1)$ when $x_1 \to 0$. Because this singularity is less strong than $1/\sqrt{(x_1)}$, this discontinuity in curvature

does not lead to infinite strain energy, hence it is a physically acceptable singularity. Let's show the previous result using the small slope approximation and assuming constant slip distribution. For a bended fault like in Fig. 15-a, the curvature can be written $\kappa^t(y_1) = B(H(y_1 - a) - H(y_1 + b))$, where B is the curvature in the bended portion of the fault. It leads to the normal traction distribution (Hilbert transform of a characteristic function):

$$\begin{aligned}\sigma^0_{\text{el}}(x_1) &= -\frac{\mu}{\pi}\left(1 - \frac{c_s^2}{c_p^2}\right)\Delta u^t \int_{-\infty}^{+\infty}\left[\frac{1}{x_1 - y_1} B(H(y_1 - a) - H(y_1 + b)\right] \mathrm{d}y_1 \\ &= -\frac{\mu}{\pi}\left(1 - \frac{c_s^2}{c_p^2}\right) B\Delta u^t \log\left|\frac{x_1 - a}{x_1 - b}\right|\end{aligned} \tag{31}$$

Where we found a log singularity when $x_1 \to a$ or $x_1 \to b$. The last comment is that, again, there is no such a problem in out-of-plane shear, because the stresses and strains are independent of the curvature term (see eq. 77 in appendix I).

3.2 Limits of linear elasticity

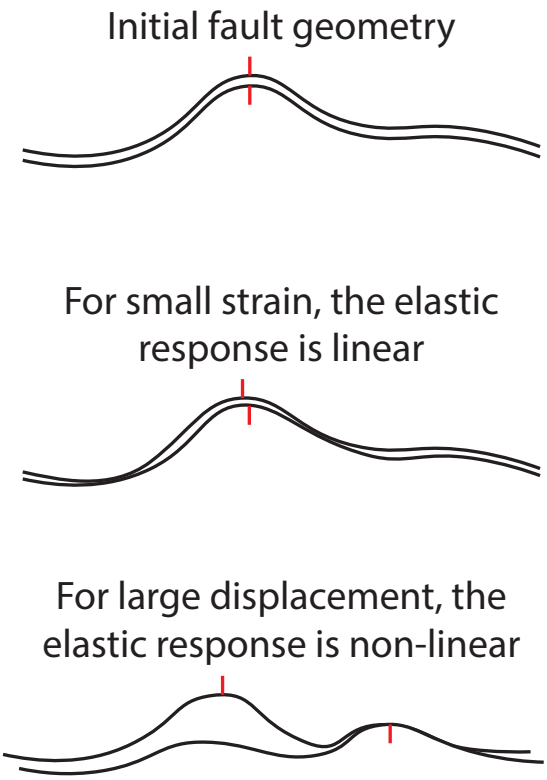

Figure 16: Figure showing the limits of linear elasticity in the modeling of non-planar fault geometries.

The small strain approximation is commonly used in seismology and is necessary to linearises the strain tensor with the displacement field. However, when considering non planar fault geometry, the strains and stresses will keep increasing with on-going slip breaking the small strain approximation. At a certain point, the small strain approximation becomes invalid as depicted in figure 16. In such cases, finite elasticity should be considered to prevent the strains and stresses from growing without bounds (*Romanet et al.*, 2020; *Tal*, 2023). Various approaches have been proposed in the litterature to address the issue of

unbounded increase or decrease in normal traction with ongoing slip (*Duan and Oglesby*, 2005; *Dunham et al.*, 2011; *Heimisson*, 2020; *Cattania and Segall*, 2021), for example the inclusion of viscosity or plasticity while retaining the small strain approximation of linear elasticity. However, this approach may lead to a significant overestimation of the effect of plasticity and viscosity in fault mechanics.

While we acknowledge the likelihood of non-linear anelastic phenomena occurring (such as damage, plasticity, or viscosity), we disagree with the interpretation that they are a necessary condition for preventing the stresses and strains from growing indefinitely with ongoing slip on non-planar faults (*Dieterich and Smith*, 2009; *Shi and Day*, 2013), as this does not consider the effect of finite elasticity.

It is important to recognize that small strain elasticity is violated when dealing with very small asperities, and even regularization techniques may not provide accurate results. One possible direction is to move towards finite elasticity and thoroughly test the limits of linear elasticity in current earthquake simulations.

4 Conclusion

	Opening fault (mode I)	**In-plane shear fault (mode II)**	**Out-of-plane shear fault (mode III)**
Shear traction τ^0 (0^{th} order)	Mainly controlled by the fault geometry $\propto \kappa^t \Delta u^n$	Same as the planar fault response	Same as the planar fault response
Shear traction τ^1 (1^{st} order)	Nearly no effect (depends on the gradient of slip)	Shear traction drag, the fault is resisting slip	$= 0$ No effect of fault geometry
Normal traction σ^0 (0^{th} order)	Same as the planar fault response	Mainly controlled by the fault geometry $\propto \kappa^t \Delta u^t$	$= 0$ No effect of fault geometry
Normal traction σ^1 (1^{st} order)	Normal traction drag, the fault is resisting opening	Slightly reduce the minimums and maximums of normal traction changes	$= 0$ No effect of fault geometry

Table 1: Summary of the results. Please note that there is an effect of geometry for out-of-plane shear, but this effect only appears at 2^{nd} order.

This work advances the limited theoretical knowledge regarding the effect of non-planar fault geometries on earthquake mechanics. By expanding the relation of fault traction and slip, up to second order relative to the deviation from a planar fault, this study allows for the interpretation of complex fault geometry and its impact on fault traction (see Table 1).

The results of this study confirm that fault geometry plays a significant role in in-plane faulting (mode II) by modifying the normal traction on the fault and increasing its resistance to slipping. We provide a general expression independent of fault geometry and fault slip for the shear traction drag (*Fang and Dunham*, 2013), making it a general result. We also provide some useful simplification for the effect of rough fault on normal traction, which can be simplified as an Hilbert transform of the curvature by using Bedrosian's theorem.

Conversely, for out-of-plane faulting (mode III), the influence of fault geometry is negligible. There is no effect of fault geometry up to the second order. We also showed that, in this case, there is no scaling between the slip distribution and the geometry.

The paper also examines singularities that arise in specific fault geometries commonly used in earthquake simulations and provides guidelines for their elimination.

Ultimately, this study highlights the limitations of the small strain approximation when considering non-planar faults, emphasizing the need to consider finite elasticity for more accurate modeling of non-planar faults.

Availability statement

The mathematica code used to develop the equation is available as supplementary material. No data was used in this research.

Acknowledgments

I would like to thank Robert Viesca for providing the non-singular analytical solution for stresses and slip. This study benefited from comments by Jean-Paul Ampuero. P.R. would also like to acknowledge the strong support by Jean-Paul Ampuero, Frédéric Cappa, and Marco Scuderi. This research was mainly funded by the NIED project on the generation mechanism of large earthquakes and partly from the European Research Council (ERC) Starting Grants 101040600 (HYQUAKE).

A Table of parameters

Symbol	Description
h	Height of the fault
m	Slope of the fault
$\mathbf{x}$	Point of evaluation
x_d	d^{th} component of the point $\mathbf{x}$
$\mathbf{y}$	Point of evaluation, usually over which an integral is performed
y_d	d^{th} component of the point $\mathbf{y}$
κ^t	Curvature of the fault
u_k	k^{th} component of the displacement vector
c_{ijpq}	$ijpq$ component of the Hooke tensor
Δu_i^n	i^{th} component of the slip vector for opening (mode I)
Δu_i^t	i^{th} component of the slip vector for in-plane shear (mode II)
Δu_i^s	i^{th} component of the slip vector for out-of-plane shear (mode III)
n_j	j^{th} of the vector normal to the fault
G_{kp}	kp component of the Green's functions
l	Length along the fault
ϵ_{cd}	cd component of the strain tensor
σ_{ab}	ab component of the stress tensor
t_j	j^{th} component of the tangential vector to the fault
$\frac{\partial}{\partial y^t}$	Derivative along the fault ($\frac{\partial}{\partial y^t} = t_1 \frac{\partial}{\partial x_1} + t_2 \frac{\partial}{\partial x_2}$)
τ_{el}	Total elastic shear traction along the fault
τ_{el}^0	Elastic shear traction at 0^{th} order along the fault
τ_{el}^1	Elastic shear traction at 1^{th} order along the fault
σ_{el}	Total elastic normal traction along the fault
σ_{el}^0	Elastic normal traction at 0^{th} order along the fault
σ_{el}^1	Elastic normal traction at 1^{th} order along the fault
L	Length of the fault, used for the prescribed slip definition
μ	Shear modulus
c_s	Shear wave speed
c_p	Compressional wave speed

Table 2: Table of parameters

Symbol	Description
σ^0_{load}	Constant normal traction loading
τ^0_{load}	Constant shear traction loading
f	Coulomb friction parameter
τ^1_{th}	Theoretical shear traction drag as given in *Fang and Dunham* (2013)
α	Amplitude to wavelength ratio for a self-similar fault
λ_{min}	Minimum roughness wavelength
H	Heaviside function
δ	Dirac function
λ	Lamé's first parameter
θ	Angle between the axis **1** and the fault (see Fig. 18)

Table 3: Table of parameters (continue)

B Derivation

In the following, the convention for stress is chosen as tension positive and compression negative.

B.1 Formulas

Here, we just recall some formulas that will be used in the following section for the derivation.

The momentum balance equation:

$$c_{ijpq}\frac{\partial}{\partial x_j}\frac{\partial}{\partial x_q}G_{pn}(\mathbf{x},\mathbf{y}) = 0 \tag{32}$$

Symmetry of the Green's function:

$$\frac{\partial}{\partial x_q}G_{ij}(\mathbf{x},\mathbf{y}) = -\frac{\partial}{\partial y_q}G_{ij}(\mathbf{x},\mathbf{y}) \tag{33}$$

Definition of the tangential differential operator on a function f (*Bonnet*, 1999):

$$D_{ij}[f(\mathbf{y})] = n_i(\mathbf{y})\frac{\partial}{\partial y_j}f(\mathbf{y}) - n_j(\mathbf{y})\frac{\partial}{\partial y_i}f(\mathbf{y}) \tag{34}$$

Definition of the derivative along the fault, if $\mathbf{t}$ is the tangential vector to the fault:

$$\frac{\partial}{\partial y^t}f = t_1\frac{\partial}{\partial y_1}f + t_2\frac{\partial}{\partial y_2}f \tag{35}$$

The expression for the Green's function can be found in *Tada and Yamashita* (1997):

$$\begin{aligned} G_{ij}(\mathbf{x},\mathbf{y}) &= \frac{1}{4\pi\mu}[\gamma_i\gamma_j(1-c_s^2/c_p^2) - \delta_{ij}(1+c_s^2/c_p^2)\log(r)], \text{ for } i,j \in \{1,2\} \\ G_{33}(\mathbf{x},\mathbf{y}) &= \frac{-1}{2\pi\mu}\log(r) \end{aligned} \tag{36}$$

where $\gamma_1 = \frac{x_1-y_1}{r}$, $\gamma_2 = \frac{x_2-y_2}{r}$, and $r = \sqrt{(x_1-y_1)^2+(x_2-y_2)^2}$ is the distance between the points $\mathbf{x}$ and $\mathbf{y}$.

B.2 Derivation

We start from the representation theorem (*Tada and Yamashita*, 1997):

$$u_k(\mathbf{x}) = -\int_{\text{fault}} c_{ijpq}n_j(\mathbf{y})\Delta u_i(\mathbf{y})\frac{\partial}{\partial x_q}G_{kp}(\mathbf{x},\mathbf{y})dl(\mathbf{y}) \tag{37}$$

From the previous equation, by deriving under the integral it can be obtained:

$$\frac{\partial}{\partial x_l}u_k(\mathbf{x}) = -\int_{\text{fault}} c_{ijpq}n_j(\mathbf{y})\Delta u_i(\mathbf{y})\frac{\partial}{\partial x_q}\left[\frac{\partial}{\partial x_l}G_{kp}(\mathbf{x},\mathbf{y})\right]dl(\mathbf{y}) \tag{38}$$

The reason to do so is that both the strains ($\epsilon_{kl} = \frac{1}{2}\left(\frac{\partial}{\partial x_k}u_l + \frac{\partial}{\partial x_l}u_k\right)$) and the stresses ($\sigma_{ab} = c_{abkl}\epsilon_{kl}$) can be obtained by linear combinaison of the previous equation. To regularise this

integral we need to work on the integrand of the previous integral. Using the symmetry of second derivatives, we can replace the derivatives with respect to x with derivatives with respect to y.

$$\frac{\partial}{\partial x_l} u_k(\mathbf{x}) = -\int_{\text{fault}} c_{ijpq} n_j(\mathbf{y}) \frac{\partial}{\partial y_q} \left[\frac{\partial}{\partial y_l} G_{kp}(\mathbf{x}, \mathbf{y}) \right] dl(\mathbf{y}) \tag{39}$$

Then, we used the definition of the tangential differential operator together with the momemtum balance equation (eq. (32)):

$$\begin{aligned} c_{ijpq} n_j(y) \frac{\partial}{\partial y_l} \frac{\partial}{\partial y_q} G_{kp} &= c_{ijpq} \left[D_{jl} \frac{\partial}{\partial y_q} G_{kp} + n_l(y) \frac{\partial}{\partial y_j} \frac{\partial}{\partial y_q} G_{kp} \right] \\ &= c_{ijpq} D_{jl} \frac{\partial}{\partial y_q} G_{kp} \end{aligned} \tag{40}$$

Please note that this derivation is due to Daisuke Sato (*Sato et al.*, 2020) for the 2D case. The equivalent 3D case derivation was done by Marc Bonnet (*Bonnet*, 1999), and can also be found in *Romanet et al.* (2020).

We then developed the differential tangential operator in the local coordinate system of the fault, and used the fact that the derivative perpendicular to the fault direction are null:

$$\begin{aligned} D_{jk}[f(y)] &= \left[n_j(y) \frac{\partial}{\partial y_k} - n_k(y) \frac{\partial}{\partial y_j} \right] f(y) \\ &= \left[n_j(y) \left(t_k(y) \frac{\partial}{\partial y^t} + n_k(y) \frac{\partial}{\partial y^n} \right) - n_k(y) \left(t_j(y) \frac{\partial}{\partial y^t} + n_j(y) \frac{\partial}{\partial y^n} \right) \right] f(y) \\ &= \left[n_j(y) t_k(y) - n_k(y) t_j(y) \right] \frac{\partial}{\partial y^t} f(y) \end{aligned} \tag{41}$$

It can be checked easily that the previous equation is 0 for any pair in $(1, 2)$, because $t_1 = n_2$ and $t_2 = -n_1$.

Then, we replace the integrand in eq. (39), using eq. (40) and eq. (41):

$$\frac{\partial}{\partial x_l}u_k(\mathbf{x}) = -\int_{\text{fault}} c_{ijpq}\Delta u_i[n_j(\mathbf{y})t_l(\mathbf{y}) - n_l(\mathbf{y})t_j(\mathbf{y})]\frac{\partial}{\partial y^t}\frac{\partial}{\partial y_q}G_{kp}(\mathbf{x},\mathbf{y})dl(\mathbf{y}) \tag{42}$$

Finally, it is possible to perform an integration by parts to regulatize the hypersingular integral given previously (eq. (43)):

$$\frac{\partial}{\partial x_l}u_k(\mathbf{x}) = -\int_{\text{fault}} c_{ijpq}[n_j(\mathbf{y})t_l(\mathbf{y}) - n_l(\mathbf{y})t_j(\mathbf{y})]\frac{\partial}{\partial y^t}\Delta u_i\frac{\partial}{\partial y_q}G_{kp}(\mathbf{x},\mathbf{y})dl(\mathbf{y}) \tag{43}$$

For numerical calculation and the discretisation of the fault slip, it is best to use eq. (43). However for facilitate interpretation, the slip vector can be projected on the local basis as:

$$\begin{aligned}
\Delta u_i &= \Delta u^n n_i, \text{ for mode I} \\
\Delta u_i &= \Delta u^t t_i, \text{ for mode II} \\
\Delta u_i &= \Delta u^s s_i, \text{ for mode III}
\end{aligned} \tag{44}$$

where Δu^n, Δu^t, and Δu^s are respectively the opening, the in-plane slip and the out-of-plane slip. The derivative of slip with respect to the direction of the fault $\frac{\partial}{\partial y^t}\Delta u_i$ can then be replaced by:

$$\begin{aligned}
\frac{\partial}{\partial y^t}[\Delta u^n n_i] &= n_i\frac{\partial}{\partial y^t}\Delta u^n - t_i\Delta u^n\kappa^t, \text{ for mode I} \\
\frac{\partial}{\partial y^t}[\Delta u^t t_i] &= t_i\frac{\partial}{\partial y^t}\Delta u^t + n_i\Delta u^n\kappa^t, \text{ for mode II} \\
\frac{\partial}{\partial y^t}[\Delta u^s s_i] &= s_i\frac{\partial}{\partial y^t}\Delta u^s = \delta_{3i}\frac{\partial}{\partial y^t}\Delta u^s, \text{ for mode III}
\end{aligned} \tag{45}$$

where δ_{3i} is the Kronecker delta.

C Discretization

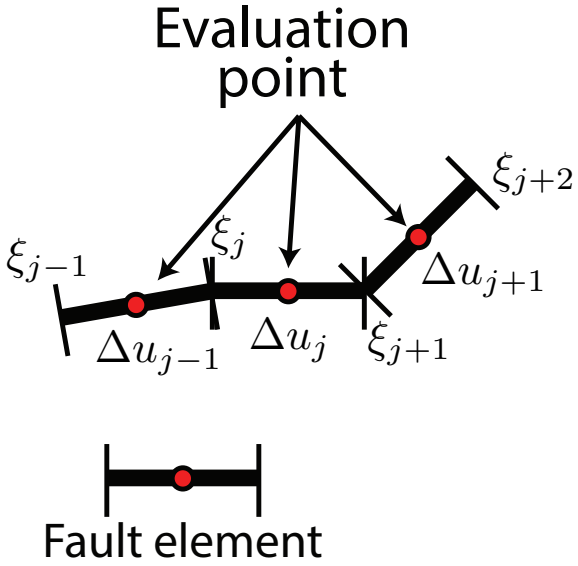

Figure 17: Figure showing the discretisation of the fault.

The discretisation is using the same strategy as in *Romanet et al.* (2020). It consists into discretizing the slip and the tangential vector as constant over a straight line. It is convenient for this part to use the curvilinear abcisse ξ instead of the position along the fault $\mathbf{y}(\xi)$. Also, to simplify the demonstration, we will just keep the scalar t instead of one component of the tangential vector t_i.

$$\begin{aligned} t(\xi) &= \sum_j t_j[H(\xi - \xi_j) - H(\xi - \xi_{j+1})] \\ \Delta u(\xi) &= \sum_j \Delta u_j[H(\xi - \xi_j) - H(\xi - \xi_{j+1})] \end{aligned} \tag{46}$$

The discretisation is using a piecewise contant slip and a straight element over.

$$
\begin{aligned}
&\int_{\text{fault}} K(\mathbf{x},\mathbf{y})\frac{\partial}{\partial y^t}\left[t\Delta u\right] dl(\mathbf{y}) = \\
&\int_{\text{fault}} K(\mathbf{x},\mathbf{y})t\frac{\partial}{\partial y^t}\left[\Delta u\right] dl(\mathbf{y}) + \\
&\int_{\text{fault}} K(\mathbf{x},\mathbf{y})\Delta u\frac{\partial}{\partial y^t}\left[t\right] dl(\mathbf{y}) = \\
&\int_{\text{fault}} K(\mathbf{x},\mathbf{y})t\frac{\partial}{\partial y^t}\left[\sum_j \Delta u_j[H(\xi-\xi_j)-H(\xi-\xi_{j+1})]\right] dl(\mathbf{y}) + \\
&\int_{\text{fault}} K(\mathbf{x},\mathbf{y})\Delta u\frac{\partial}{\partial y^t}\left[\sum_j t_j[H(\xi-\xi_j)-H(\xi-\xi_{j+1})]\right] dl(\mathbf{y}) = \\
&\sum_j [K[\mathbf{x},\mathbf{y}(\xi_j)]t(\xi_j) - K[\mathbf{x},\mathbf{y}(\xi_{j+1})]t(\xi_{j+1})]\Delta u_j + \\
&\sum_j [K[\mathbf{x},\mathbf{y}(\xi_j)]\Delta u(\xi_j) - K[\mathbf{x},\mathbf{y}(\xi_{j+1})]\Delta u(\xi_{j+1})]t_j
\end{aligned}
\tag{47}
$$

We can then replace $t(\xi_j)$ and $\Delta u(\xi_j)$ by ($H(0) = 1/2$):

$$
\begin{aligned}
t(\xi_j) &= (1-0.5)t_{j-1} + 0.5t_j = \frac{t_{j-1}+t_j}{2} \\
\Delta u(\xi_j) &= \frac{\Delta u_{j-1}+\Delta u_j}{2}
\end{aligned}
\tag{48}
$$

which gives:

$$
\begin{aligned}
&\int_{\text{fault}} K(\mathbf{x},\mathbf{y})\frac{\partial}{\partial y^t}\left[t\Delta u\right] dl(\mathbf{y}) = \\
&\underbrace{\sum_j [K[\mathbf{x},\mathbf{y}(\xi_j)]\frac{t_j+t_{j-1}}{2} - K[\mathbf{x},\mathbf{y}(\xi_{j+1})]\frac{t_{j+1}+t_j}{2})]\Delta u_j +}_{\text{Gradient term}} \\
&\underbrace{\sum_j [K[\mathbf{x},\mathbf{y}(\xi_j)]\frac{\Delta u_j+\Delta u_{j-1}}{2} - K[\mathbf{x},\mathbf{y}(\xi_{j+1})]\frac{\Delta u_{j+1}+\Delta u_j}{2}]t_j}_{\text{Curvature term}}
\end{aligned}
\tag{49}
$$

This way of discretising the integral allows for the separation of the curvature and gradient

terms.

D The small slope approximation

D.1 It transforms the integrals along the fault to integral along a straight line

Starting from a regularized boundary element method, and applying the small slope approximation, it is possible to obtain the 0^{th} and 1^{st} order solution of the stress on the fault due to a slip distribution for the different mode of slip. Please notice that all the integrals that were along the fault become along the y_1 axis only. This is due to the fact that if $y_2 = h(y_1)$ and the slope derivative is small $\frac{d}{dy_1}h(y_1) << 0$, and changing the variable of the integral:

$$\begin{aligned}\int_{\text{fault}} f(y_1)dl(y_1) &= \int_{-\infty}^{+\infty} f(y_1)\sqrt{1+h'^2(y_1)}dy_1 \\ &\simeq \int_{-\infty}^{+\infty} f(y_1)(1+h'^2(y_1)/2)dy_1 \\ &\simeq \int_{-\infty}^{+\infty} f(y_1)dy_1\end{aligned} \tag{50}$$

D.2 It provides an expression for the normal and tangential vector to the fault

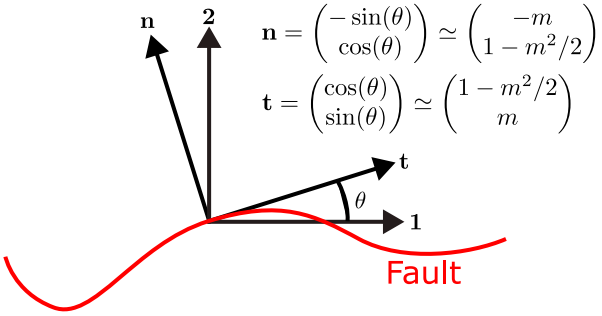

Figure 18: Figure showing the simplification that happens in the small slope approximation for the normal and tangential vectors.

The normal and tangential vectors can be simplified in the small slope approximation (see Fig. 18), indeed:

$$m(y_1) = \tan[\theta(y_1)] \simeq \theta(y_1) \tag{51}$$

so that in the small slope approximation:

$$\begin{aligned} \mathbf{n}(y_1) &= \begin{pmatrix} -\sin(\theta(y_1)) \\ \cos(\theta(y_1)) \end{pmatrix} \simeq \begin{pmatrix} -m(y_1) \\ 1 \end{pmatrix} \\ \mathbf{t}(y_1) &= \begin{pmatrix} \cos(\theta(y_1)) \\ \sin(\theta(y_1)) \end{pmatrix} \simeq \begin{pmatrix} 1 \\ m(y_1) \end{pmatrix} \end{aligned} \tag{52}$$

E A particular solution for the semi-analytical formulation

The slip/opening distribution for the result section is chosen as following:

$$\Delta u(y_1) = (1 - y_1^2)^{3/2} \tag{53}$$

The reason for this particular form of slip (or opening) distribution compared to the classic distribution in linear fracture mechanics ($\Delta u(y_1) = \sqrt{1 - y_1^2}$) is because it brings finite stress concentrations outside the fault (hence the numerical result are converging) and that there is an analytical solution for the stresses in the case of planar fault:

$$\frac{1}{2\pi}\int_{-1}^{1} \frac{1}{x_1 - y_1}\frac{\mathrm{d}}{\mathrm{d}y_1}\Delta u(y_1)\mathrm{d}y_1 = \frac{3}{4}\begin{cases} 1 - 2x_1^2 - 2x_1\sqrt{x_1^2 - 1}, & \text{if } x_1 < -1 \\ 1 - 2x_1^2, & \text{if } -1 \leq x_1 \leq 1, \text{ inside the fault} \\ 1 - 2x_1^2 + 2x_1\sqrt{x_1^2 - 1}, & \text{if } x_1 > 1 \end{cases} \tag{54}$$

The previous solution was used to check our numerical scheme against the analytical formulation. Obtaining this solution is not straightforward. For the case $-1 < x_1 < 1$, the solution can be obtained by using Chebychev polynomial (*Mason and Handscomb* (2002), section 9.5.1). The solution outside $|x_1| > 1$ can be obtained by doing a first change of variable $y_1 \rightarrow sin(\theta)$ and checking that $\frac{\sin(\theta)\cos^2(\theta)}{x_1 - \sin(\theta)}$ is symmetric at $\pi/2$. That allows us to make the integration over the whole circle and take half the value. If we start from the following integral:

$$\frac{1}{2\pi}\int_{-1}^{1} \frac{1}{x_1 - y_1}\frac{\mathrm{d}}{\mathrm{d}y_1}\Delta u(y_1)\mathrm{d}y_1 = -\frac{3}{2\pi}\int_{-1}^{1} \frac{y_1\sqrt{1 - y_1^2}}{x_1 - y_1}\mathrm{d}y_1 \tag{55}$$

And then do the first change of variable:

$$\begin{aligned}\frac{1}{2\pi}\int_{-1}^{1}\frac{1}{x_1-y_1}\frac{\mathrm{d}}{\mathrm{d}y_1}\Delta u(y_1)\mathrm{d}y_1 &= -\frac{3}{2\pi}\int_{-\pi/2}^{\pi/2}\frac{\sin(\theta)\cos(\theta)|\cos(\theta)|}{x_1-\sin(\theta)}\mathrm{d}\theta \\ &= -\frac{3}{2\pi}\int_{-\pi/2}^{\pi/2}\frac{\sin(\theta)\cos^2(\theta)}{x_1-\sin(\theta)}\mathrm{d}\theta \\ &= -\frac{3}{4\pi}\int_{-\pi/2}^{3\pi/2}\frac{\sin(\theta)\cos^2(\theta)}{x_1-\sin(\theta)}\mathrm{d}\theta\end{aligned} \tag{56}$$

A second change of variable is using $z = e^{i\theta}$, where $\sin(\theta) = \frac{z-1/z}{2i}$ and $\cos(\theta) = \frac{z+1/z}{2}$.

$$-\frac{3}{4\pi}\int_{-\pi/2}^{3\pi/2}\frac{\sin(\theta)\cos^2(\theta)}{x_1-\sin(\theta)}\mathrm{d}\theta = -\frac{3i}{16\pi}\int_C \frac{(z^2-1)(1+z^2)^2}{z^3[z-(ix+\sqrt{1-x^2})][z-(ix-\sqrt{1-x^2})]}\mathrm{d}z \tag{57}$$

For $x < -1$, there are two poles at $z = 0$ and $z = i(x + \sqrt{x^2-1})$, so that applying the residue theorem gives:

$$\begin{aligned}\frac{1}{2\pi}\int_{-1}^{1}\frac{1}{x_1-y_1}\frac{\mathrm{d}}{\mathrm{d}y_1}\Delta u(y_1)\mathrm{d}y_1 &= 2\pi i\mathrm{Res}(f, z=0) + 2\pi i\mathrm{Res}(f, z = i(x_1+\sqrt{x_1^2-1}) \\ &= \frac{3}{4}(1-2x_1^2-2x_1\sqrt{x_1^2-1})\end{aligned} \tag{58}$$

where Res(f,z) is the residue of f in z

For $x > 1$, there are also two poles at $z = 0$ and $z = i(x_1 - \sqrt{x_1^2-1})$, so that the residue theorem yields:

$$\begin{aligned}\frac{1}{2\pi}\int_{-1}^{1}\frac{1}{x_1-y_1}\frac{\mathrm{d}}{\mathrm{d}y_1}\Delta u(y_1)\mathrm{d}y_1 &= 2\pi i\mathrm{Res}(f, z=0) + 2\pi i\mathrm{Res}(f, z = i(x_1-\sqrt{x_1^2-1}) \\ &= \frac{3}{4}(1-2x_1^2+2x_1\sqrt{x_1^2-1})\end{aligned} \tag{59}$$

F Definition of the Fourier Transform

In the following part, the 0^{th} and 1^{st} order solution for both normal and shear traction are provided. Their expression depends on the choose of the definition of the Fourier transform. We define the Fourier transform as following:

$$\mathcal{F}[f](k) = \int_{-\infty}^{+\infty} f(x_1) e^{-ikx_1} dx_1 \tag{60}$$

$$\mathcal{F}^{-1}[f](x_1) = \frac{1}{2\pi} \int_{-\infty}^{+\infty} f(x_1) e^{ikx_1} dk \tag{61}$$

where k is the wavenuber and is linked to the wavelength λ by $k = 2\pi/\lambda$. In particular, we will use the two Fourier transform:

$$\begin{aligned} \mathcal{F}[1/x_1](k) &= -i\pi \text{sign}(k) \\ \mathcal{F}[1/x_1^2](k) &= -\pi |k| \end{aligned} \tag{62}$$

G In-plane opening (mode I)

The mode I correspond to opening. One common assumption for an opening fault is the traction free condition at the surface.

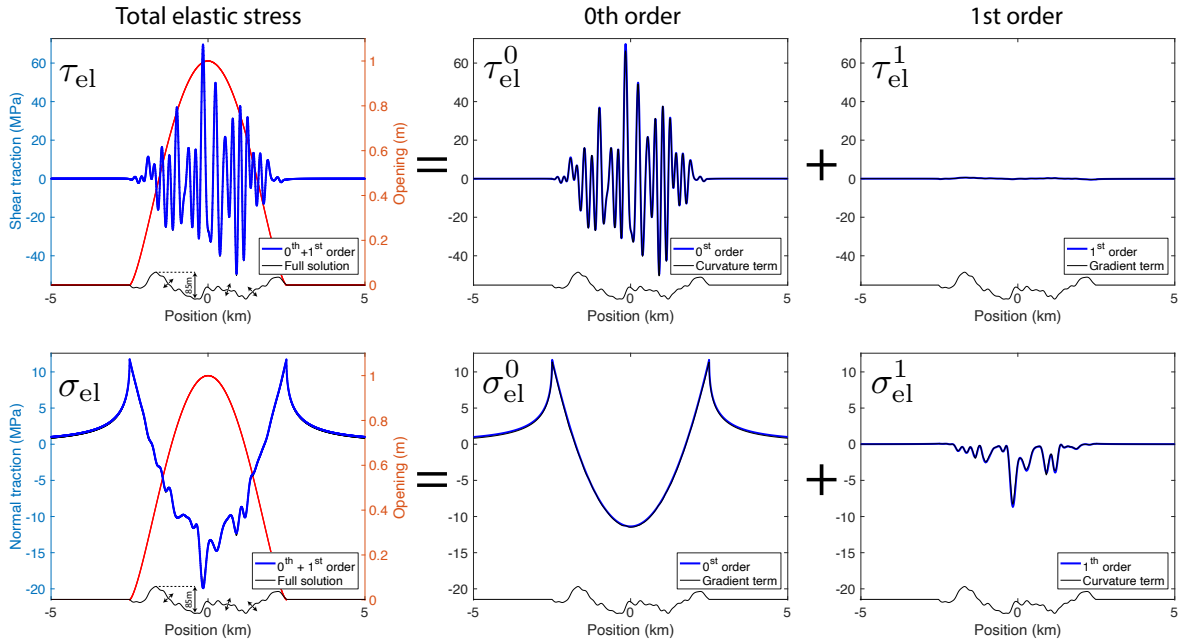

Figure 19: Assuming the fault geometry and the opening distribution $\Delta u(y_1) = (1-4\frac{y_1^2}{L^2})^{3/2}$ in meter (red curve), the full solution, the gradient term and the curvature term can be calculated using equation (67). The 0^{th} order and the 1^{st} order, are respectively calculated using the expressions (65) and (66).

By making the small slope approximation is can be shown that the main contribution for the shear and normal tractions are:

$$\underbrace{\tau_{el}}_{\substack{\text{Elastic shear traction}\\ \text{Only if the fault is non-planar}}} = \underbrace{\tau^0_{el}}_{\substack{\text{Shear traction perturbation}\\ \propto \kappa^t \Delta u^t}} + \underbrace{\tau^1_{el}}_{\substack{1^{\text{st}}\text{order}\\ \text{Shear traction pertubation}}} + \underbrace{\ldots}_{\text{Higher order terms}} \tag{63}$$

$$\underbrace{\sigma_{el}}_{\substack{\text{Elastic normal traction}\\ \text{Of non-planar fault}}} = \underbrace{\sigma^0_{el}}_{\text{Planar fault response}} + \underbrace{\sigma^1_{el}}_{\text{Normal traction drag}} + \underbrace{\ldots}_{\text{Higher order terms}} \tag{64}$$

with

$$\begin{aligned}\tau_t^0(x_1) &= \frac{\mu}{\pi}\left(1-\frac{c_s^2}{c_p^2}\right)\int_{-\infty}^{+\infty}\frac{1}{x_1-y_1}\kappa^t(y_1)\Delta u^n(y_1)\mathrm{d}y_1 \\ \sigma_n^0(x_1) &= -\frac{\mu}{\pi}\left(1-\frac{c_s^2}{c_p^2}\right)\int_{-\infty}^{+\infty}\frac{1}{x_1-y_1}\frac{d}{dy_1}\Delta u^n(y_1)\mathrm{d}y_1\end{aligned} \tag{65}$$

$$\begin{aligned}\tau_t^1(x_1) &= \frac{\mu}{\pi}\left(1-\frac{c_s^2}{c_p^2}\right)\int_{-\infty}^{+\infty}\left[\frac{m(y_1)}{x_1-y_1}-\frac{x_2-y_2}{(x_1-y_1)^2}\right]\frac{d}{dy_1}\Delta u^n(y_1)\mathrm{d}y_1 \\ \sigma_n^1(x_1) &= \frac{\mu}{\pi}\left(1-\frac{c_s^2}{c_p^2}\right)\int_{-\infty}^{+\infty}\left[\frac{-2m(x_1)}{x_1-y_1}+\frac{m(y_1)}{x_1-y_1}+\frac{x_2-y_2}{(x_1-y_1)^2}\right]\kappa^t(y_1)\Delta u^n(y_1)\mathrm{d}y_1\end{aligned} \tag{66}$$

On figure 19 an example of a in-plane opening fault is given for a rough geometry. An interesting feature is that the on-fault shear traction mainly (0th order) depends upon the geometry, because it the 0th order shear traction depends on the local curvature (a geometrical parameter) that multiplies the opening. On the contrary, the normal traction depends mainly on the derivative of opening along the fault. That means that it is more dependent on the opening distribution than the fault geometry. By looking at the 0^{th} order solution, it is interesting to see that the result of opening on a non -planar fault leads to the apparition of shear traction on this fault. If we assume traction free condition, the only solution to remove the shear traction that appears it that mode II is also involve. One result from that is that mode I on a non-planar fault, with the traction free condition cannot exist without the existence of mode II.

G.1 Full solution

In the following $*$ represents the convolution operation.

$$\begin{aligned}\epsilon_{11}(\mathbf{x}) = &\frac{1}{2\pi(\lambda+2\mu)}\int_{\text{fault}}\left[n_1\frac{\gamma_2}{r}(2\lambda\gamma_1^2+\mu(3\gamma_1^2+\gamma_2^2))+n_2\frac{\gamma_1}{r}(2\lambda\gamma_2^2+\mu(\gamma_2^2-\gamma_1^2))\right]\frac{d}{dy^t}\Delta u^n(\mathbf{y})\mathrm{d}l(\mathbf{y})\\ &+\frac{1}{2\pi(\lambda+2\mu)}\int_{\text{fault}}\left[-n_2\frac{\gamma_2}{r}(2\lambda\gamma_1^2+\mu(3\gamma_1^2+\gamma_2^2))+n_1\frac{\gamma_1}{r}(2\lambda\gamma_2^2+\mu(\gamma_2^2-\gamma_1^2))\right]\kappa^t(\mathbf{y})\Delta u^n(\mathbf{y})\mathrm{d}l(\mathbf{y})\end{aligned}$$

$$\begin{aligned}\epsilon_{22}(\mathbf{x}) = &-\frac{1}{2\pi(\lambda+2\mu)}\int_{\text{fault}}\left[n_2\frac{\gamma_1}{r}(2\lambda\gamma_2^2+\mu(\gamma_1^2+3\gamma_2^2))+n_1\frac{\gamma_2}{r}(2\lambda\gamma_1^2+\mu(\gamma_1^2-\gamma_2^2))\right]\frac{d}{dy^t}\Delta u^n(\mathbf{y})\mathrm{d}l(\mathbf{y})\\ &-\frac{1}{2\pi(\lambda+2\mu)}\int_{\text{fault}}\left[n_1\frac{\gamma_1}{r}(2\lambda\gamma_2^2+\mu(\gamma_1^2+3\gamma_2^2))-n_2\frac{\gamma_2}{r}(2\lambda\gamma_1^2+\mu(\gamma_1^2-\gamma_2^2))\right]\kappa^t(\mathbf{y})\Delta u^n(\mathbf{y})\mathrm{d}l(\mathbf{y})\end{aligned}$$

$$\begin{aligned}\epsilon_{12}(\mathbf{x}) = &-\frac{\lambda+\mu}{2\pi(\lambda+2\mu)}\int_{\text{fault}}\left[(n_1\frac{\gamma_1}{r}+n_2\frac{\gamma_2}{r})(\gamma_1^2-\gamma_2^2)\right]\frac{d}{dy^t}\Delta u^n(\mathbf{y})\mathrm{d}l(\mathbf{y})\\ &-\frac{\lambda+\mu}{2\pi(\lambda+2\mu)}\int_{\text{fault}}\left[(-n_2\frac{\gamma_1}{r}+n_1\frac{\gamma_2}{r})(\gamma_1^2-\gamma_2^2)\right]\kappa^t(\mathbf{y})\Delta u^n(\mathbf{y})\mathrm{d}l(\mathbf{y})\end{aligned}$$

$$\begin{aligned}\sigma_{11}(\mathbf{x}) = &\frac{\mu}{\pi}\left(1-\frac{c_s^2}{c_p^2}\right)\int_{\text{fault}}\left[n_1(\mathbf{y})(3\gamma_1^2+\gamma_2^2)\frac{\gamma_2}{r}-n_2(\mathbf{y})(\gamma_1^2-\gamma_2^2)\frac{\gamma_1}{r}\right]\frac{d}{dy^t}\Delta u^n(\mathbf{y})\mathrm{d}l(\mathbf{y})\\ &-\frac{\mu}{\pi}\left(1-\frac{c_s^2}{c_p^2}\right)\int_{\text{fault}}\left[n_2(\mathbf{y})(3\gamma_1^2+\gamma_2^2)\frac{\gamma_2}{r}+n_1(\mathbf{y})(\gamma_1^2-\gamma_2^2)\frac{\gamma_1}{r}\right]\kappa^t(\mathbf{y})\Delta u^n(\mathbf{y})\mathrm{d}l(\mathbf{y})\end{aligned}$$

$$\begin{aligned}\sigma_{22}(\mathbf{x}) = &-\frac{\mu}{\pi}\left(1-\frac{c_s^2}{c_p^2}\right)\int_{\text{fault}}\left[n_2(\mathbf{y})(\gamma_1^2+3\gamma_2^2)\frac{\gamma_1}{r}+n_1(\mathbf{y})(\gamma_1^2-\gamma_2^2)\frac{\gamma_2}{r}\right]\frac{d}{dy^t}\Delta u^n(\mathbf{y})\mathrm{d}l(\mathbf{y})\\ &-\frac{\mu}{\pi}\left(1-\frac{c_s^2}{c_p^2}\right)\int_{\text{fault}}\left[n_1(\mathbf{y})(\gamma_1^2+3\gamma_2^2)\frac{\gamma_1}{r}-n_2(\mathbf{y})(\gamma_1^2-\gamma_2^2)\frac{\gamma_2}{r}\right]\kappa^t(\mathbf{y})\Delta u^n(\mathbf{y})\mathrm{d}l(\mathbf{y})\end{aligned}$$

$$\begin{aligned}\sigma_{12}(\mathbf{x}) = &-\frac{\mu}{\pi}\left(1-\frac{c_s^2}{c_p^2}\right)\int_{\text{fault}}\left[(n_1\gamma_1+n_2\gamma_2)\left(\frac{\gamma_1^2}{r}-\frac{\gamma_2^2}{r}\right)\right]\frac{d}{dy^t}\Delta u^n(\mathbf{y})\mathrm{d}l(\mathbf{y})\\ &-\frac{\mu}{\pi}\left(1-\frac{c_s^2}{c_p^2}\right)\int_{\text{fault}}\left[(n_1\gamma_2-n_2\gamma_1)\left(\frac{\gamma_1^2}{r}-\frac{\gamma_2^2}{r}\right)\right]\kappa^t(\mathbf{y})\Delta u^n(\mathbf{y})\mathrm{d}l(\mathbf{y})\end{aligned}$$

$$\begin{aligned}\tau_t(\mathbf{x}) &= n_1(\mathbf{x})n_2(\mathbf{x})(\sigma_{11}(\mathbf{x})-\sigma_{22}(\mathbf{x}))+(n_2^2(\mathbf{x})-n_1^2(\mathbf{x}))\sigma_{12}(\mathbf{x})\\ \sigma_n(\mathbf{x}) &= n_1^2(\mathbf{x})\sigma_{11}(\mathbf{x})+2n_1(\mathbf{x})n_2(\mathbf{x})\sigma_{12}(\mathbf{x})+n_2^2(\mathbf{x})\sigma_{22}(\mathbf{x})\end{aligned}$$

(67)

G.2 Zeroth Order

G.2.1 Space-time

$$
\begin{aligned}
\sigma_{11}(x_1) &= -\frac{\mu}{\pi}\left(1-\frac{c_s^2}{c_p^2}\right)\int_{-\infty}^{+\infty}\frac{1}{x_1-y_1}\frac{d}{dy^t}\Delta u^n(y_1)\mathrm{d}y_1 \\
\sigma_{22}(x_1) &= -\frac{\mu}{\pi}\left(1-\frac{c_s^2}{c_p^2}\right)\int_{-\infty}^{+\infty}\frac{1}{x_1-y_1}\frac{d}{dy^t}\Delta u^n(y_1)\mathrm{d}y_1 \\
\sigma_{12}(x_1) &= \frac{\mu}{\pi}\left(1-\frac{c_s^2}{c_p^2}\right)\int_{-\infty}^{+\infty}\frac{1}{x_1-y_1}\kappa^t(y_1)\Delta u^n(y_1)\mathrm{d}y_1 \\
\tau_t(x_1) &= \sigma_{12}^0 \\
&= \frac{\mu}{\pi}\left(1-\frac{c_s^2}{c_p^2}\right)\int_{-\infty}^{+\infty}\frac{1}{x_1-y_1}\kappa^t(y_1)\Delta u^n(y_1)\mathrm{d}y_1 \\
\sigma_n(x_1) &= \sigma_{22}^0 \\
&= -\frac{\mu}{\pi}\left(1-\frac{c_s^2}{c_p^2}\right)\int_{-\infty}^{+\infty}\frac{1}{x_1-y_1}\frac{d}{dy^t}\Delta u^n(y_1)\mathrm{d}y_1
\end{aligned}
\tag{68}
$$

G.2.2 Spectral-time

$$
\begin{aligned}
\sigma_{11}(k) &= -\frac{\mu}{\pi}\left(1-\frac{c_s^2}{c_p^2}\right)\pi|k|\mathcal{F}[\Delta u^n] \\
\sigma_{22}(k) &= -\frac{\mu}{\pi}\left(1-\frac{c_s^2}{c_p^2}\right)\pi|k|\mathcal{F}[\Delta u^n] \\
\sigma_{12}(k) &= -\frac{\mu}{\pi}\left(1-\frac{c_s^2}{c_p^2}\right)i\pi\mathrm{sign}(k)\mathcal{F}[\kappa^t(y_1)\Delta u^n(y_1)] \\
\tau_t(k) &= -\frac{\mu}{\pi}\left(1-\frac{c_s^2}{c_p^2}\right)i\pi\mathrm{sign}(k)\mathcal{F}[\kappa^t(y_1)\Delta u^n(y_1)] \\
\sigma_n(k) &= -\frac{\mu}{\pi}\left(1-\frac{c_s^2}{c_p^2}\right)\pi|k|\mathcal{F}[\Delta u^n]
\end{aligned}
\tag{69}
$$

G.3 First Order

G.3.1 Space-time

$$
\begin{aligned}
\sigma_{11}(x_1) &= -\frac{\mu}{\pi}\left(1-\frac{c_s^2}{c_p^2}\right)\int_{-\infty}^{+\infty}\left[3\frac{x_2-y_2}{(x_1-y_1)^2}-\frac{m(y_1)}{x_1-y_1}\right]\kappa^t(y_1)\Delta u^n(y_1)\mathrm{d}y_1\\
\sigma_{22}(x_1) &= -\frac{\mu}{\pi}\left(1-\frac{c_s^2}{c_p^2}\right)\int_{-\infty}^{+\infty}\left[-\frac{m(y_1)}{x_1-y_1}-\frac{x_2-y_2}{(x_1-y_1)^2}\right]\kappa^t(y_1)\Delta u^n(y_1)\mathrm{d}y_1\\
\sigma_{12}(x_1) &= -\frac{\mu}{\pi}\left(1-\frac{c_s^2}{c_p^2}\right)\int_{-\infty}^{+\infty}\left[-\frac{m(y_1)}{x_1-y_1}+\frac{x_2-y_2}{(x_1-y_1)^2}\right]\frac{d}{dy^t}\Delta u^n(y_1)\mathrm{d}y_1\\
\tau_t(x_1) &= -m(\sigma_{11}^0-\sigma_{22}^0)+\sigma_{12}^1\\
&= \frac{\mu}{\pi}\left(1-\frac{c_s^2}{c_p^2}\right)\int_{-\infty}^{+\infty}\left[\frac{m(y_1)}{x_1-y_1}-\frac{x_2-y_2}{(x_1-y_1)^2}\right]\frac{d}{dy^t}\Delta u^n(y_1)\mathrm{d}y_1\\
\sigma_n(x_1) &= -2m\sigma_{12}^0+\sigma_{22}^1\\
&= \frac{\mu}{\pi}\left(1-\frac{c_s^2}{c_p^2}\right)\int_{-\infty}^{+\infty}\left[\frac{-2m(x_1)}{x_1-y_1}+\frac{m(y_1)}{x_1-y_1}+\frac{x_2-y_2}{(x_1-y_1)^2}\right]\kappa^t(y_1)\Delta u^n(y_1)\mathrm{d}y_1
\end{aligned}
\tag{70}
$$

G.3.2 Spectral-time

$$
\begin{aligned}
\sigma_{11}(k) &= -\frac{\mu}{\pi}\left(1-\frac{c_s^2}{c_p^2}\right)(-3\pi|k|(h*\mathcal{F}[\kappa^t\Delta u^n]-\mathcal{F}[h\kappa^t\Delta u^n])+i\pi\mathrm{sign}(k)\mathcal{F}[m\kappa^t\Delta u^n])\\
\sigma_{22}(k) &= -\frac{\mu}{\pi}\left(1-\frac{c_s^2}{c_p^2}\right)(i\pi\mathrm{sign}(k)\mathcal{F}[m\kappa^t\Delta u^n]+\pi|k|(h*\mathcal{F}[\kappa^t\Delta u^n]-\mathcal{F}[h\kappa^t\Delta u^n]))\\
\sigma_{12}(k) &= -\frac{\mu}{\pi}\left(1-\frac{c_s^2}{c_p^2}\right)\left(i\pi\mathrm{sign}(k)\mathcal{F}\left[m\frac{d}{dy_1}\Delta u^n\right]-\pi|k|\left(h*\mathcal{F}\left[\frac{d}{dy_1}\Delta u^n\right]-\mathcal{F}\left[h\frac{d}{dy_1}\Delta u^n\right]\right)\right)\\
\tau_t(k) &= \frac{\mu}{\pi}\left(1-\frac{c_s^2}{c_p^2}\right)\left(-i\pi\mathrm{sign}(k)\mathcal{F}\left[m\frac{d}{dy_1}\Delta u^n\right]+\pi|k|\left(h*\mathcal{F}\left[\frac{d}{dy_1}\Delta u^n\right]-\mathcal{F}\left[h\frac{d}{dy_1}\Delta u^n\right]\right)\right)\\
\sigma_n(k) &= \frac{\mu}{\pi}\left(1-\frac{c_s^2}{c_p^2}\right)(2i\pi\mathrm{sign}(k)m*\mathcal{F}\left[\kappa^t\Delta u^n\right]-i\pi\mathrm{sign}(k)\mathcal{F}\left[m\kappa^t\Delta u^n\right]\\
&\quad -\pi|k|(h*\mathcal{F}\left[\kappa^t\Delta u^n\right]-\mathcal{F}\left[h\kappa^t\Delta u^n\right]))
\end{aligned}
\tag{71}
$$

H In-plane shear (mode II)

In the following, $\gamma_1 = \frac{x_1 - y_1}{r}$, $\gamma_2 = \frac{x_2 - y_2}{r}$, and $*$ represents the convolution operation.

H.1 Full solution

$$
\begin{aligned}
\epsilon_{11}(\mathbf{x}) &= \frac{1}{2\pi(\lambda+2\mu)} \int_{\text{fault}} \left[n_2 \frac{\gamma_2}{r} (2\lambda\gamma_1^2 + \mu(3\gamma_1^2 + \gamma_2^2)) - n_1 \frac{\gamma_1}{r} (2\lambda\gamma_2^2 + \mu(\gamma_2^2 - \gamma_1^2)) \right] \frac{d}{dy^t} \Delta u^t(\mathbf{y}) \mathrm{d}l(\mathbf{y}) \\
&+ \frac{1}{2\pi(\lambda+2\mu)} \int_{\text{fault}} \left[n_1 \frac{\gamma_2}{r} (2\lambda\gamma_1^2 + \mu(3\gamma_1^2 + \gamma_2^2)) + n_2 \frac{\gamma_1}{r} (2\lambda\gamma_2^2 + \mu(\gamma_2^2 - \gamma_1^2)) \right] \kappa^t(\mathbf{y}) \Delta u^t(\mathbf{y}) \mathrm{d}l(\mathbf{y}) \\
\epsilon_{22}(\mathbf{x}) &= \frac{1}{2\pi(\lambda+2\mu)} \int_{\text{fault}} \left[n_1 \frac{\gamma_1}{r} (2\lambda\gamma_2^2 + \mu(\gamma_1^2 + 3\gamma_2^2)) - n_2 \frac{\gamma_2}{r} (2\lambda\gamma_1^2 + \mu(\gamma_1^2 - \gamma_2^2)) \right] \frac{d}{dy^t} \Delta u^t(\mathbf{y}) \mathrm{d}l(\mathbf{y}) \\
&- \frac{1}{2\pi(\lambda+2\mu)} \int_{\text{fault}} \left[n_2 \frac{\gamma_1}{r} (2\lambda\gamma_2^2 + \mu(\gamma_1^2 + 3\gamma_2^2)) + n_1 \frac{\gamma_2}{r} (2\lambda\gamma_1^2 + \mu(\gamma_1^2 - \gamma_2^2)) \right] \kappa^t(\mathbf{y}) \Delta u^t(\mathbf{y}) \mathrm{d}l(\mathbf{y}) \\
\epsilon_{12}(\mathbf{x}) &= -\frac{\lambda+\mu}{2\pi(\lambda+2\mu)} \int_{\text{fault}} \left[\left(n_2 \frac{\gamma_1}{r} - n_1 \frac{\gamma_2}{r} \right) (\gamma_1^2 - \gamma_2^2) \right] \frac{d}{dy^t} \Delta u^t(\mathbf{y}) \mathrm{d}l(\mathbf{y}) \\
&- \frac{\lambda+\mu}{2\pi(\lambda+2\mu)} \int_{\text{fault}} \left[\left(n_1 \frac{\gamma_1}{r} + n_2 \frac{\gamma_2}{r} \right) (\gamma_1^2 - \gamma_2^2) \right] \kappa^t(\mathbf{y}) \Delta u^t(\mathbf{y}) \mathrm{d}l(\mathbf{y}) \\
\sigma_{11}(\mathbf{x}) &= \frac{\mu}{\pi} \left(1 - \frac{c_s^2}{c_p^2} \right) \int_{\text{fault}} \left[n_2 (3\gamma_1^2 + \gamma_2^2) \frac{\gamma_2}{r} + n_1 (\gamma_1^2 - \gamma_2^2) \frac{\gamma_1}{r} \right] \frac{d}{dy^t} \Delta u^t(\mathbf{y}) \mathrm{d}l(\mathbf{y}) \\
&+ \frac{\mu}{\pi} \left(1 - \frac{c_s^2}{c_p^2} \right) \int_{\text{fault}} \left[n_1 (3\gamma_1^2 + \gamma_2^2) \frac{\gamma_2}{r} - n_2 (\gamma_1^2 - \gamma_2^2) \frac{\gamma_1}{r} \right] \kappa^t(\mathbf{y}) \Delta u^t(\mathbf{y}) \mathrm{d}l(\mathbf{y}) \\
\sigma_{22}(\mathbf{x}) &= \frac{\mu}{\pi} \left(1 - \frac{c_s^2}{c_p^2} \right) \int_{\text{fault}} \left[n_1 (\gamma_1^2 + 3\gamma_2^2) \frac{\gamma_1}{r} - n_2 (\gamma_1^2 - \gamma_2^2) \frac{\gamma_2}{r} \right] \frac{d}{dy^t} \Delta u^t(\mathbf{y}) \mathrm{d}l(\mathbf{y}) \\
&- \frac{\mu}{\pi} \left(1 - \frac{c_s^2}{c_p^2} \right) \int_{\text{fault}} \left[n_2 (\gamma_1^2 + 3\gamma_2^2) \frac{\gamma_1}{r} + n_1 (\gamma_1^2 - \gamma_2^2) \frac{\gamma_2}{r} \right] \kappa^t(\mathbf{y}) \Delta u^t(\mathbf{y}) \mathrm{d}l(\mathbf{y}) \\
\sigma_{12}(\mathbf{x}) &= \frac{\mu}{\pi} \left(1 - \frac{c_s^2}{c_p^2} \right) \int_{\text{fault}} \left[(n_1 \frac{\gamma_2}{r} - n_2 \frac{\gamma_1}{r}) (\gamma_1^2 - \gamma_2^2) \right] \frac{d}{dy^t} \Delta u^t(\mathbf{y}) \mathrm{d}l(\mathbf{y}) \\
&- \frac{\mu}{\pi} \left(1 - \frac{c_s^2}{c_p^2} \right) \int_{\text{fault}} \left[(n_1 \frac{\gamma_1}{r} + n_2 \frac{\gamma_2}{r}) (\gamma_1^2 - \gamma_2^2) \right] \kappa^t(\mathbf{y}) \Delta u^t(\mathbf{y}) \mathrm{d}l(\mathbf{y}) \\
\tau_t(\mathbf{x}) &= n_1(\mathbf{x}) n_2(\mathbf{x}) (\sigma_{11}(\mathbf{x}) - \sigma_{22}(\mathbf{x})) + (n_2^2(\mathbf{x}) - n_1^2(\mathbf{x})) \sigma_{12}(\mathbf{x}) \\
\sigma_n(\mathbf{x}) &= n_1^2(\mathbf{x}) \sigma_{11}(\mathbf{x}) + 2 n_1(\mathbf{x}) n_2(\mathbf{x}) \sigma_{12}(\mathbf{x}) + n_2^2(\mathbf{x}) \sigma_{22}(\mathbf{x})
\end{aligned}
\tag{72}
$$

H.2 Zeroth Order

H.2.1 Space-time

$$
\begin{aligned}
\sigma_{11}(x_1) &= -\frac{\mu}{\pi}\left(1-\frac{c_s^2}{c_p^2}\right)\int_{-\infty}^{+\infty}\left[\frac{1}{x_1-y_1}\kappa^t(y_1)\Delta u^t(y_1)\right]\mathrm{d}y_1 \\
\sigma_{22}(x_1) &= -\frac{\mu}{\pi}\left(1-\frac{c_s^2}{c_p^2}\right)\int_{-\infty}^{+\infty}\left[\frac{1}{x_1-y_1}\kappa^t(y_1)\Delta u^t(y_1)\right]\mathrm{d}y_1 \\
\sigma_{12}(x_1) &= -\frac{\mu}{\pi}\left(1-\frac{c_s^2}{c_p^2}\right)\int_{-\infty}^{+\infty}\left[\frac{1}{x_1-y_1}\frac{d}{dy^t}\Delta u^t(y_1)\right]\mathrm{d}y_1 \\
\tau_t(x_1) &= \sigma_{12}^0 \\
&= -\frac{\mu}{\pi}\left(1-\frac{c_s^2}{c_p^2}\right)\int_{-\infty}^{+\infty}\left[\frac{1}{x_1-y_1}\frac{d}{dy^t}\Delta u^t(y_1)\right]\mathrm{d}y_1 \\
\sigma_n(x_1) &= \sigma_{22}^0 \\
&= -\frac{\mu}{\pi}\left(1-\frac{c_s^2}{c_p^2}\right)\int_{-\infty}^{+\infty}\left[\frac{1}{x_1-y_1}\kappa^t(y_1)\Delta u^t(y_1)\right]\mathrm{d}y_1
\end{aligned}
\tag{73}
$$

H.2.2 Spectral-time

$$
\begin{aligned}
\sigma_{11}(k) &= \frac{\mu}{\pi}\left(1-\frac{c_s^2}{c_p^2}\right) i\pi\mathrm{sign}(k)\mathcal{F}[\kappa^t\Delta u^t] \\
\sigma_{22}(k) &= \frac{\mu}{\pi}\left(1-\frac{c_s^2}{c_p^2}\right) i\pi\mathrm{sign}(k)\mathcal{F}[\kappa^t\Delta u^t] \\
\sigma_{12}(k) &= -\frac{\mu}{\pi}\left(1-\frac{c_s^2}{c_p^2}\right) \pi|k|\mathcal{F}[\Delta u^t] \\
\tau_t(k) &= -\frac{\mu}{\pi}\left(1-\frac{c_s^2}{c_p^2}\right) \pi|k|\mathcal{F}[\Delta u^t] \\
\sigma_n(k) &= \frac{\mu}{\pi}\left(1-\frac{c_s^2}{c_p^2}\right) i\pi\mathrm{sign}(k)\mathcal{F}[\kappa^t\Delta u^t]
\end{aligned}
\tag{74}
$$

H.3 First Order

H.3.1 Space-time

$$
\begin{aligned}
\sigma_{11}(x_1) &= \frac{\mu}{\pi}\left(1-\frac{c_s^2}{c_p^2}\right)\int_{-\infty}^{+\infty}\left[3\frac{x_2-y_2}{(x_1-y_1)^2}-\frac{m(y_1)}{x_1-y_1}\right]\frac{d}{dy^t}\Delta u^t(y_1)\mathrm{d}y_1\\
\sigma_{22}(x_1) &= \frac{\mu}{\pi}\left(1-\frac{c_s^2}{c_p^2}\right)\int_{-\infty}^{+\infty}\left[-\frac{m(y_1)}{x_1-y_1}-\frac{x_2-y_2}{(x_1-y_1)^2}\right]\frac{d}{dy^t}\Delta u^t(y_1)\mathrm{d}y_1\\
\sigma_{12}(x_1) &= \frac{\mu}{\pi}\left(1-\frac{c_s^2}{c_p^2}\right)\int_{-\infty}^{+\infty}\left[\frac{m(y_1)}{x_1-y_1}-\frac{x_2-y_2}{(x_1-y_1)^2}\right]\kappa^t(y_1)\Delta u^t(y_1)\mathrm{d}y_1\\
\tau_t(x_1) &= -m(\sigma_{11}^0-\sigma_{22}^0)+\sigma_{12}^1\\
&= \frac{\mu}{\pi}\left(1-\frac{c_s^2}{c_p^2}\right)\int_{-\infty}^{+\infty}\left[\frac{m(y_1)}{x_1-y_1}-\frac{x_2-y_2}{(x_1-y_1)^2}\right]\kappa^t(y_1)\Delta u^t(y_1)\mathrm{d}y_1\\
\sigma_n(x_1) &= -2m\sigma_{12}^0+\sigma_{22}^1\\
&= \frac{\mu}{\pi}\left(1-\frac{c_s^2}{c_p^2}\right)\int_{-\infty}^{+\infty}\left[\frac{2m(x_1)}{x_1-y_1}-\frac{m(y_1)}{x_1-y_1}-\frac{x_2-y_2}{(x_1-y_1)^2}\right]\frac{d}{dy^t}\Delta u^t(y_1)\mathrm{d}y_1
\end{aligned}
\tag{75}
$$

H.3.2 Spectral-time

$$
\begin{aligned}
\sigma_{11}(k) &= \frac{\mu}{\pi}\left(1-\frac{c_s^2}{c_p^2}\right)\left(-3\pi|k|\left(h*\mathcal{F}\left[\frac{d}{y_1}\Delta u^t\right]-\mathcal{F}\left[h\frac{d}{y_1}\Delta u^t\right]\right)+i\pi\mathrm{sign}(k)\mathcal{F}\left[m\frac{d}{y_1}\Delta u^t\right]\right)\\
\sigma_{22}(k) &= \frac{\mu}{\pi}\left(1-\frac{c_s^2}{c_p^2}\right)\left(i\pi\mathrm{sign}(k)\mathcal{F}\left[m\frac{d}{y_1}\Delta u^t\right]+\pi|k|\left(h*\mathcal{F}\left[\frac{d}{y_1}\Delta u^t\right]-\mathcal{F}\left[h\frac{d}{y_1}\Delta u^t\right]\right)\right)\\
\sigma_{12}(k) &= \frac{\mu}{\pi}\left(1-\frac{c_s^2}{c_p^2}\right)(-i\pi\mathrm{sign}(k)\mathcal{F}[m\kappa^t\Delta u^t]+\pi|k|(h*\mathcal{F}[\kappa^t\Delta u^t]-\mathcal{F}[h\kappa^t\Delta u^t]))\\
\tau_t(k) &= \frac{\mu}{\pi}\left(1-\frac{c_s^2}{c_p^2}\right)(-i\pi\mathrm{sign}(k)\mathcal{F}[m\kappa^t\Delta u^t]+\pi|k|(h*\mathcal{F}[\kappa^t\Delta u^t]-\mathcal{F}[h\kappa^t\Delta u^t]))\\
\sigma_n(k) &= \frac{\mu}{\pi}\left(1-\frac{c_s^2}{c_p^2}\right)\left(-2i\pi\mathrm{sign}(k)m*\mathcal{F}\left[\frac{d}{dy_1}\Delta u^t\right]+i\pi\mathrm{sign}(k)\mathcal{F}\left[m\frac{d}{dy_1}\Delta u^t\right]\right.\\
&\quad\left.+\,\pi|k|\left(h*\mathcal{F}\left[\frac{d}{dy_1}\Delta u^t\right]-\mathcal{F}\left[h\frac{d}{dy_1}\Delta u^t\right]\right)\right)
\end{aligned}
\tag{76}
$$

I Out-of-plane (mode III)

In the following, $\gamma_1 = \frac{x_1 - y_1}{r}$, $\gamma_2 = \frac{x_2 - y_2}{r}$, and $*$ represents the convolution operation.

I.1 Full solution

$$
\begin{aligned}
\epsilon_{13}(\mathbf{x}) &= \frac{1}{4\pi} \int_{\text{fault}} \frac{\gamma_2}{r} \frac{d}{dy^t} \Delta u^s(\mathbf{y}) \mathrm{d}l(\mathbf{y}) \\
\epsilon_{23}(\mathbf{x}) &= -\frac{1}{4\pi} \int_{\text{fault}} \frac{\gamma_1}{r} \frac{d}{dy^t} \Delta u^s(\mathbf{y}) \mathrm{d}l(\mathbf{y}) \\
\sigma_{13}(\mathbf{x}) &= \frac{\mu}{2\pi} \int_{\text{fault}} \frac{\gamma_2}{r} \frac{d}{dy^t} \Delta u^s(\mathbf{y}) \mathrm{d}l(\mathbf{y}) \\
\sigma_{23}(\mathbf{x}) &= -\frac{\mu}{2\pi} \int_{\text{fault}} \frac{\gamma_1}{r} \frac{d}{dy^t} \Delta u^s(\mathbf{y}) \mathrm{d}l(\mathbf{y}) \\
\tau_t(\mathbf{x}) &= \frac{\mu}{2\pi} \int_{\text{fault}} \frac{\gamma_1}{r} \frac{d}{dy^t} \Delta u^s(\mathbf{y}) \mathrm{d}l(\mathbf{y})
\end{aligned}
\tag{77}
$$

$$
\sigma_n(\mathbf{x}) = 0
$$

I.2 Zeroth Order

I.2.1 Space-time

$$
\begin{aligned}
\sigma_{13}(x_1) &= 0 \\
\sigma_{23}(x_1) &= -\frac{\mu}{2\pi} \int_{-\infty}^{+\infty} \frac{1}{x_1 - y_1} \frac{d}{dy_1} \Delta u^s(y_1) \mathrm{d}y_1 \\
\tau_t(x_1) &= -\frac{\mu}{2\pi} \int_{-\infty}^{+\infty} \frac{1}{x_1 - y_1} \frac{d}{dy_1} \Delta u^s(y_1) \mathrm{d}y_1 \\
\sigma_n(x_1) &= 0
\end{aligned}
\tag{78}
$$

I.2.2 Spectral-time

$$\begin{aligned}\sigma_{13}(k) &= 0\\ \sigma_{23}(k) &= -\frac{\mu}{2\pi}\pi|k|\mathcal{F}[\Delta u^s]\\ \tau_t(k) &= -\frac{\mu}{2\pi}\pi|k|\mathcal{F}[\Delta u^s]\\ \sigma_n(k) &= 0\end{aligned} \tag{79}$$

I.3 First Order

I.3.1 Space-time

$$\begin{aligned}\sigma_{13}(x_1) &= \frac{\mu}{2\pi}\int_{-\infty}^{+\infty}\frac{x_2-y_2}{(x_1-y_1)^2}\frac{d}{dy^t}\Delta u^s(y_1)\mathrm{d}y_1\\ \sigma_{23}(x_1) &= 0\\ \tau_t(x_1) &= 0\\ \sigma_n(x_1) &= 0\end{aligned} \tag{80}$$

I.3.2 Spectral-time

$$\begin{aligned}\sigma_{13}(k) &= -\frac{\mu}{2\pi}\left(\pi kh * \mathcal{F}[\Delta u^s] + \pi i k^2\mathcal{F}[h\Delta u^s]\right)\\ \sigma_{23}(k) &= 0\\ \tau_t(k) &= 0\\ \sigma_n(k) &= 0\end{aligned} \tag{81}$$

References

Aki, K. (1979), Characterization of barriers on an earthquake fault, *J. Geophys. Res.*, *84*(B11), 6140–6148.

Aki, K., and P. G. Richards (2002), *Quantitative Seismology*, University Science Books.

Andrews, D. (1989), Mechanics of fault junctions, *J. Geophys. Res.*, *94*(B7), 9389–9397.

Aochi, H., E. Fukuyama, and M. Matsu'ura (2000a), Spontaneous rupture propagation on a non-planar fault in 3d elastic medium, *Pure Appl. Geophys.*, *157*, 2003–2027.

Bedrosian, E. (1963), A product theorem for hilbert transforms, *Proceedings of the IEEE*, *51*(5), 868–869, doi:10.1109/PROC.1963.2308.

Bonnet, M. (1999), *Boundary integral equation methods for solids and fluids*, vol. 34, 301–302 pp., Springer.

Bruhat, L., Y. Klinger, A. Vallage, and E. M. Dunham (2020), Influence of fault roughness on surface displacement: from numerical simulations to coseismic slip distributions, *Geophys. J. Int.*, *220*(3), 1857–1877, doi:10.1093/gji/ggz545.

Cattania, C., and P. Segall (2021), Precursory slow slip and foreshocks on rough faults, *J. Geophys. Res.*, *126*(4), e2020JB020,430, doi:10.1029/2020JB020430.

Chester, F. M., and J. S. Chester (2000), Stress and deformation along wavy frictional faults, *J. Geophys. Res.*, *105*(B10), 23,421–23,430.

Dieterich, J. H., and D. E. Smith (2009), Nonplanar faults: Mechanics of slip and off-fault damage, in *Mechanics, Structure and Evolution of Fault Zones*, edited by Y. Ben-Zion and C. Sammis, pp. 1799–1815, Springer, doi:10.1007/s00024-009-0517-y.

Duan, B., and D. D. Oglesby (2005), Multicycle dynamics of nonplanar strike-slip faults, *J. Geophys. Res.*, *110*, doi:10.1029/2004JB003298.

Dunham, E. M., D. Belanger, L. Cong, and J. E. Kozdon (2011), Earthquake ruptures with strongly rate-weakening friction and off-fault plasticity, part 2: Nonplanar faults, *Bull. Seism. Soc. Am.*, *101*(5), 2308–2322, doi:10.1785/0120100076.

Ely, G. P., S. M. Day, and J.-B. Minster (2009), A support-operator method for 3-d rupture dynamics, *Geophys. J. Int.*, *177*(3), 1140–1150, doi:10.1111/j.1365-246X.2009.04117.x.

Fang, Z., and E. M. Dunham (2013), Additional shear resistance from fault roughness and stress levels on geometrically complex faults, *Journal of Geophysical Research: Solid Earth*, *118*(7), 3642–3654, doi:10.1002/jgrb.50262.

Fukuyama, E., and S. Hok (2015), Dynamic overshoot near trench caused by large asperity break at depth, *Pure Appl. Geophys.*, *172*(8), 2157–2165, doi:10.1007/s00024-013-0745-z.

Geubelle, P. H., and J. R. Rice (1995), A spectral method for three-dimensional elastodynamic fracture problems, *J. Mech. Phys. Solids*, *43*(11), 1791–1824.

Heimisson, E. R. (2020), Crack to pulse transition and magnitude statistics during earthquake cycles on a self-similar rough fault, *Earth Planet. Sc. Lett.*, *537*, 116,202.

King, G. C. P., and J. Nabelek (1985), The role of bends in faults in the initiation and termination of earthquake rupture, *Science*, *228*, 984–987.

Klinger, Y., R. Michel, and G. C. P. King (2006), Evidence for an earthquake barrier model from mw $\sim$ 7.8 kokoxili (tibet) earthquake slip-distribution, *Earth Planet. Sc. Lett.*, *242*, 354–364.

Koller, M. G., M. Bonnet, and R. Madariaga (1992), Modelling of dynamical crack propagation using time-domain boundary integral equations, *Wave Motion*, *16*(4), 339–366.

Lozos, J. C., D. D. Oglesby, B. Duan, and S. G. Wesnousky (2011), The effects of double fault bends on rupture propagation: A geometrical parameter study, *Bull. Seism. Soc. Am.*, *101*(1), 385–398.

Mason, J. C., and D. C. Handscomb (2002), *Chebyshev polynomials*, Chapman and Hall/CRC.

Milliner, C. W., J. F. Dolan, J. Hollingsworth, S. Leprince, F. Ayoub, and C. G. Sammis (2015), Quantifying near-field and off-fault deformation patterns of the 1992 mw 7.3 l anders earthquake, *Geochem. Geophys. Geosyst.*, *16*(5), 1577–1598, doi: 10.1002/2014GC005693.

Nielsen, S. B., and L. Knopoff (1998), The equivalent strength of geometrical barriers to earthquakes, *J. Geophys. Res.*, *103*(B5), 9953–9965.

Romanet, P., and S. Ozawa (2021), Fully dynamic earthquake cycle simulations on a nonplanar fault using the spectral boundary integral element method (sbiem), *Bull. Seism. Soc. Am.*, doi:10.1785/0120210178.

Romanet, P., D. S. Sato, and R. Ando (2020), Curvature, a mechanical link between the geometrical complexities of a fault: application to bends, kinks and rough faults., *Geophys. J. Int.*, doi:10.1093/gji/ggaa308.

Sathiakumar, S., and S. Barbot (2021), The stop-start control of seismicity by fault bends along the main himalayan thrust, *Communications Earth & Environment*, *2*(1), 1–11, doi:10.1038/s43247-021-00153-3.

Sato, D. S., P. Romanet, and R. Ando (2020), Paradox of modelling curved faults revisited with general non-hypersingular stress green's functions, *Geophys. J. Int.*, *223*(1), 197–210.

603 Saucier, F., E. Humphreys, and R. Weldon (1992), Stress near geometrically complex
604 strike-slip faults: Application to the san andreas fault at cajon pass, southern california,
605 *J. Geophys. Res.*, *97*(B4), 5081–5094.

606 Schwartz, D. P., and R. H. Sibson (1989), Fault segmentation and controls of rupture
607 initiation and termination, *USGS Open-File Report*, *89315*, 445.

608 Segall, P. (2010), *Earthquake and volcano deformation*, Princeton University Press.

609 Shi, Z., and S. M. Day (2013), Rupture dynamics and ground motion from 3-d rough-fault
610 simulations, *Journal of Geophysical Research: Solid Earth*, *118*(3), 1122–1141.

611 Tada, T., and T. Yamashita (1996), The paradox of smooth and abrupt bends in two-
612 dimensional in-plane shear-crack mechanics, *Geophys. J. Int.*, *127*(3).

613 Tada, T., and T. Yamashita (1997), Non-hypersingular boundary integral equations for
614 two dimensional non-planar crack analysis, *Geophys. J. Int.*, *130*(2), 269–282.

615 Tal, Y. (2023), Modeling earthquake cycles and wear on rough faults with the mortar finite
616 element method, *Geophys. J. Int.*, *234*(1), 190–209, doi:10.1093/gji/ggad063.

617 Wesnousky, S. G. (2006), Predicting the endpoints of earthquake ruptures, *Nature*,
618 *444*(7117), 358–360.

619 Wesnousky, S. G. (2008), Displacement and geometrical characteristics of earthquake sur-
620 face ruptures: Issues and implications for seismic-hazard analysis and the process of
621 earthquake rupture, *Bull. Seism. Soc. Am.*, *98*(4), 1609–1632, doi:10.1785/0120070111.

Figure 1.

In-plane opening (mode I)

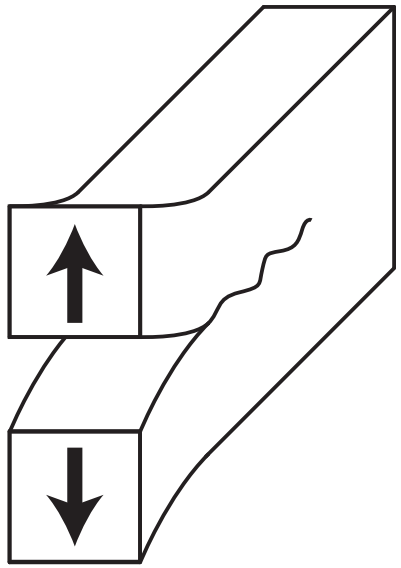

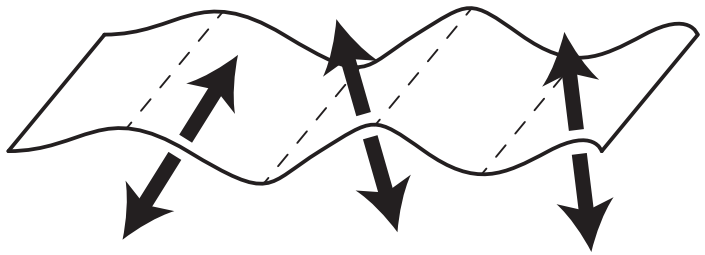

The opening direction is changing along the fault

In-plane shear (mode II)

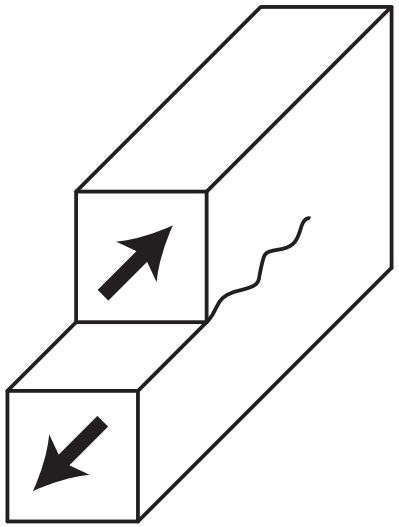

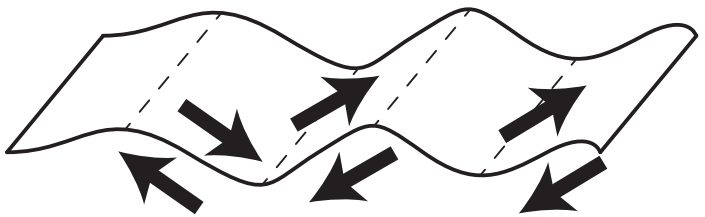

The slip direction is changing along the fault

Out-of-plane shear (mode III)

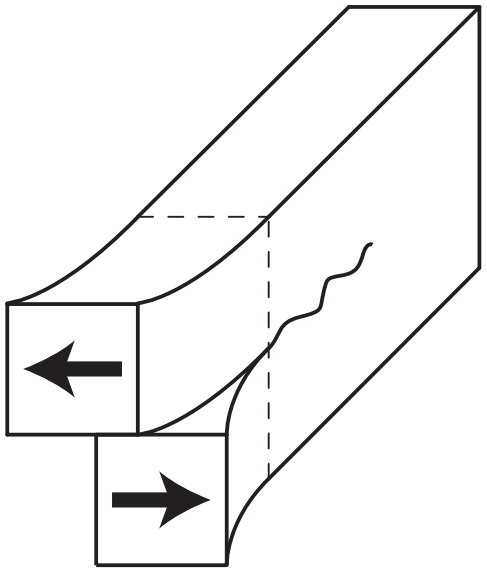

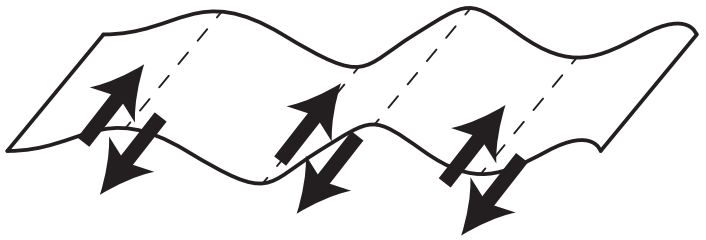

The slip direction is constant

Figure 2.

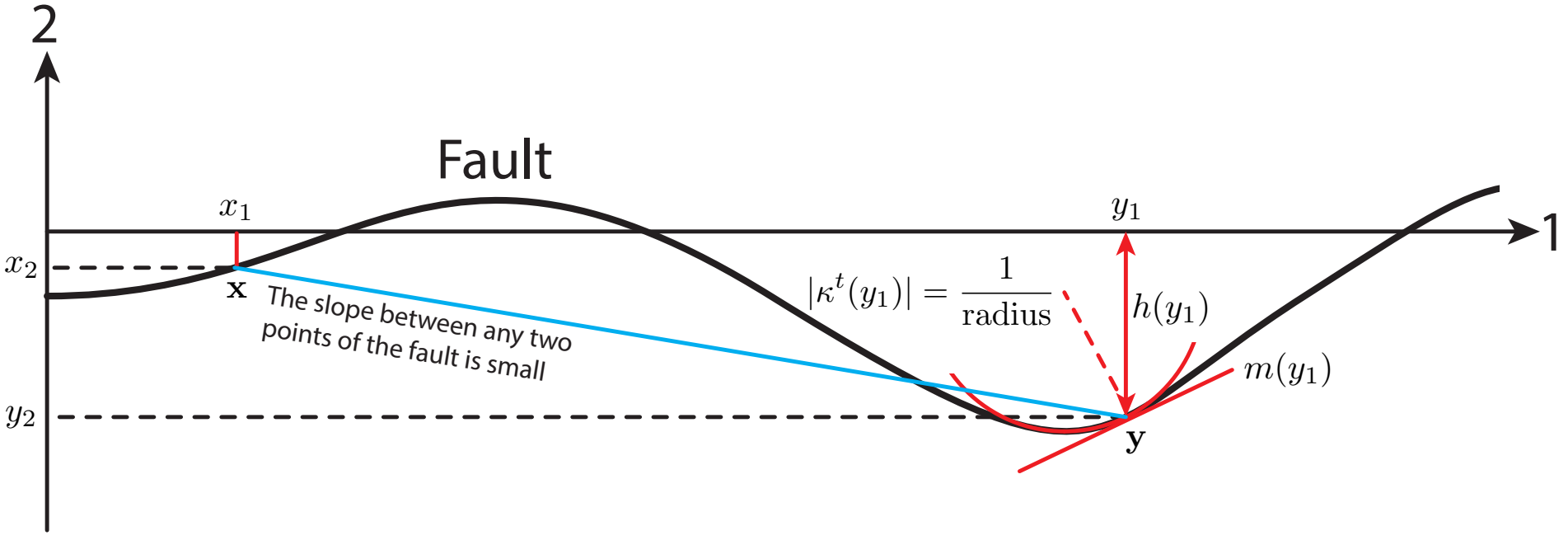
2
Fault
x_1
y_1
1
x_2
x
The slope between any two points of the fault is small
$|\kappa^t(y_1)| = \frac{1}{\text{radius}}$
$h(y_1)$
$m(y_1)$
y_2
y

Figure 3.

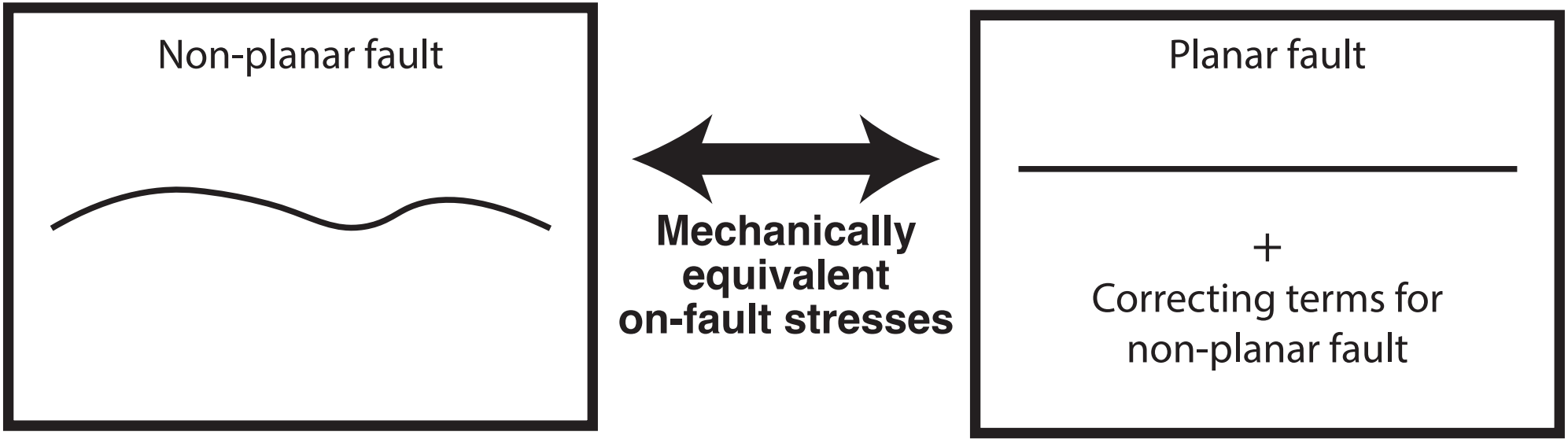
Non-planar fault
Mechanically equivalent on-fault stresses
Planar fault
+
Correcting terms for non-planar fault

Figure 4.

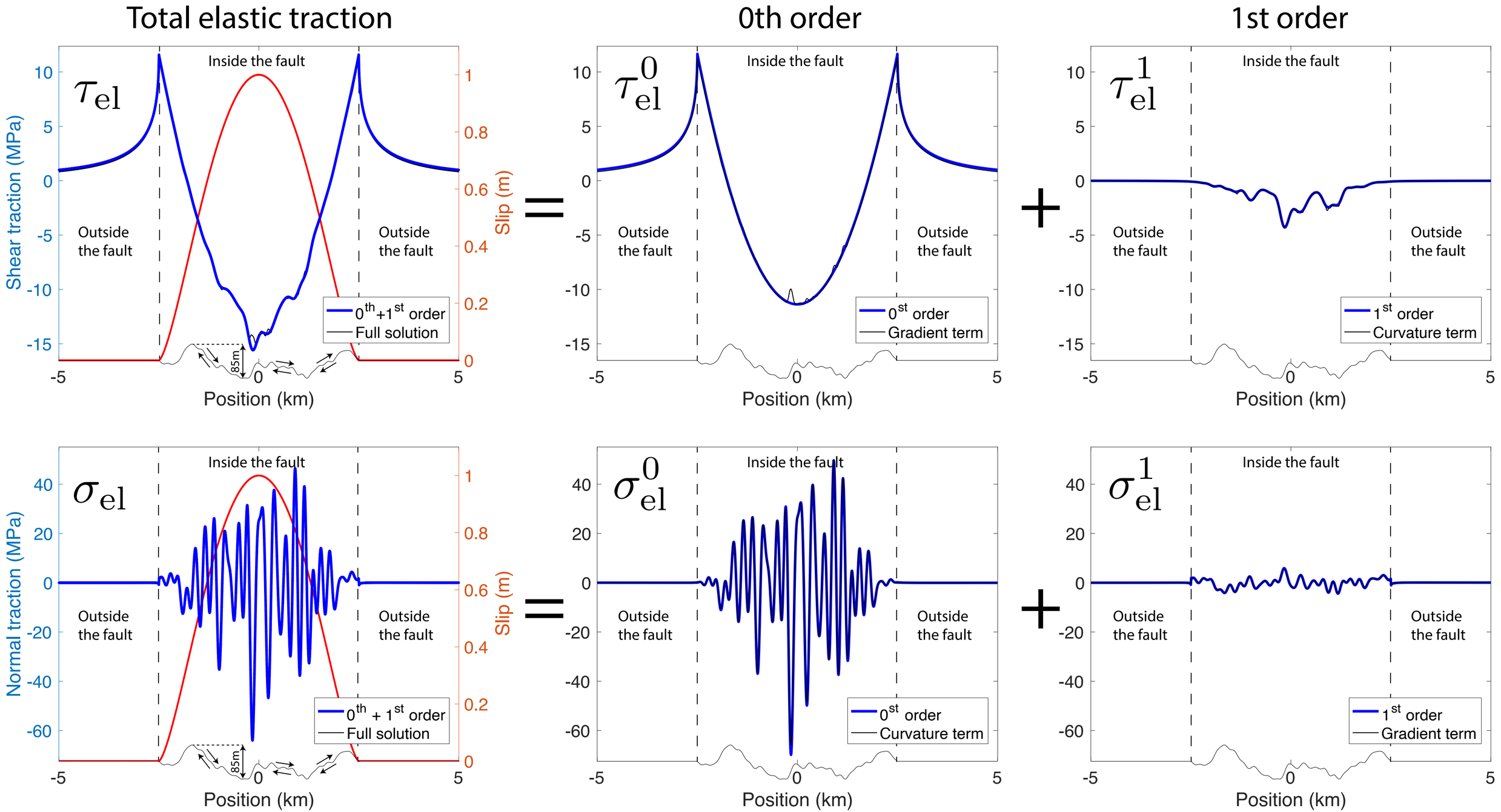
Total elastic traction
0th order
1st order
τ_{el}
τ_{el}^0
τ_{el}^1
σ_{el}
σ_{el}^0
σ_{el}^1
Inside the fault
Outside the fault
Outside the fault
Shear traction (MPa)
Normal traction (MPa)
Slip (m)
Position (km)
85m
0th+1st order
Full solution
0st order
Gradient term
1st order
Curvature term
0th + 1st order
0st order
Curvature term
1st order
Gradient term

Figure 5.

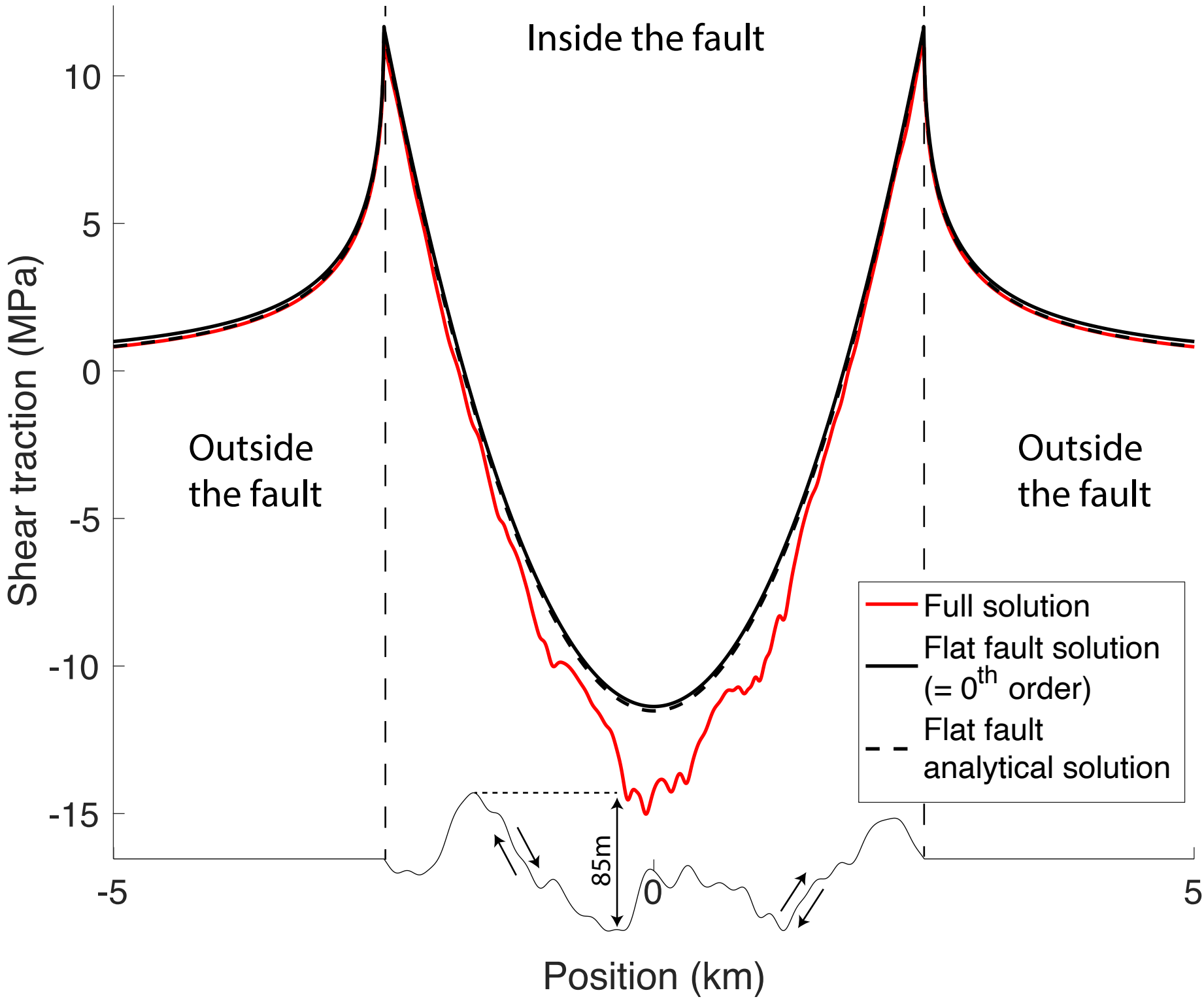
Inside the fault
Outside the fault
Outside the fault
Shear traction (MPa)
10
5
0
-5
-10
-15
-5
0
5
Position (km)
85m
Full solution
Flat fault solution (= 0th order)
Flat fault analytical solution

Figure 6.

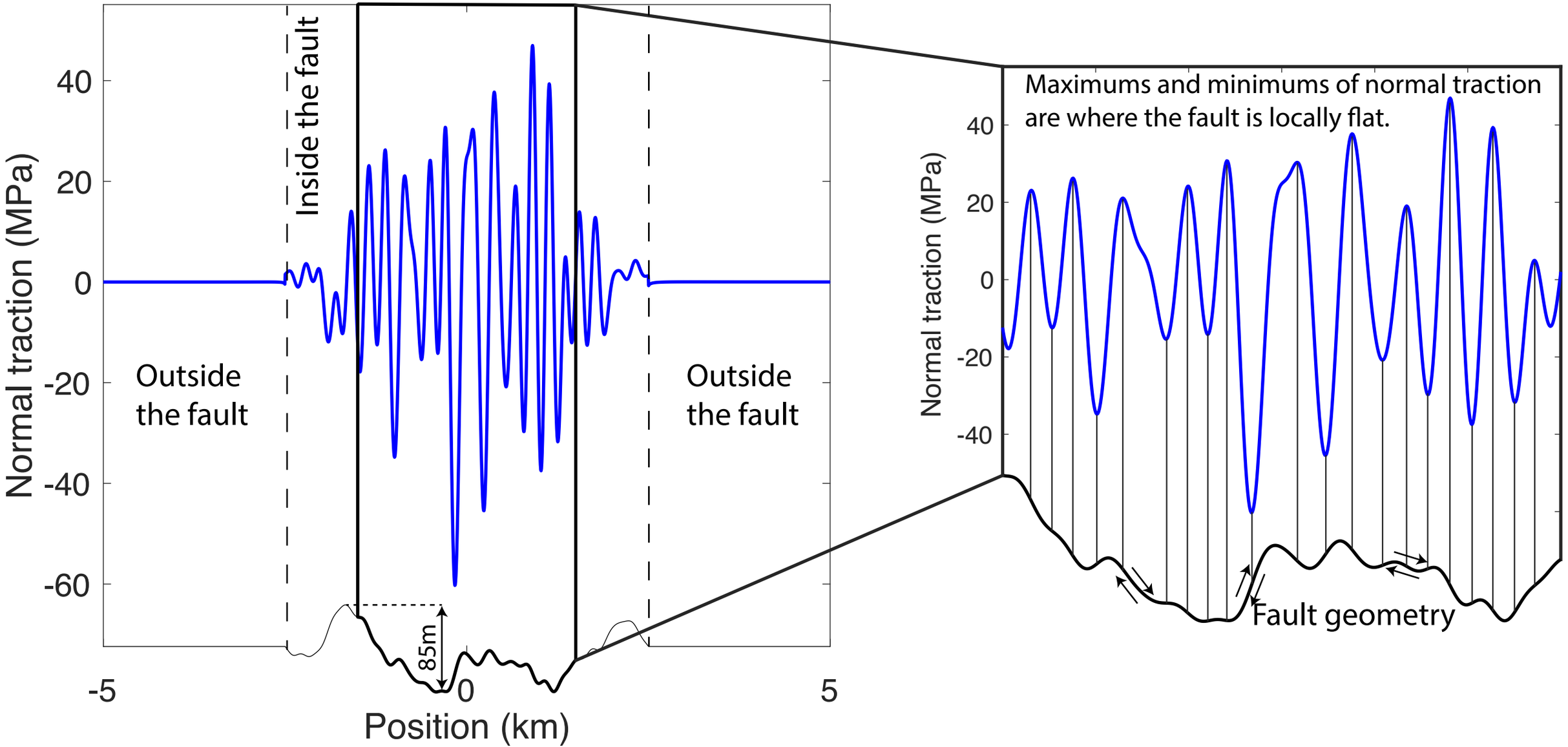
Inside the fault
Outside
the fault
Outside
the fault
Normal traction (MPa)
40
20
0
-20
-40
-60
-5
0
5
Position (km)
85m
Maximums and minimums of normal traction
are where the fault is locally flat.
Normal traction (MPa)
40
20
0
-20
-40
Fault geometry

Figure 7.

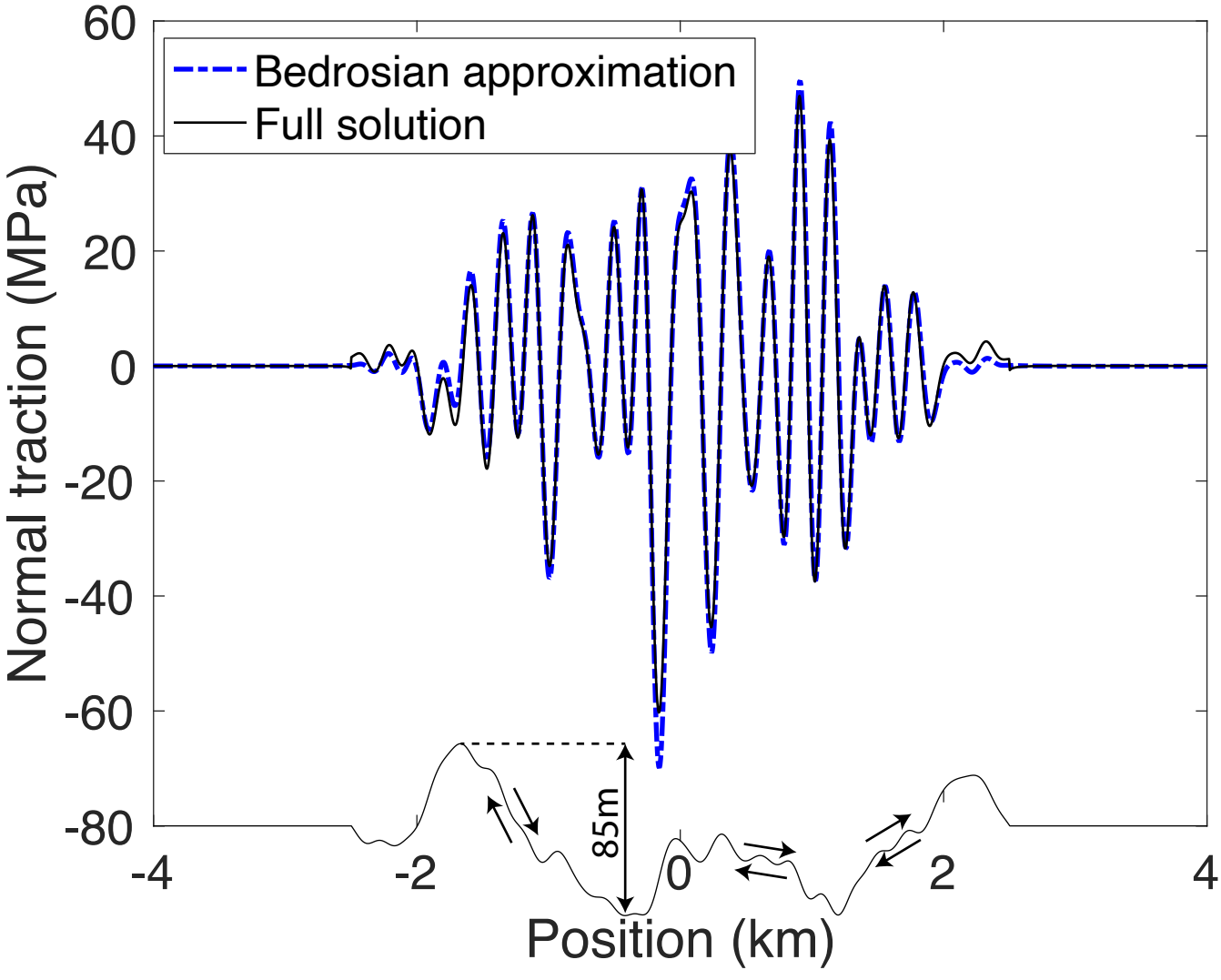
Bedrosian approximation
Full solution
Normal traction (MPa)
60
40
20
0
-20
-40
-60
-80
-4
-2
0
2
4
Position (km)
85m

Figure 8.

Scaling of slip distribution vs geometry
for different fault geometries in in-plane shear faulting (mode II)

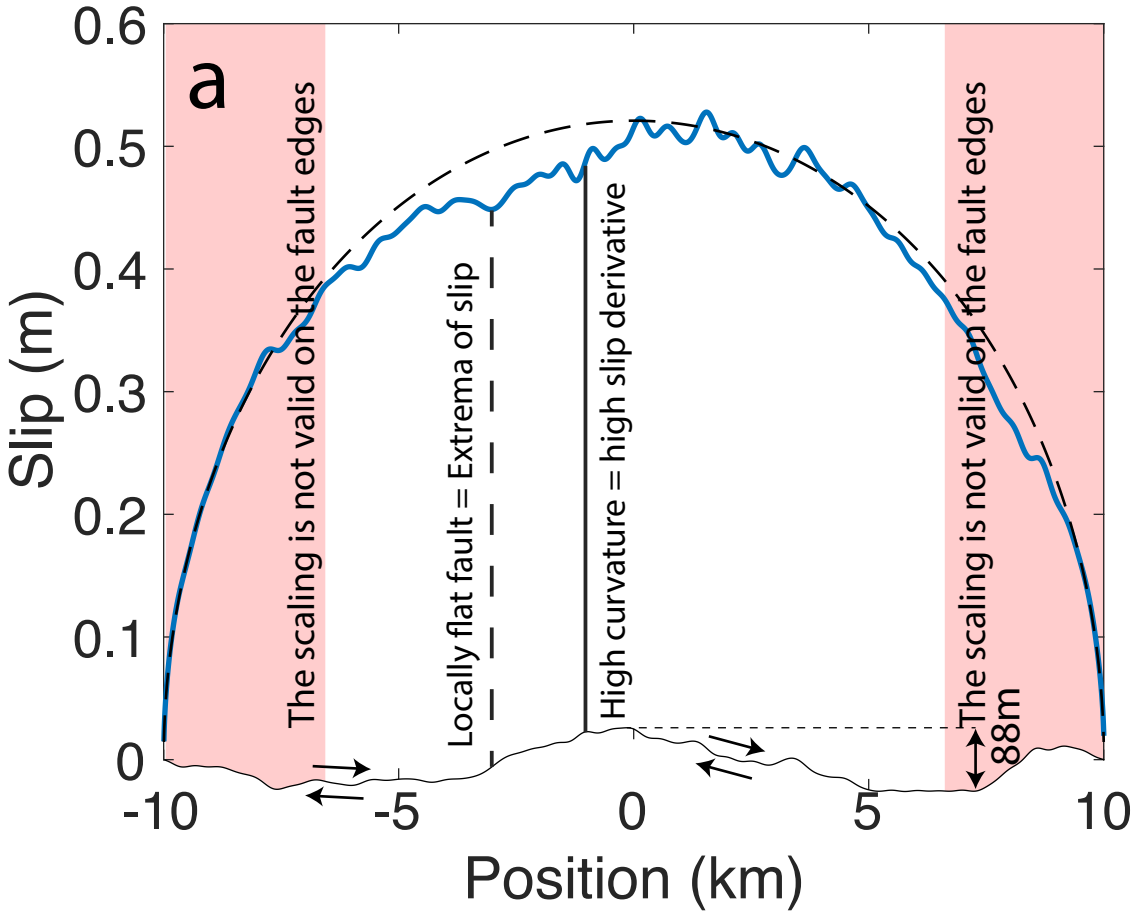

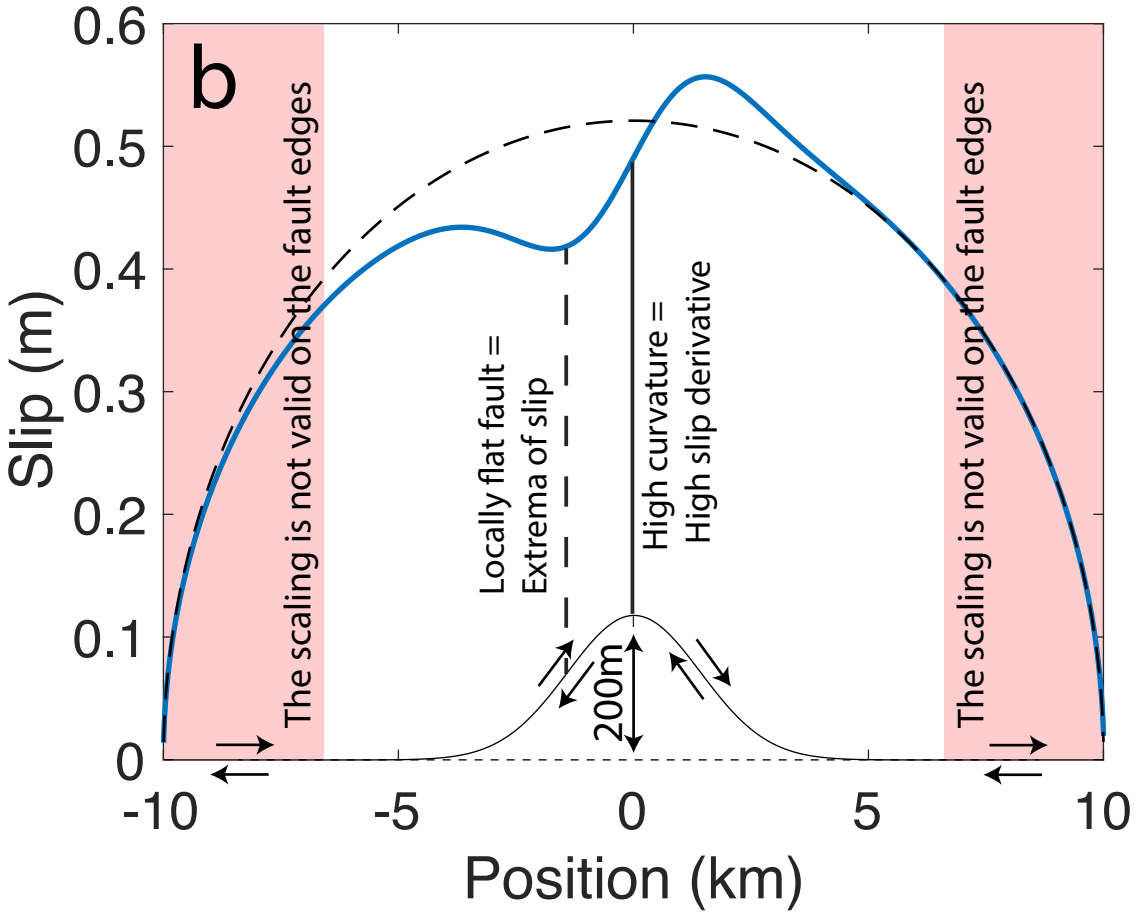

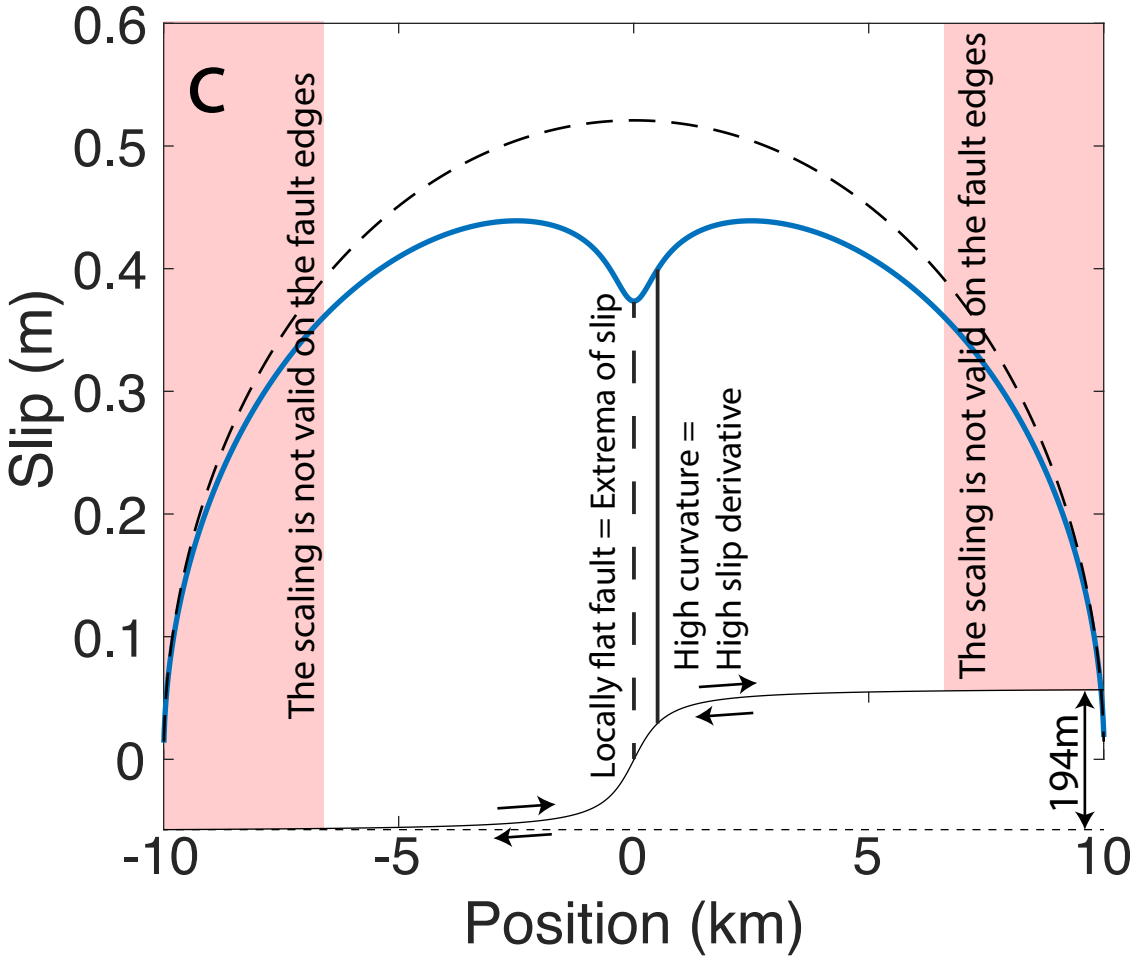

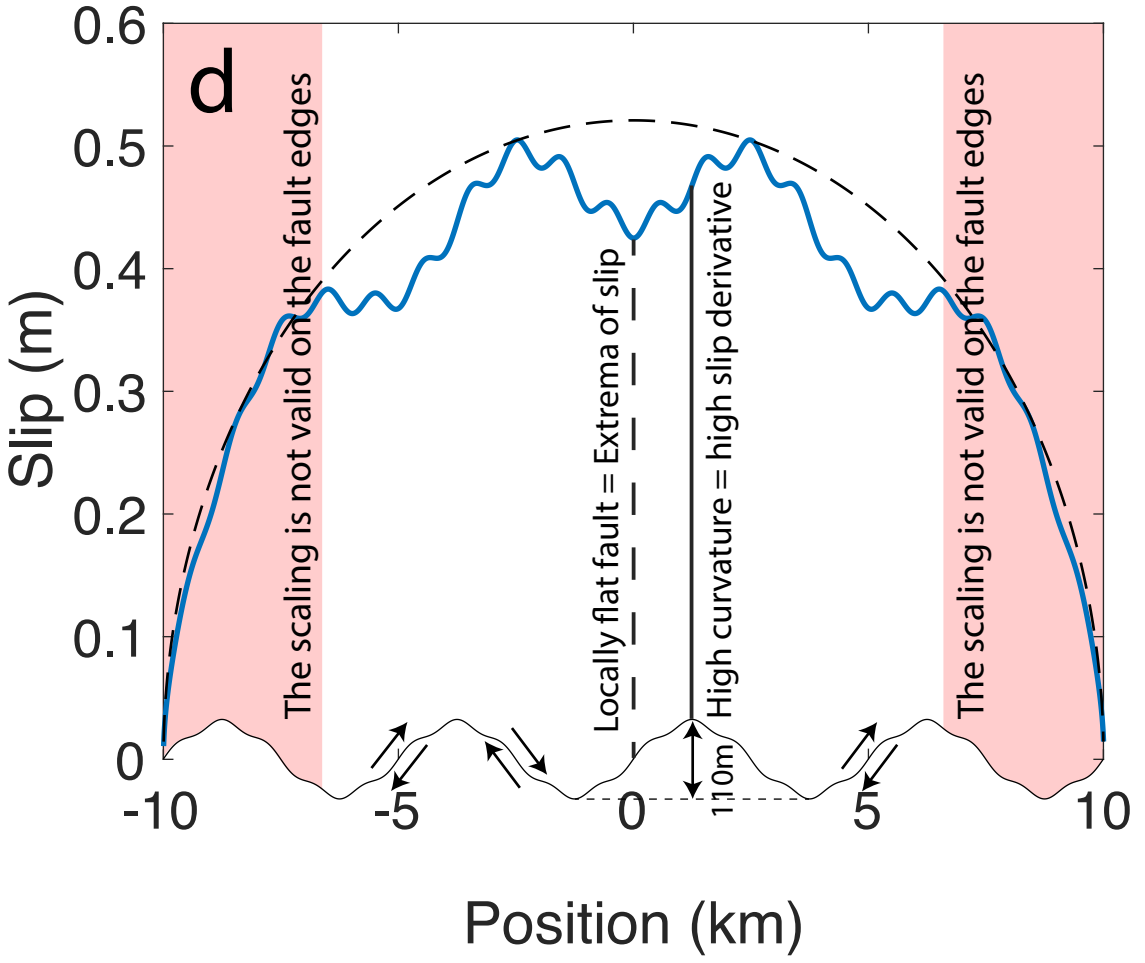

Figure 9.

Shear traction drag for different fault geometries

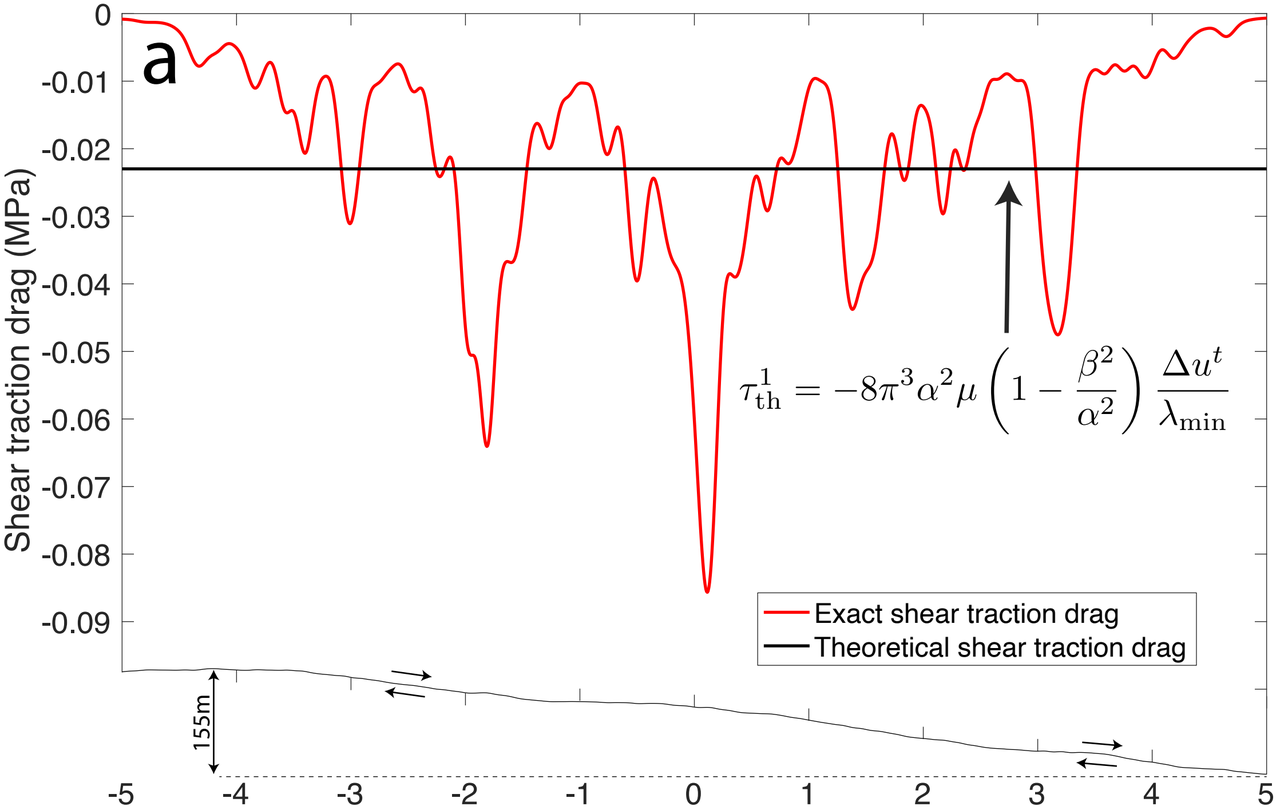

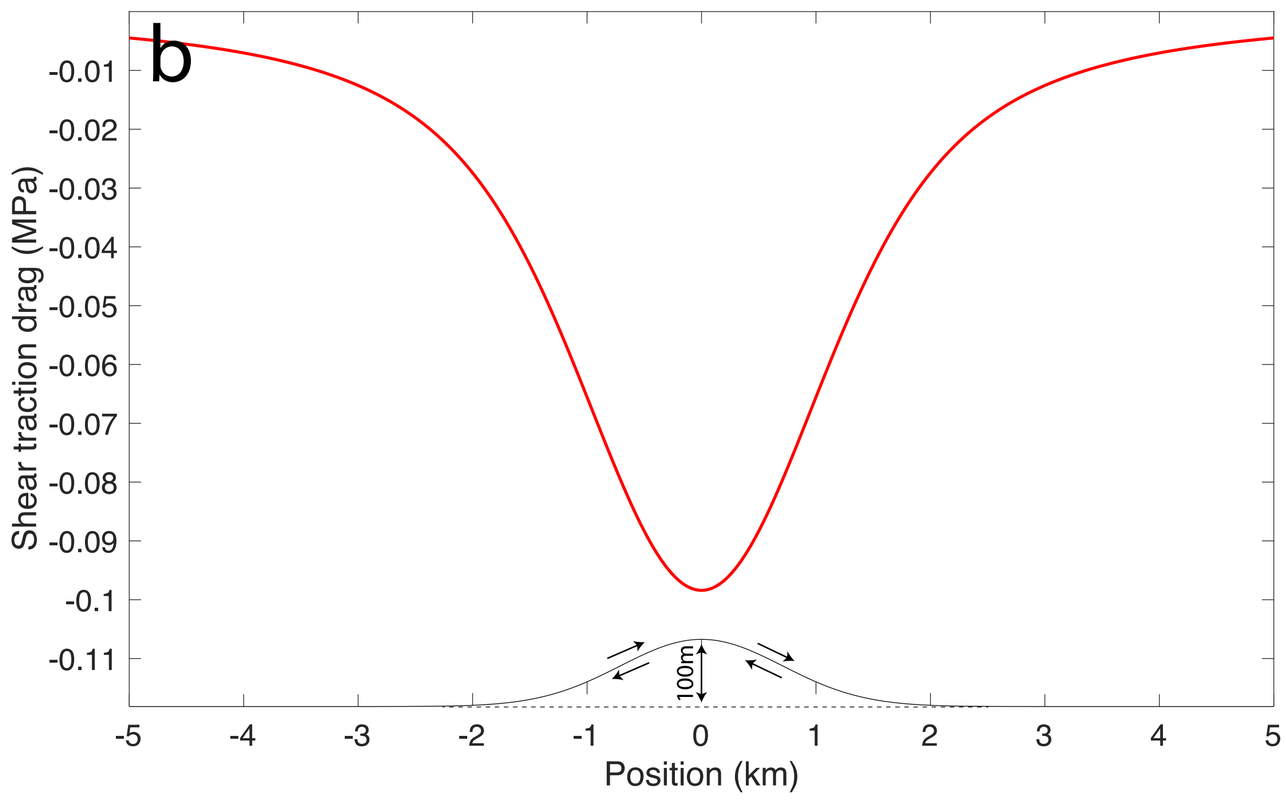

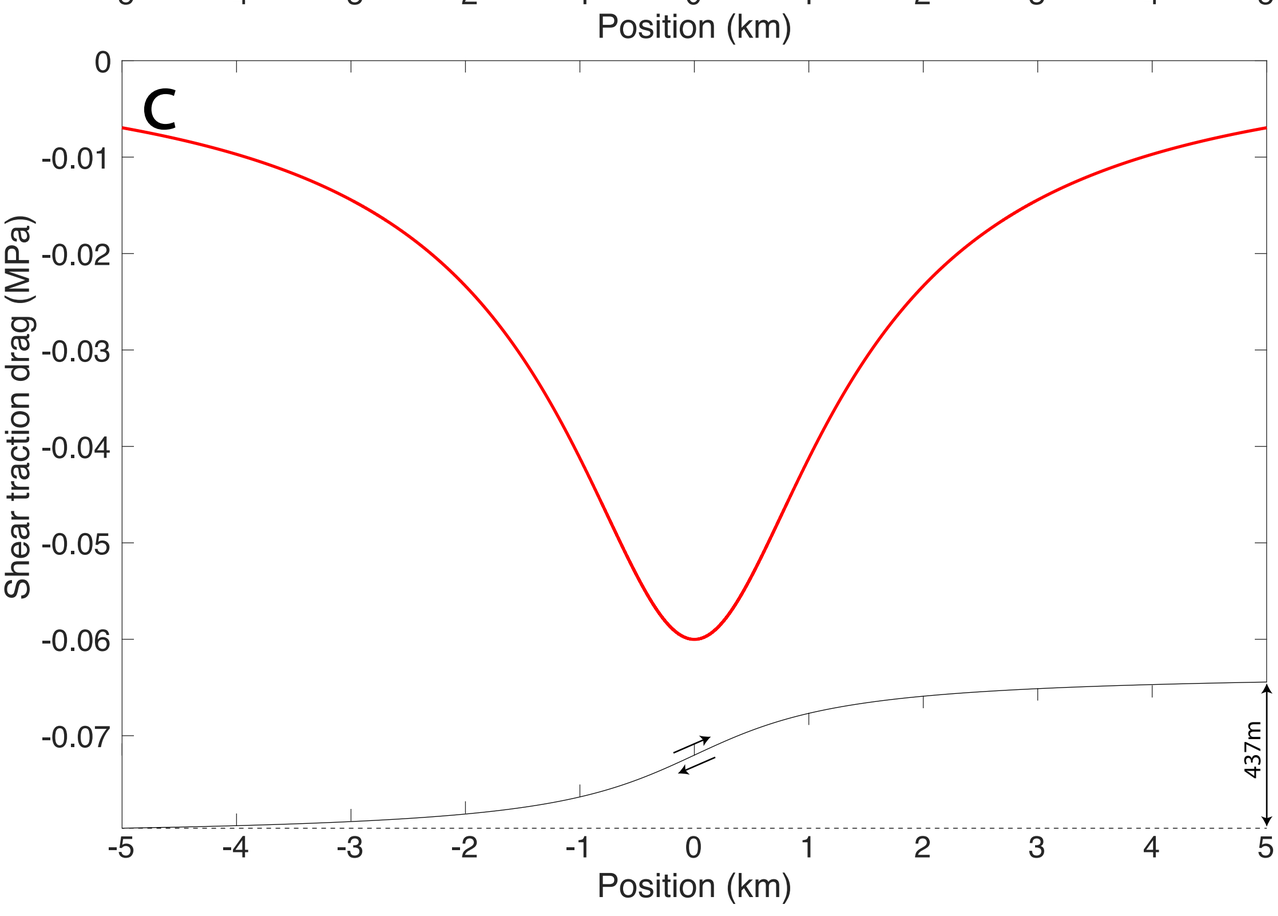

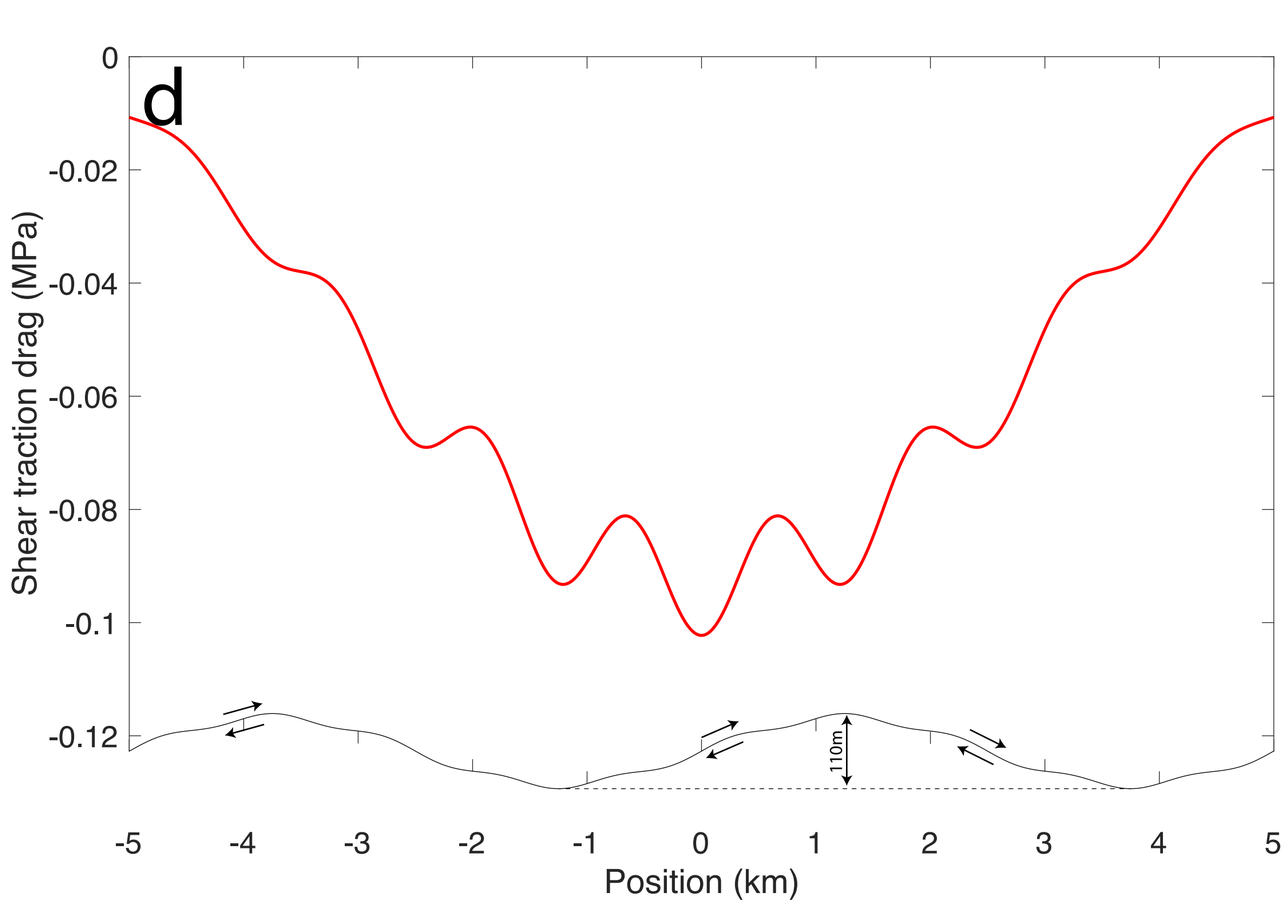

Figure 10.

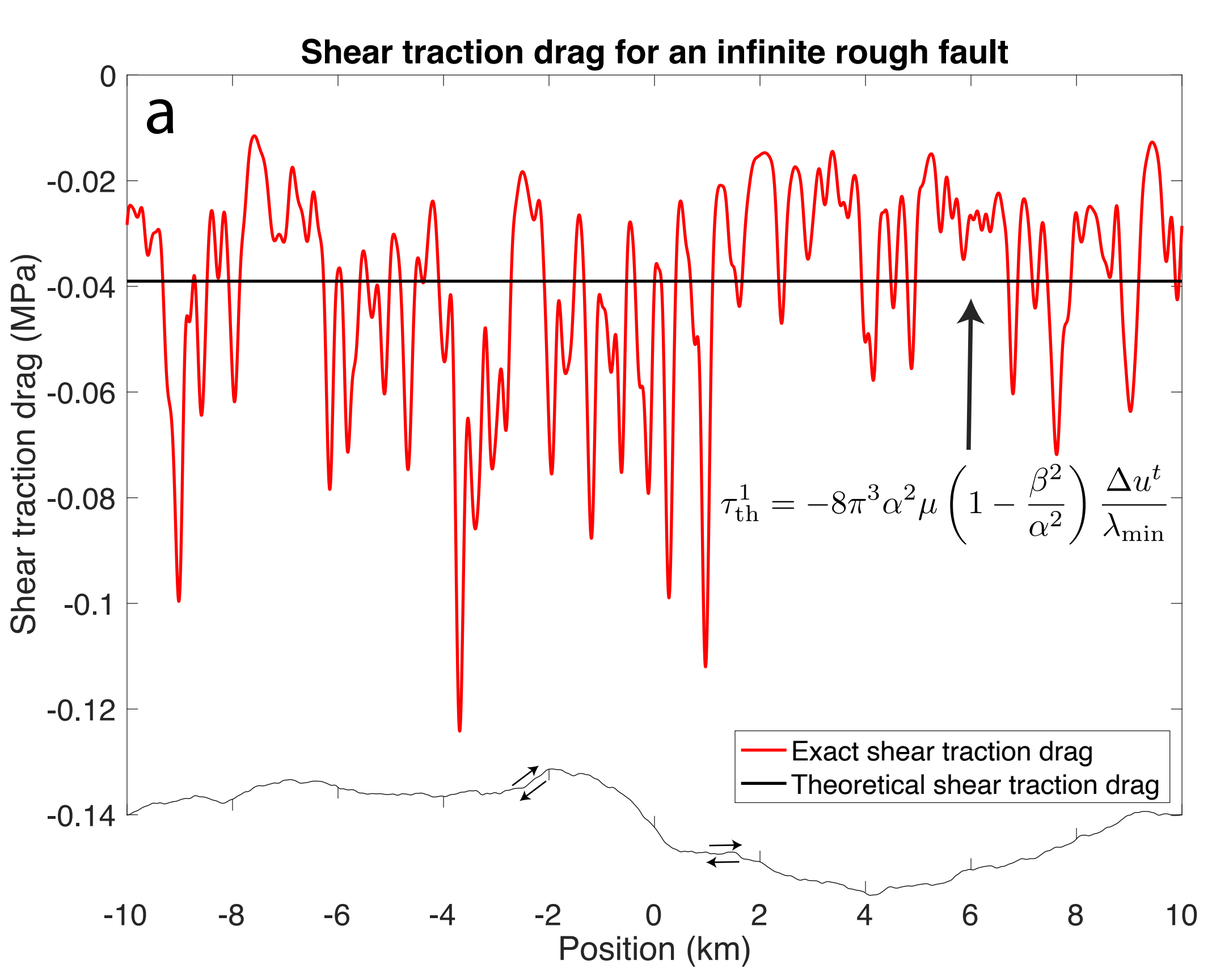
Shear traction drag for an infinite rough fault
a
Shear traction drag (MPa)
Position (km)
$\tau^1_{\mathrm{th}} = -8\pi^3\alpha^2\mu\left(1-\frac{\beta^2}{\alpha^2}\right)\frac{\Delta u^t}{\lambda_{\min}}$
Exact shear traction drag
Theoretical shear traction drag

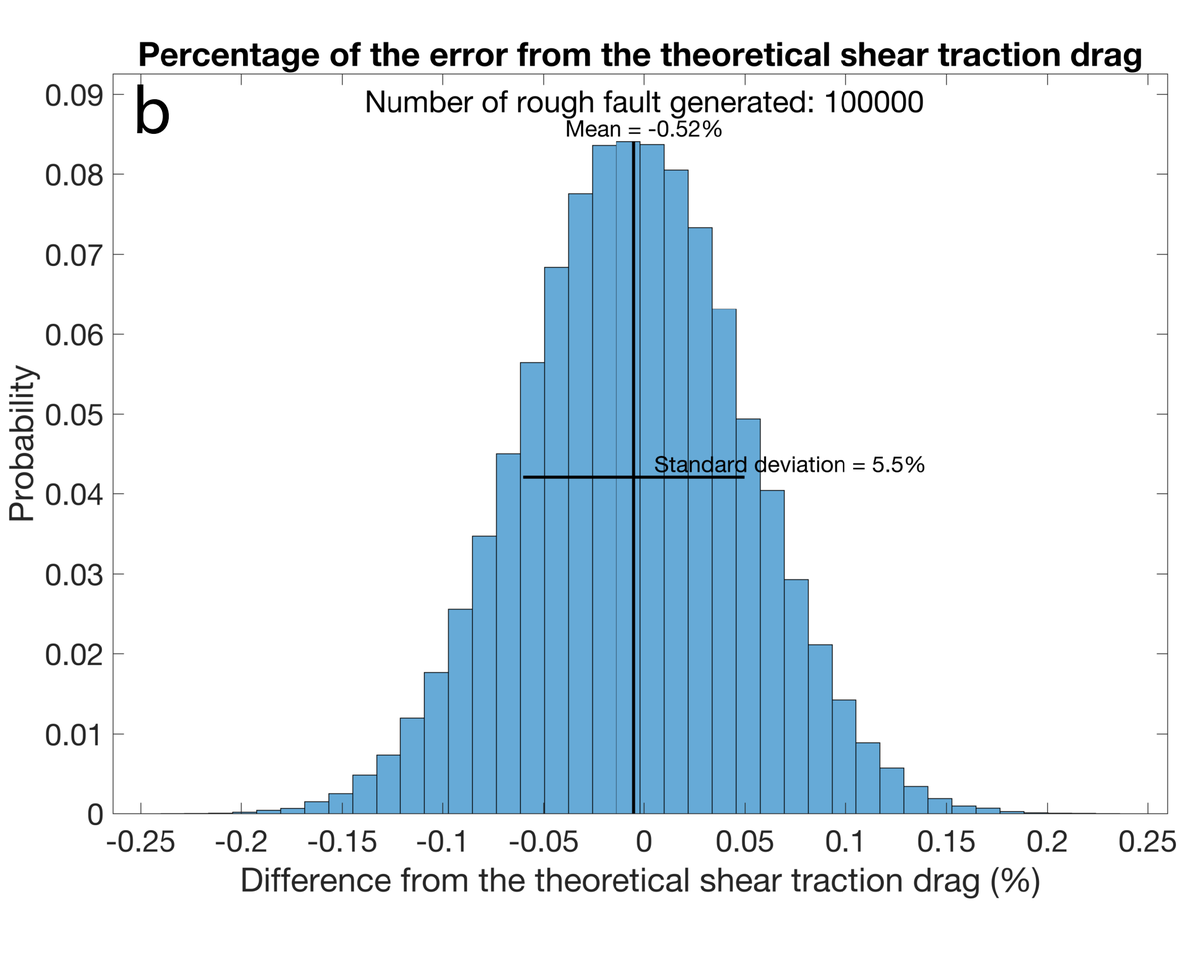
Percentage of the error from the theoretical shear traction drag
b
Number of rough fault generated: 100000
Mean = -0.52%
Standard deviation = 5.5%
Probability
Difference from the theoretical shear traction drag (%)

Figure 11.

Slighly decrease the maximums and minimums
of normal traction in the center of the fault

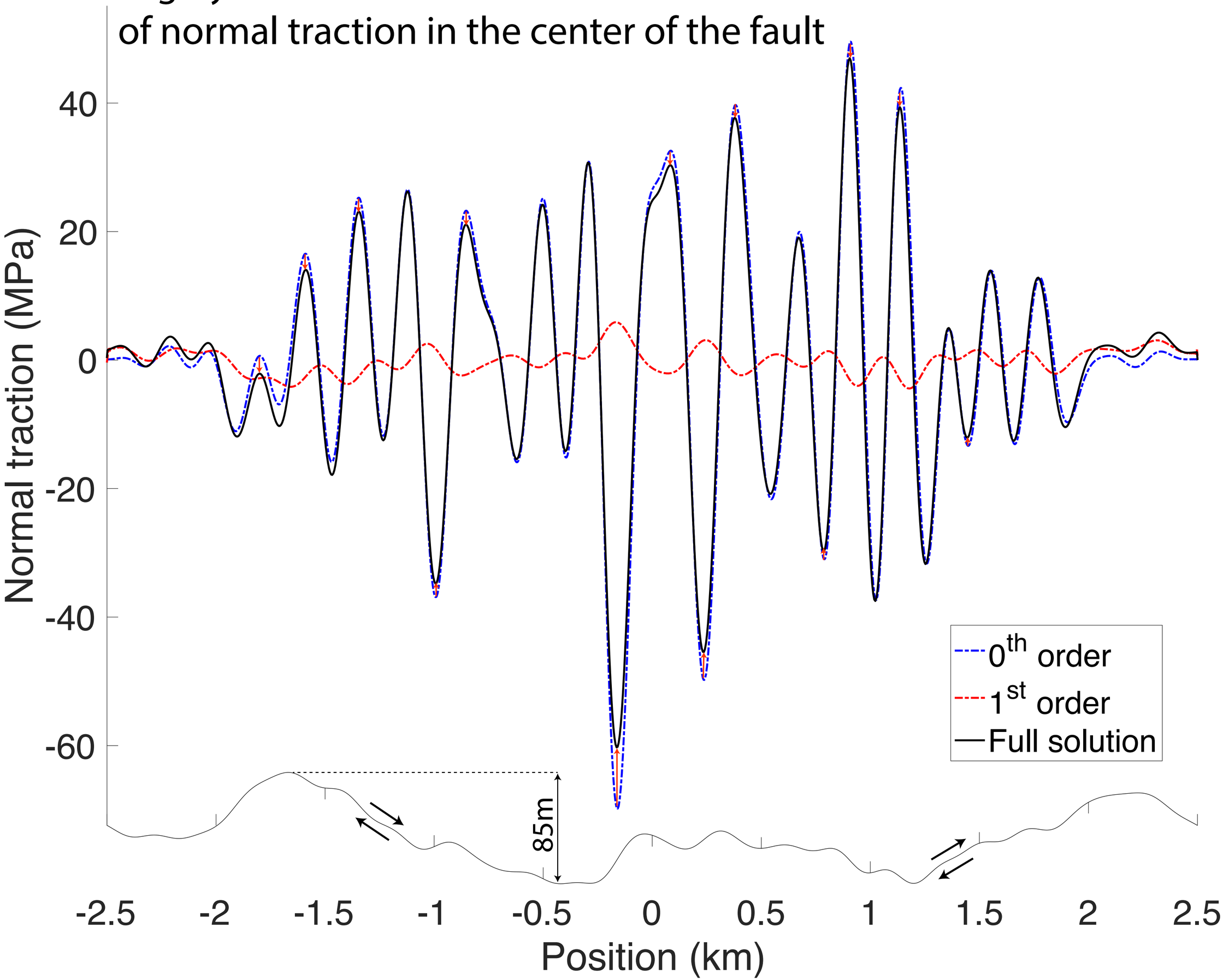

Figure 12.

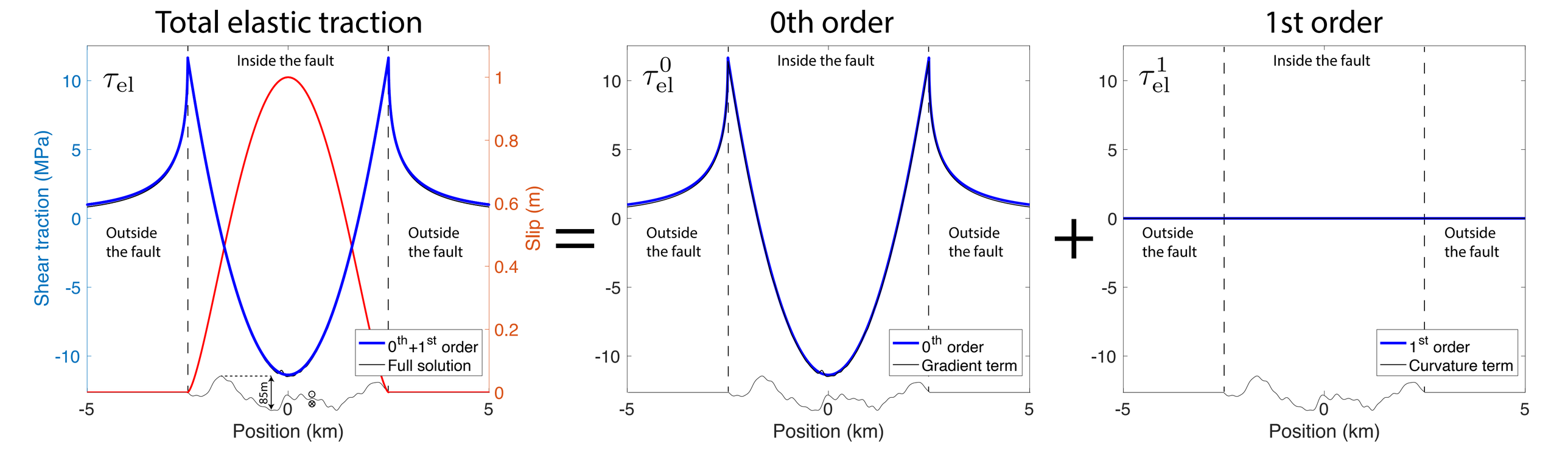
Total elastic traction
τ_{el}
Inside the fault
Outside the fault
Outside the fault
Shear traction (MPa)
Slip (m)
85m
0^{th}+1^{st} order
Full solution
Position (km)
=
0th order
τ_{el}^{0}
Inside the fault
Outside the fault
Outside the fault
0^{th} order
Gradient term
Position (km)
+
1st order
τ_{el}^{1}
Inside the fault
Outside the fault
Outside the fault
1^{st} order
Curvature term
Position (km)

Figure 13.

Absence of scaling of slip distribution vs geometry for different fault geometries in out-of-plane shear faulting (mode III)

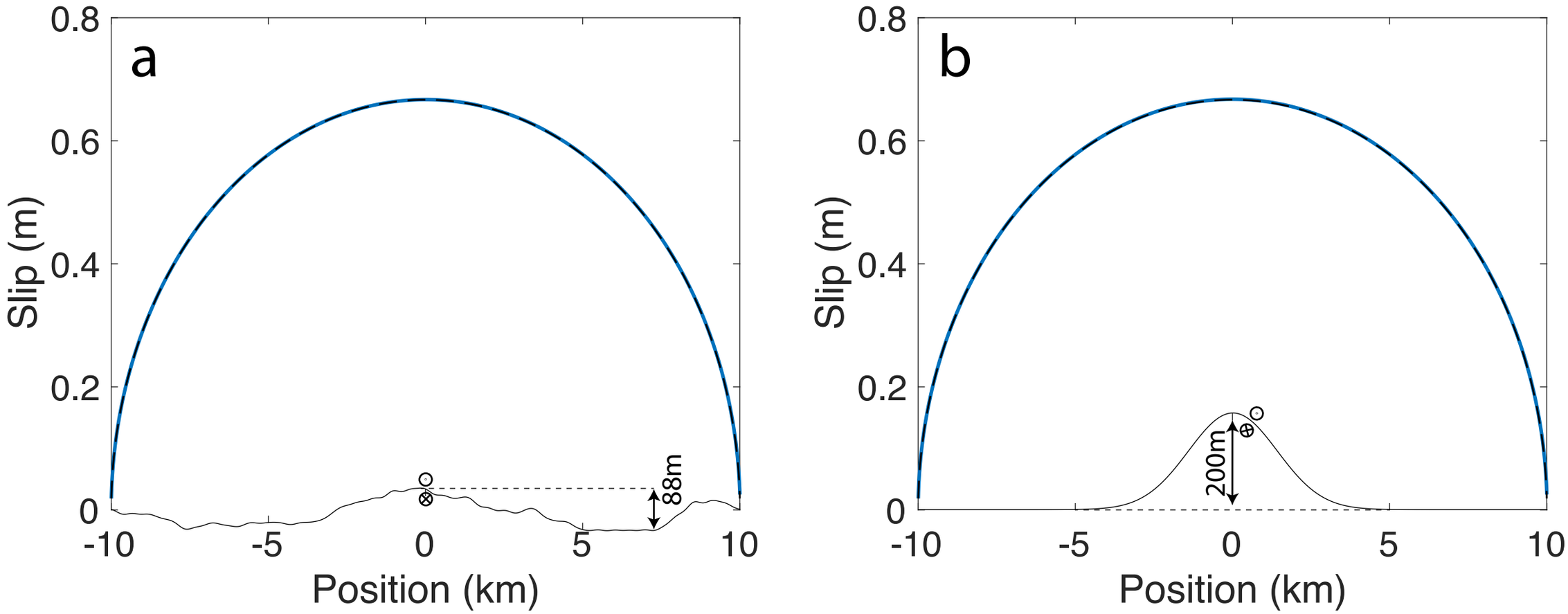

---- Planar fault slip distribution

—— Non-planar fault slip distribution

Figure 14.

a

Kinked fault with Coulomb friction

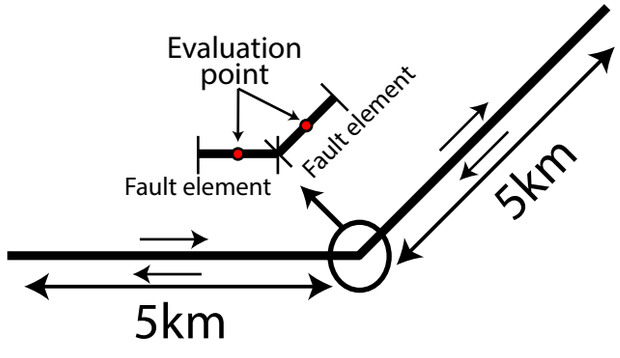

$$\tau^{\mathrm{el}} + \tau^{\mathrm{load}} = -f_0(\sigma_n^{\mathrm{el}} + \sigma_n^{\mathrm{load}})$$

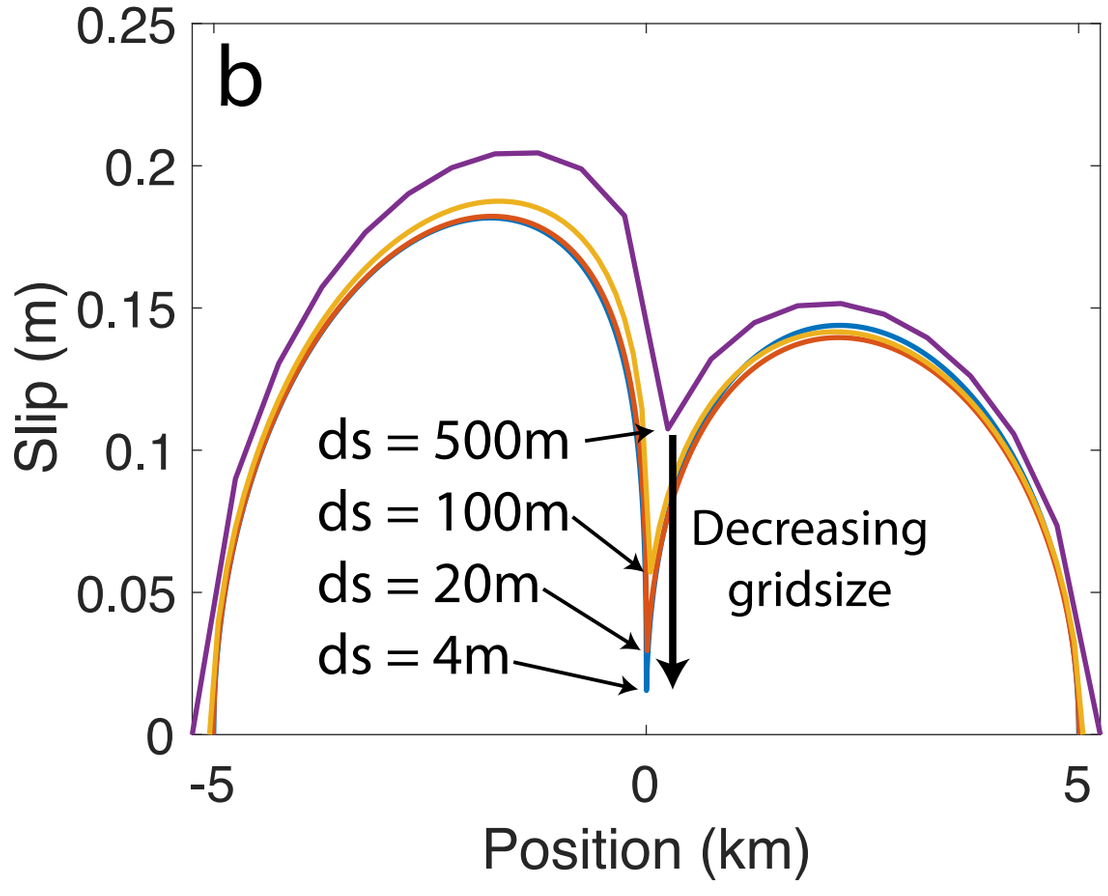

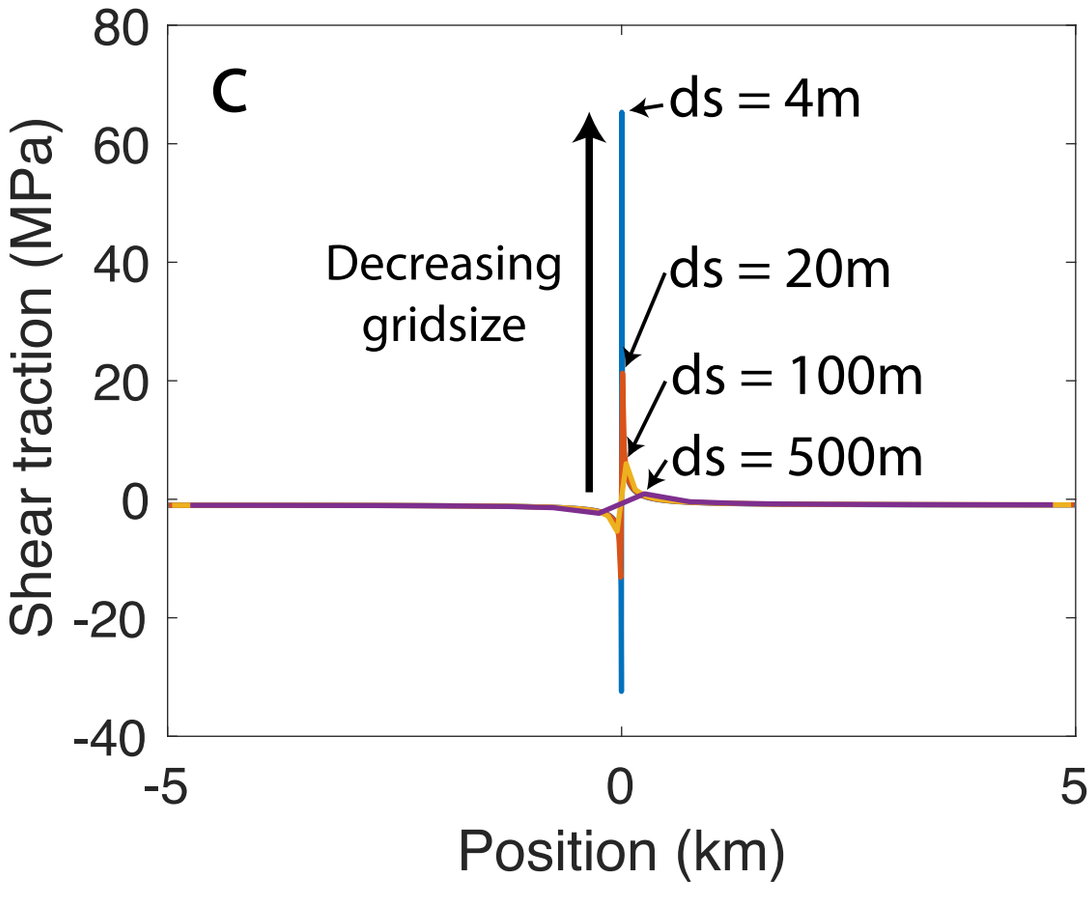

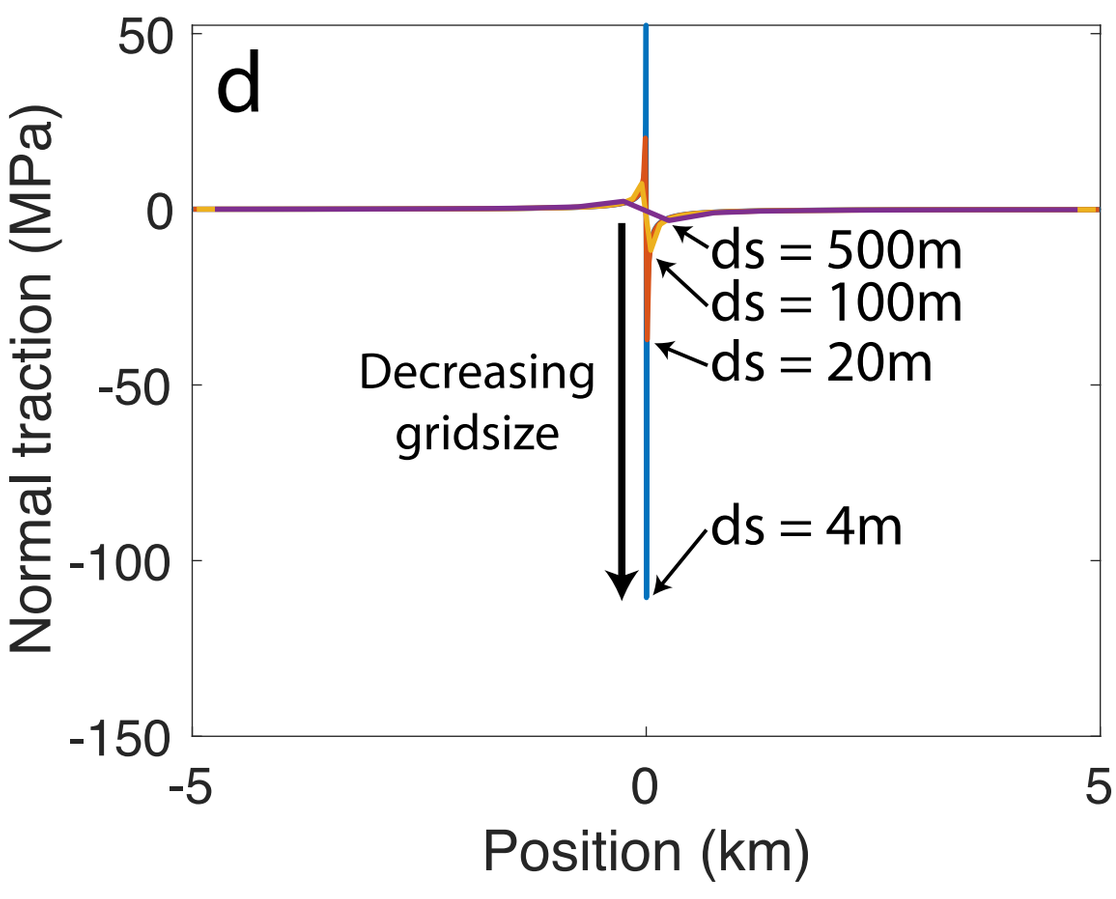

Figure 15.

a

Bended fault with Coulomb friction
(Non-continous curvature)

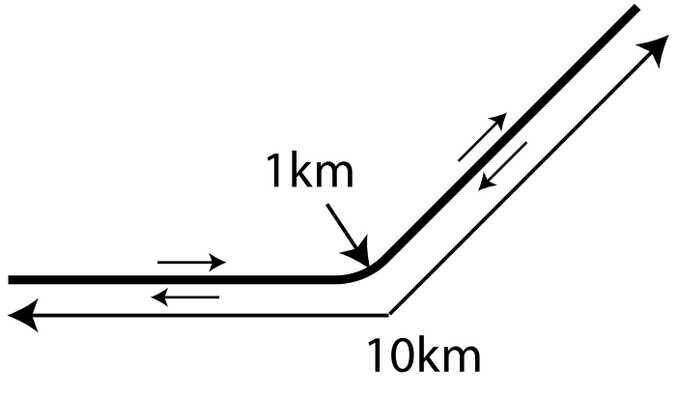

$$\tau^{\mathrm{el}} + \tau^{\mathrm{load}} = -f_0(\sigma_n^{\mathrm{el}} + \sigma_n^{\mathrm{load}})$$

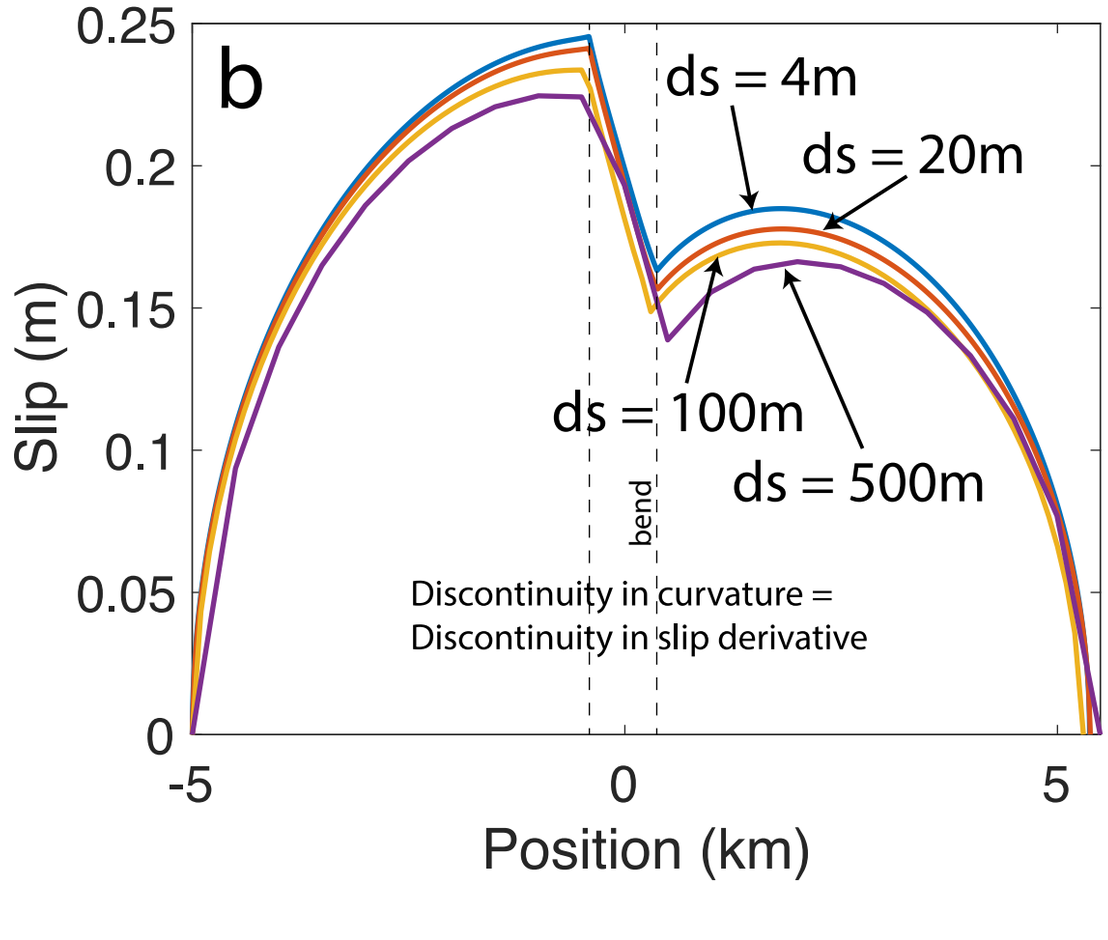

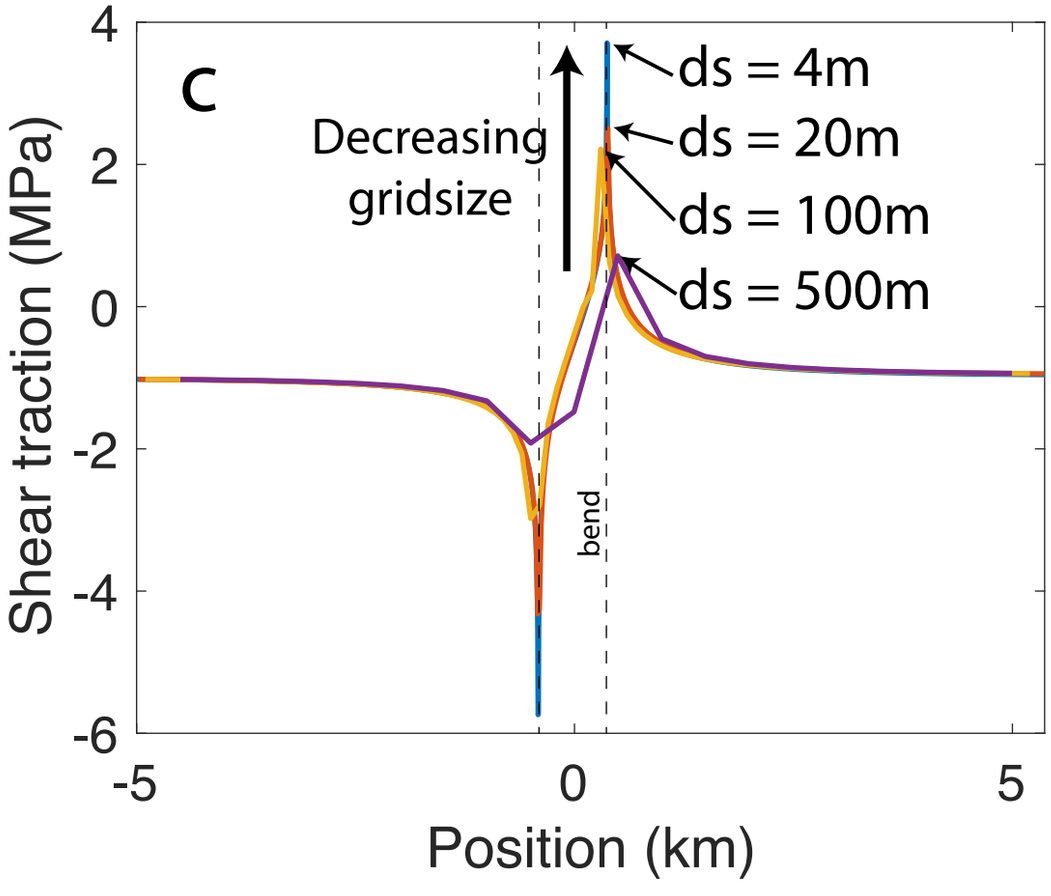

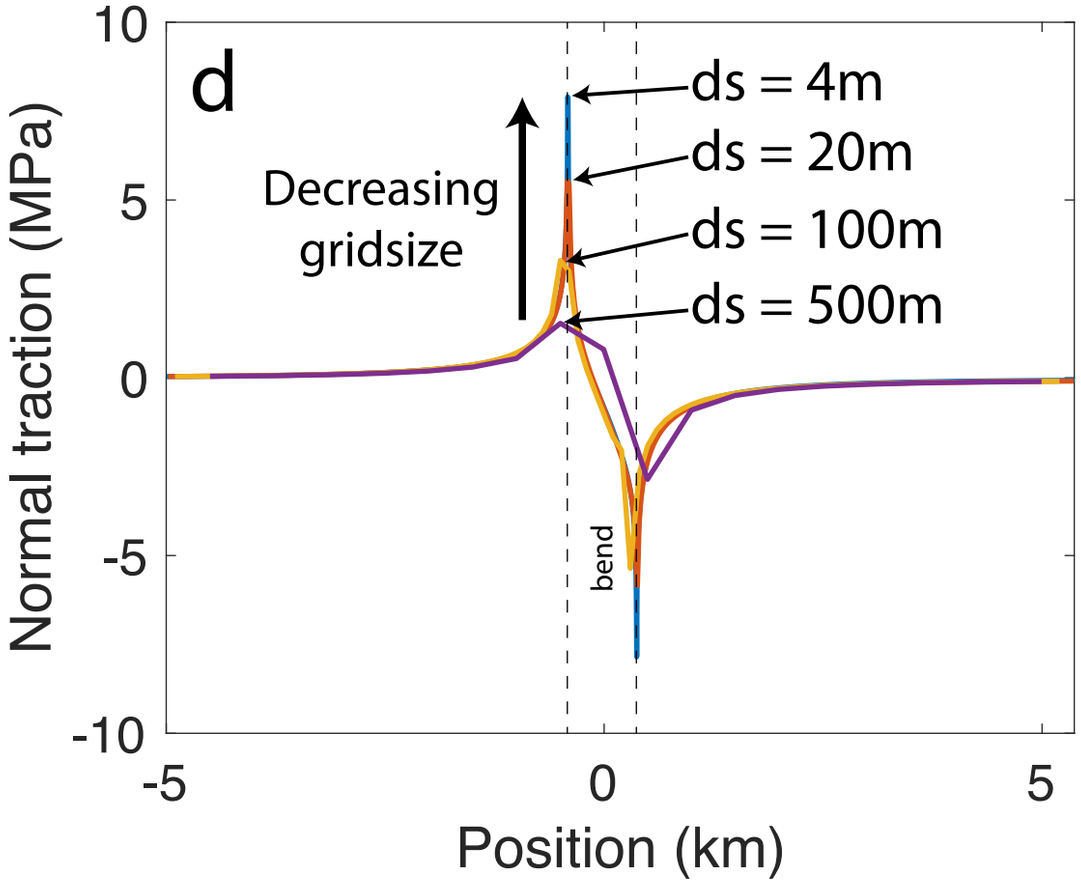

Figure 16.

Initial fault geometry

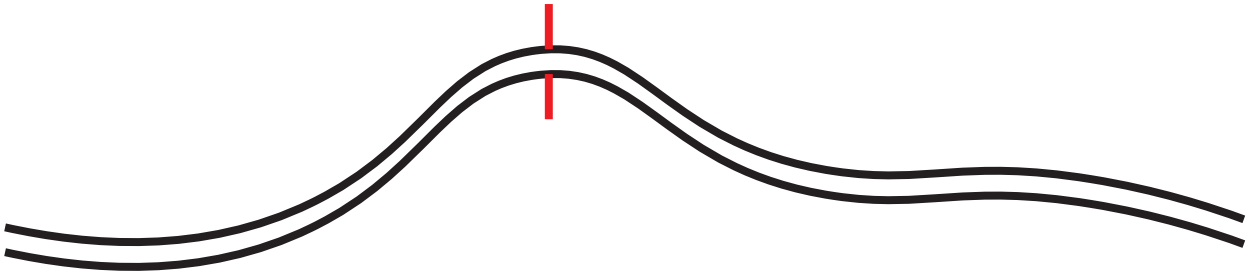

For small strain, the elastic response is linear

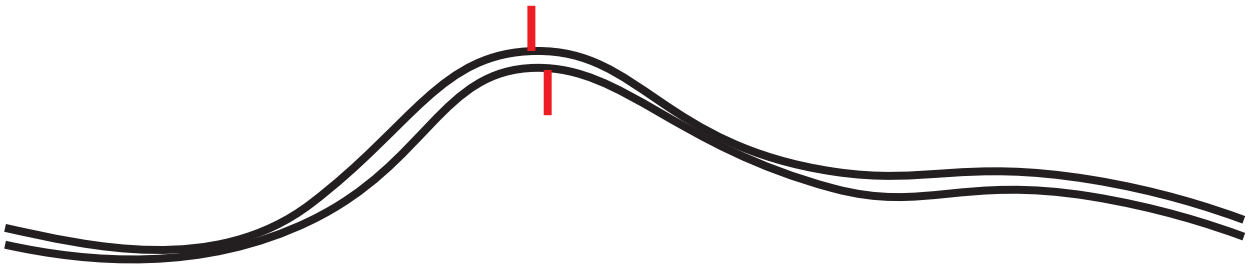

For large displacement, the elastic response is non-linear

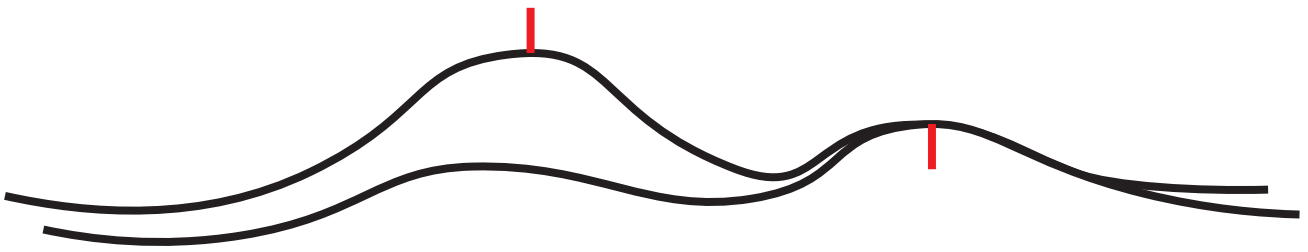

Figure 17.

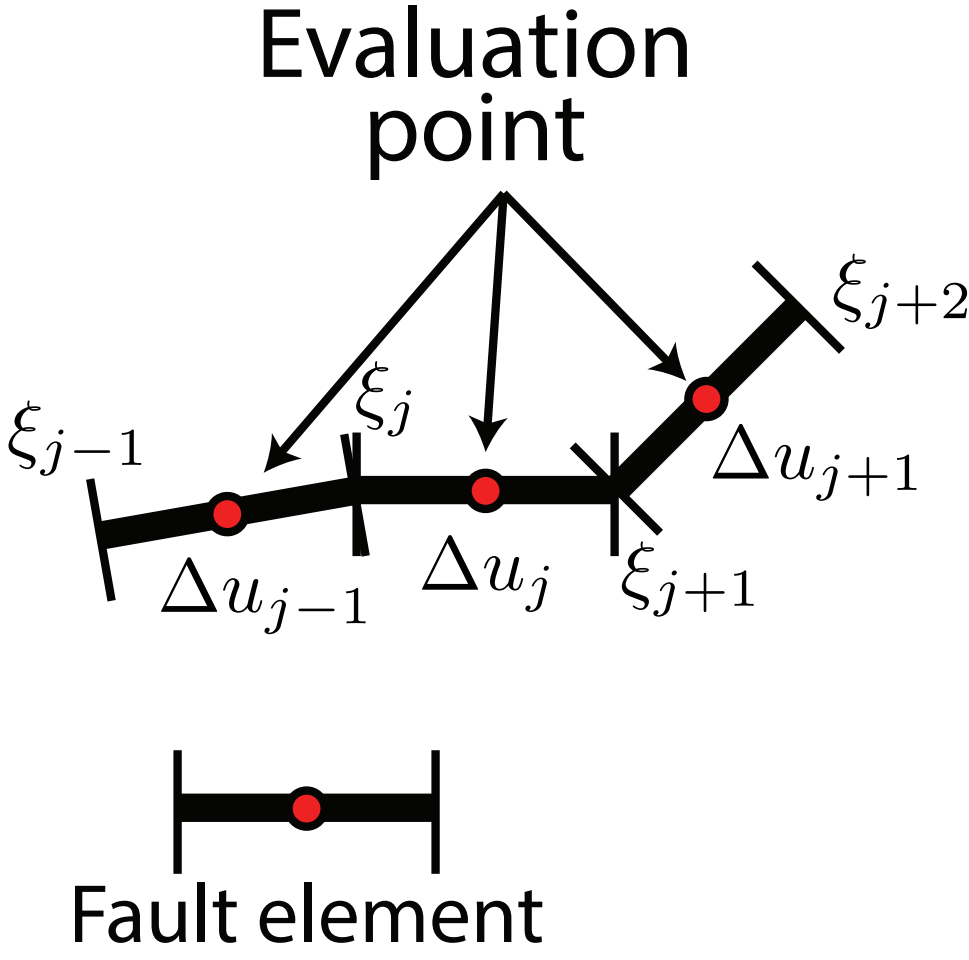
Evaluation point
ξ_{j+2}
ξ_j
ξ_{j-1}
Δu_{j+1}
Δu_{j-1}
Δu_j
ξ_{j+1}
Fault element

Figure 18.

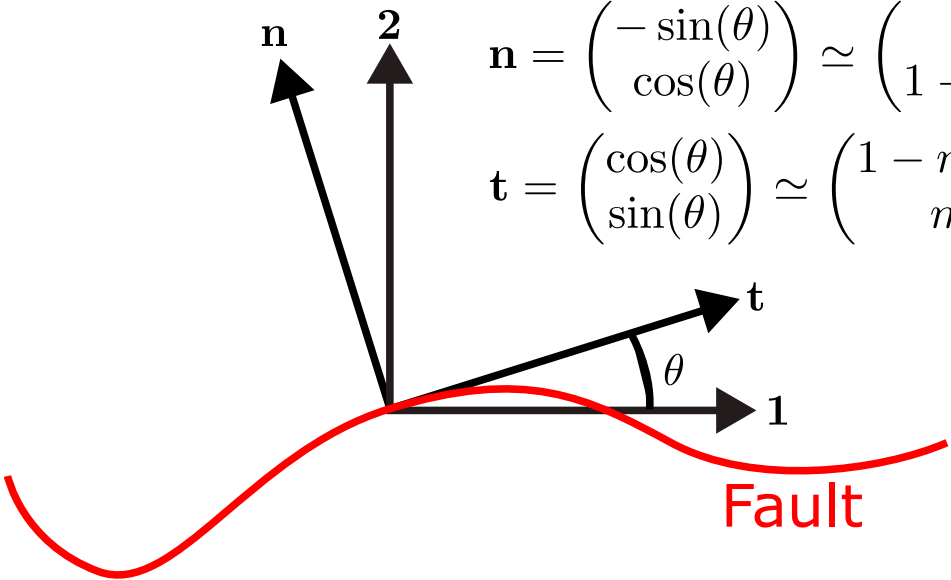

$$\mathbf{n} = \begin{pmatrix} -\sin(\theta) \\ \cos(\theta) \end{pmatrix} \simeq \begin{pmatrix} -m \\ 1 - m^2/2 \end{pmatrix}$$

$$\mathbf{t} = \begin{pmatrix} \cos(\theta) \\ \sin(\theta) \end{pmatrix} \simeq \begin{pmatrix} 1 - m^2/2 \\ m \end{pmatrix}$$

Figure19.

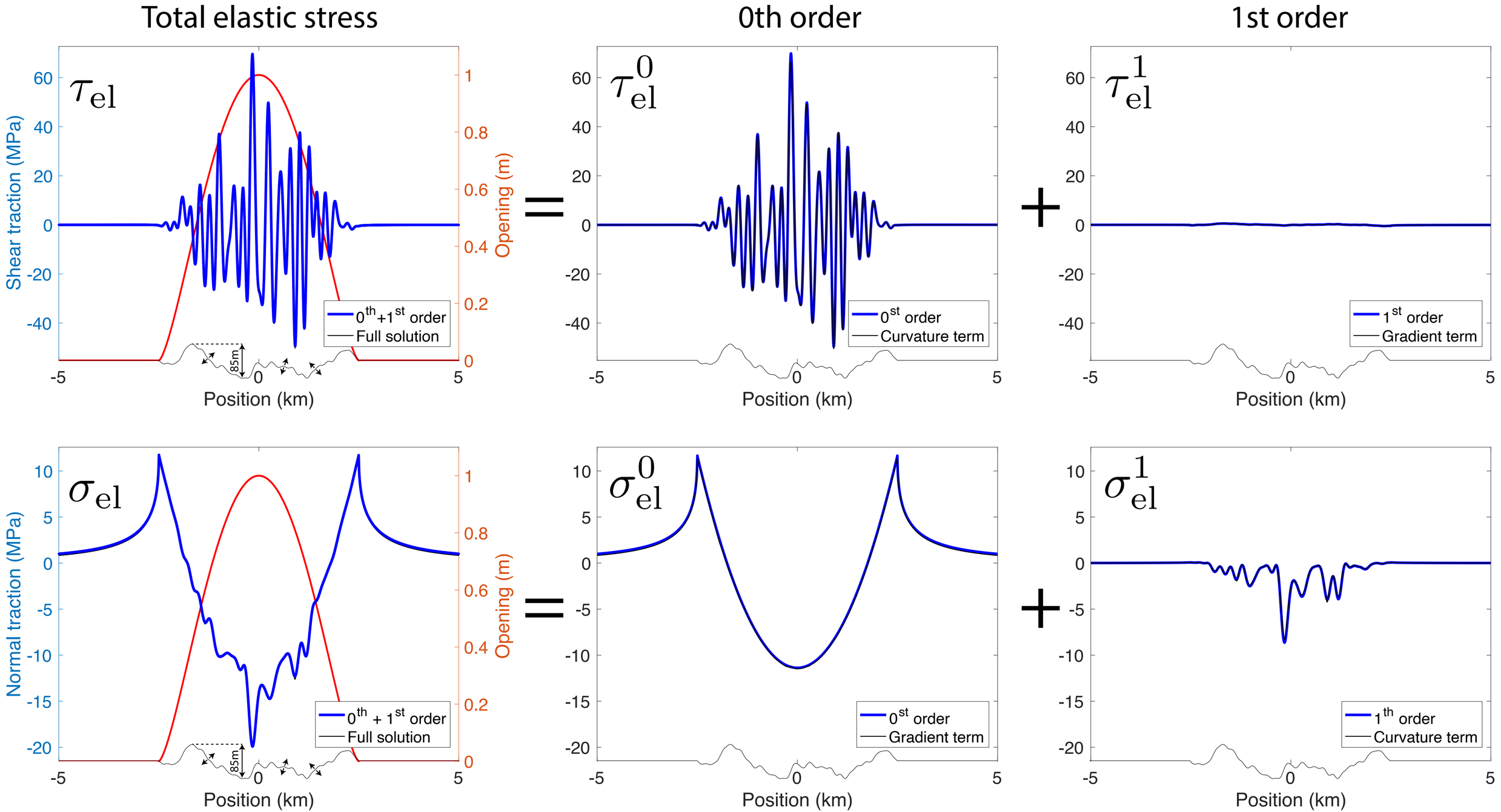
Total elastic stress
0th order
1st order
τ_{el}
τ^0_{el}
τ^1_{el}
Shear traction (MPa)
Opening (m)
0th+1st order
Full solution
0st order
Curvature term
1st order
Gradient term
85m
Position (km)
σ_{el}
σ^0_{el}
σ^1_{el}
Normal traction (MPa)
0th + 1st order
0st order
Gradient term
1th order
Curvature term